SERDP

FINAL REPORT

Lithium Based Red Colorants in Environmentally Friendly Pyrotechnical Illuminants

Thomas Klapoetke
Alicia Dufter
Alexander Schweiger
Joerg Stierstorfer
University of Munich (LMU)

Jared Moretti
Anthony Shaw
US Army, CCDC Armaments Center

May 2022

SERDP Project WP19-1287

REPORT DOCUMENTATION PAGE

Form Approved
OMB No. 0704-0188

1. REPORT DATE *(DD-MM-YYYY)*	**2. REPORT TYPE**	**3. DATES COVERED** *(From - To)*
27/05/2022	SERDP Final Report	5/21/2019 - 5/27/2022

4. TITLE AND SUBTITLE

Lithium Based Red Colorants in Environmentally Friendly Pyrotechnical Illuminants

5a. CONTRACT NUMBER
19-C-0033

5b. GRANT NUMBER

5c. PROGRAM ELEMENT NUMBER

6. AUTHOR(S)

Thomas Klapoetke, Alicia Dufter, Alexander Schweiger and Joerg Stierstorfer
University of Munich (LMU)

Jared Moretti and Anthony Shaw
US Army, CCDC Armaments Center

5d. PROJECT NUMBER WP19-1287

5e. TASK NUMBER

5f. WORK UNIT NUMBER

7. PERFORMING ORGANIZATION NAME(S) AND ADDRESS(ES)

Ludwig-Maximilians-University
Munich Department Chemistry
Butenandstraße 5-13
81377 Munich
Germany

DEVCOM Armaments Center
Pyrotechnics Technology Devision
Picatinny Arsenal,
NJ 07806
United States of America

8. PERFORMING ORGANIZATION REPORT NUMBER

WP19-1287

9. SPONSORING/MONITORING AGENCY NAME(S) AND ADDRESS(ES)

Strategic Environmental Research and Development Program
4800 Mark Center Drive, Suite 16F16
Alexandria, VA 22350-3605

10. SPONSOR/MONITOR'S ACRONYM(S)

SERDP

11. SPONSOR/MONITOR'S REPORT NUMBER(S)

WP19-1287

12. DISTRIBUTION/AVAILABILITY STATEMENT

DISTRIBUTION STATEMENT A. Approved for public release: distribution unlimited.

13. SUPPLEMENTARY NOTES

14. ABSTRACT

● Traditional red-light-emitting pyrotechnic formulations are based on strontium and chlorinated organic materials. During the combustion highly, carcinogenic polychlorinated compounds are formed. Additionally, strontium is classified as potentially harmful to human health by the United States Environmental Protection Agency (U.S. EPA). Therefore, the goal of the project WP19-1287 is to find a novel pyrotechnic system that will significantly reduce the environmental impact of pyrotechnics. These pyrotechnic systems are required to be free of chlorine (perchlorate), heavy metals and strontium and weight reduced. Furthermore, they should have high color purity and luminous intensity and no toxic solvents should be involved in synthesis and purification. To achieve these requirements, new lithium based pyrotechnical compositions with a high nitrogen content are tested. The lithium salt synthesis should be simple and easily up-scalable.

15. SUBJECT TERMS

New Fluorine-Free, Green Surfactant Mixtures, AFFF

16. SECURITY CLASSIFICATION OF:			**17. LIMITATION OF ABSTRACT**	**18. NUMBER OF PAGES**	**19a. NAME OF RESPONSIBLE PERSON** Thomas Klapoetke
a. REPORT	**b. ABSTRACT**	**c. THIS PAGE**			**19b. TELEPHONE NUMBER** *(Include area code)*
UNCLASS	UNCLASS	UNCLASS	UNCLASS	141	+49 (0)89 2180 77491

Table of Contents

1 Abstract 1

1.1 Introduction and Objective 1

1.2 Technical Approach 1

1.3 Performance and cost assessment 1

1.4 Implementation Issues 1

1.5 Publications 2

2 Results and Discussion 3

2.1 Synthesis and characterization of new lithium compounds 3

2.1.1 1*N*-Nitro-1*H*-pyrazole 3

2.1.2 3-Nitro-1*H*-pyrazole 3

2.1.3 Lithium 3-nitropyrazolate 4

2.1.4 3,4-Dinitro-1*H*-pyrazole 6

2.1.5 Lithium 3,4-dinitropyrazolate monohydrate 7

2.1.6 3,5-Dinitro-1*H*-pyrazole 9

2.1.7 Lithium 3,5-dinitropyrazole monohydrate 9

2.1.8 4-Amino-3,5-dinitro-1*H*-pyrazole 11

2.1.9 Lithium 4-amino-3,5-dinitropyrazolate sesquihydrate 11

2.1.10 3,4,5-Trinitro-1*H*-pyrazole 13

2.1.11 Lithium 3,4,5-trinitropyrazolate trihydrate 13

2.1.12 Lithium tetrazolate 15

2.1.13 Lithium 5-aminotetrazolate 16

2.1.14 4,5-Dihydro-5-(nitrimino)-1*H*-tetrazole 16

2.1.15 Lithium 5-nitriminotetrazolate monohydrate 17

2.1.16 Dilithium 5,5`-bistetrazolate dihydrate 18

2.1.17 Dilithium 5,5`-bis(tetrazole-1-oxide) tetrahydrate 19

2.1.18 Dilithium 4,6-bis(nitrimino-1,3,5-triazinan)-2-one • 3.5 H_2O 20

2.1.19 Lithium picramate sesquihydrate 21

2.1.20 Lithium dinitromethanide monohydrate 23

2.1.21 Lithium 2,2,2-trinitroethyl nitrocarbamate monohydrate 26

2.1.22 Tetralithium pentaerythritol tetranitrocarbamate 29

2.1.23 Potassium dihydrobis(pyrazol-1-yl)borate 29

2.1.24 Lithium dihydrobis(pyrazol-1-yl)borate monohydrate 31

2.1.25 Potassium dihydrobis(3-nitropyrazol-1-yl)borate 34
2.1.26 Lithium dihydrobis(3-nitropyrazol-1-yl)borate 36
2.1.27 Potassium dihydrobis(4-amino-3,5-dinitropyrazol-1-yl)borate 39
2.1.28 Lithium dihydrobis(4-amino-3,5-dinitropyrazol-1-yl)borate 40
2.1.29 Potassium dihydrobis(1,2,4-triazol-1-yl)borate 40
2.1.30 Lithium dihydrobis(1,2,4-triazol-1-yl)borate sesquihydrate 44
2.1.31 Lithium dihydrobis(tetrazol-1-yl)borate monohydrate 45
2.1.32 Lithium dihydrobis(5-aminotetrazol-1-yl)borate monohydrate 47
2.1.33 Overview of all lithium salts 51
2.2 Selection process 53
2.2.1 Sensitivity measurements 53
2.2.2 Toxicity measurement 58
2.3 Pyrotechnical measurements 62
2.3.1 Drop-in formulations 63
2.3.2 Modified pyrotechnical systems 64
2.3.3 Variation of lithium content 67
2.3.4 Variation of magnesium content 71
2.3.5 Variation grain size of magnesium 74
2.3.6 Different fuel and grain size 78
2.3.7 Variation of the mixtures with different additives 81
2.3.8 Thermal measurement 86
2.3.9 Overview of the selected salts after measuring pyrotechnical formulations 88
2.4 Preparation of prototypes 90
2.4.1 Objective 90
2.4.2 Approach 90
2.4.3 Blending of illuminant compositions 91
2.4.4 Assembly of cluster flares 92
2.4.5 Assembly of parachute flares 93
2.5 Prototype testing and results 94
3 Executive Summery 110
3.1 Introduction 110
3.2 Objectives 111
3.3 Technology Description 111

3.4 Performance Assessment 114
3.5 Cost Assessment 119
3.6 Implementation Issues 120
4 Publications 122
4.1 In peer reviewed journals 122
4.2 Poster 122
5 Literature Cited 124

List of Figures

Figure 1: Color change and weight gain of a sample of lithium 3-nitropyrazolate after exposure to air for 0 or 1 days (from left to right). 5

Figure 2: DTA curves of a freshly prepared sample of lithium 3-nitropyrazolate or after exposure to air for one day (from top to bottom). 6

Figure 3: Crystal structure of lithium 3,4-dinitropyrazolate monohydrate (**6**). 8

Figure 4: Crystal structure of lithium 3,5-dinitropyrazolate trihydrate (**9**). 10

Figure 5: Crystal structure of lithium 4-amino-3,5-dinitropyrazolate sesquihydrate (**14**). . 12

Figure 6: DTA plots of lithium 3,4,5-trinitropyrazolate • H_2O from top to bottom directly after synthesis and after storage at ambient conditions for one day. 14

Figure 7: Crystal structure of lithium 3,4,5-trinitropyrazolate monohydrate..... 14

Figure 8: Dimer of lithium picramate · 1.5 H_2O (**36**). 22

Figure 9: Crystal structure of lithium dinitromethanide monohydrate (**40**)..... 24

Figure 10: Crystal structure of lithium 2,2,2-trinitroethyl nitrocarbamate monohydrate (**44**). 27

Figure 11: ^{1}H-coupled ^{11}B NMR spectra of samples prepared using different reaction temperatures and times: red curve – 90 °C, 22.5 hours; green curve – 110 °C, 20.5 hours; blue curve – 110 °C, 40.25 hours. 30

Figure 12: ^{1}H NMR spectrum of a freshly prepared sample of lithium dihydrobis(pyrazol-1-yl)borate monohydrate (**50**). 32

Figure 13: Crystal structure of lithium dihydrobis(pyrazol-1-yl)borate monohydrate (**50**)... 33

Figure 14: Change in color and weight of a sample of potassium dihydrobis(3-nitropyrazol-1-yl)borate (**51**) after exposure to air for one, seven and 14 days, respectively. 35

Figure 15: ^{1}H NMR spectra of a sample of potassium dihydrobis(3-nitropyrazol-1-yl)borate (**51**) after exposure to air directly after reaction (red graph), for one day (green graph), after seven days (blue graph) and after 14 days (violet graph). 35

Figure 16: DTA curves of lithium dihydrobis(3-nitropyrazol-1-yl)borate monohydrate (**52**) and lithium dihydrobis(3-nitropyrazol-1-yl)borate (**53**) (top to bottom). 37

Figure 17: Color change of a sample of lithium dihydrobis(3-nitropyrazol-1-yl)borate (**53**) after exposure to air for 0, 1, 7 or 14 days (from left to right). 38

Figure 18: Dimer of lithium dihydrobis(3-nitropyrazol-1-yl)borate monohydrate (**52**). 38

Figure 19: ^{1}H-coupled ^{11}B NMR spectra of samples prepared using different reaction times at constant concentrations ([KBH_4] = 1.63–2.68 mol L^{-1}, [$C_2H_3N_3$] = 3.26–5.36 mol L^{-1}). 41

Figure 20: ^{1}H-coupled ^{11}B NMR spectra of samples prepared using different concentrations at a constant reaction time of six days: red curve – [KBH_4] = 2.25 mol L^{-1}, [$C_2H_3N_3$] = 4.51 mol L^{-1}; green curve – [KBH_4] = 4.64 mol L^{-1}, [$C_2H_3N_3$] = 9.28 mol L^{-1}; blue curve – [KBH_4] = 10.06 mol L^{-1}, [$C_2H_3N_3$] = 20.12 mol L^{-1}. 42

Figure 21: Molecular unit of potassium dihydrobis(1,2,4-triazol-1-yl)borate (**57**). 43

Figure 22: Crystal structure of lithium dihydrobis(1,2,4-triazol-1-yl)borate sesquihydrate (**59**)..... 44

Figure 23: Advanced molecular unit of lithium dihydrobis(tetrazol-1-yl)borate monohydrate (**60**)..... 46
Figure 24: DTA curves of lithium dihydrobis(5-aminotetrazol-1-yl)borate monohydrate (**63**) and lithium dihydrobis(5-aminotetrazol-1-yl)borate (**64**) (top to bottom). 48
Figure 25: Crystal structure of lithium dihydrobis(5-aminotetrazol-1-yl)borate monohydrate (**63**)..... 50
Figure 26: BAM Fallhammer tester with impact device and classification chart.[34] 54
Figure 27: BAM friction tester with porcelain plate, peg and classification chart.[34] 55
Figure 28: OZM Electric Spark Tester XSpark10 for measuring the electrostatic discharge.. 56
Figure 29: Differential thermal analysis device (DTA) for determination of decomposition temperatures..... 56
Figure 30: Scheme of the dilution series, adapted from HACH LANGE GmbH (Düsseldorf, Germany)..... 59
Figure 31: Demonstration of the LUMIStox 300. Row A contained the substance diluted in a range from 1:1 to 1:16, Row B and C contained each 0.5 ml of the reactivated bacteria in sodium chloride stock solution. 60
Figure 32: Burning images of the “drop-in” formulations with KNO3 as oxidizer and nitrocellulose as binder, with the respective number of the formulation. 67
Figure 33: Burning images of the best mixtures with the respective number of the formulation, with a variation of the lithium salt content. 71
Figure 34: Burning images of the mixtures with the respective number of the formulation, with a variation of the magnesium content..... 74
Figure 35: Burning images of the mixtures with the respective number of the formulation, with a variation of the magnesium grain size. 78
Figure 36: Burning images of the mixtures with the respective number of the formulation, with aluminum as the fuel..... 80
Figure 37: Burning images of the mixtures with the respective number of the formulation, with pyrotechnical additives. 85
Figure 38: Thermal measurements of the most promising formulations..... 88
Figure 39: Photographs of the granulated pyrotechnic mixes..... 92
Figure 40: Images of a finished cluster flare; (left) top and side view, (right) inner diameter view showing igniter (black) and illuminant (gray) layers..... 92
Figure 41: Images of all finished cluster flares; (left) top view, (right) angled view..... 93
Figure 42: Top and side view of a finished parachute flare. 93
Figure 43: Images of all finished flares; (top left) top view, (top right/bottom left) side view, (bottom right) angled view of the flares. 94
Figure 44: Set up for the measurement of the cluster flares; (left/middle) angled view, (right) frontal view..... 94
Figure 45: Set up for the measurement of the parachute flares from different angles..... 95
Figure 46: Photometric and spectrometric waveform for **Control - 3** cluster flare..... 99
Figure 47: Photometric and spectrometric waveform for **Control - 3** parachute flare..... 99

Figure 48: The **Control** composition, containing strontium nitrate, burns in the hand-held signal parachute flare configuration on a test stand (picture 1). 100
Figure 49: The **Control** composition, containing strontium nitrate, burns in the hand-held signal parachute flare configuration on a test stand (picture 2). 100
Figure 50: The **Control** composition, containing strontium nitrate, burns in the hand-held signal parachute flare configuration on a test stand (picture 3). 101
Figure 51: Photometric and spectrometric waveform for cluster flare **I - 3**. 101
Figure 52: Photometric and spectrometric waveform for parachute flare **I – 3**..... 102
Figure 53: Composition **I**, which contained 33 wt-% Li2CO3, produced large amounts of slag upon combustion, as shown by this photograph taken after a test of a parachute flare..... 102
Figure 54: Photometric and spectrometric waveform for cluster flare **II - 3**. 103
Figure 55: Photometric and spectrometric waveform for parachute flare **II – 3**. 103
Figure 56: Photometric and spectrometric waveform for cluster flare **III – 3**. 103
Figure 57: Photometric and spectrometric waveform for parachute flare **III – 3**. 104
Figure 58: Composition **III**, containing 33 wt-% Li 5-aminotetrazole and 30 wt-% Mg, burns in the hand-held signal parachute flare configuration on a test stand (picture 1). 104
Figure 59: Composition **III**, containing 33 wt-% Li 5-aminotetrazole and 30 wt-% Mg, burns in the hand-held signal parachute flare configuration on a test stand (picture 2). 105
Figure 60: Composition **III**, containing 33 wt-% Li 5-aminotetrazole and 30 wt-% Mg, burns in the hand-held signal parachute flare configuration on a test stand (picture 3). 105
Figure 61: Photometric and spectrometric waveform for cluster flare **IV – 3**. 106
Figure 62: Photometric and spectrometric waveform for parachute flare **IV – 3**. 106
Figure 63: Composition **IV**, containing 33 wt-% Li 5-aminotetrazole and 12 wt-% Mg, burns in the hand-held signal parachute flare configuration on a test stand (picture 1). 107
Figure 64: Composition **IV**, containing 33 wt-% Li 5-aminotetrazole and 12 wt-% Mg, burns in the hand-held signal parachute flare configuration on a test stand (picture 2). 107
Figure 65: Composition **IV**, containing 33 wt-% Li 5-aminotetrazole and 12 wt-% Mg, burns in the hand-held signal parachute flare configuration on a test stand (picture 3). 108
Figure 66: Photometric and spectrometric waveform for cluster flare **V – 3**. 108
Figure 67: Photometric and spectrometric waveform for parachute flare **V – 3**. 109
Figure 68: Photometric and spectrometric waveform for cluster flare **VI – 3**. 109
Figure 69: Photometric and spectrometric waveform for parachute flare **VI – 3**. 109
Figure 70: Analytical devices: Xcalibur Sapphire 3 for X-ray measurements, OZM DTA 552-Ex for differential thermal analysis, BAM standardized friction and impact device and an OZM Electric Spark Tester XSpark10, respectively. 112
Figure 71: Representation of the pyrometric setup: Press, fume hood for the burn-off, spectrometer (Ocean Optics), FLIR thermal camera and display of the thermal measurement. 112
Figure 72: Display of a parachute flare manufactured by DEVCOM. 113
Figure 73: Images of a finished cluster flare; (left) top and side view, (right) inner diameter view showing igniter (black) and illuminant (gray) layers. 113

Figure 74: Top and side view of a finished parachute flare. 113
Figure 75: Comparison of a strontium-based control formulation and the tested formulation containing lithium-5-aminotetrazol (**20**). 120
Figure 76: Poster presented at SERDP ESTCP SYMPOSSIUM in 2019. 122
Figure 77: Poster presented at NTREM 2022. 123

List of Schemes

Scheme 1: Reaction toward 1N-Nitro-1H-pyrazole (**2**)..... 3
Scheme 2: Reaction toward 3-Nitro-1H-pyrazole (**3**). 3
Scheme 3: Reaction toward lithium 3-nitropyrazolate (**4**). 4
Scheme 4: Reaction toward 3,4-dinitro-1H-pyrazole (**5**)..... 6
Scheme 5: Reaction toward lithium 3,4-dinitropyrazolate monohydrate (**6**). 7
Scheme 6: Reaction toward 3,5-dinitro-1H-pyrazole (**8**)..... 9
Scheme 7: Reaction toward lithium 3,5-dinitropyrazolate monohydrate (**10**). 9
Scheme 8: Reaction toward 4-amino-3,5-dinitro-1H-pyrazole (**13**). 11
Scheme 9: Reaction toward lithium 4-amino-3,5-dinitropyrazolate sesquihydrate (**14**). ... 11
Scheme 10: Reaction toward 3,4,5-trinitro-1H-pyrazole (**15**). 13
Scheme 11: Reaction toward lithium 3,4,5-trinitropyrazolate trihydrate (**16**). 13
Scheme 12: Reaction toward lithium tetrazolate (**18**). 15
Scheme 13: Reaction toward lithium 5-aminotetrazolate (**20**). 16
Scheme 14: Reaction toward 4,5-dihydro-5-(nitrimino)-1H-tetrazole (**21**). 16
Scheme 15: Reaction toward lithium 5-nitriminotetrazolate · H_2O (**22**). 17
Scheme 16: Synthesis toward the neutral compound 5,5`-bistetrazole (**25**). 18
Scheme 17: Reaction toward dilithium 5,5‘-bistetrazolate dihydrate (**26**). 18
Scheme 18: Reaction toward dilithium 5,5`-bistetrazole dihydrate (**26**) over the respective diammonium salt (**27**). 19
Scheme 19: Reaction toward dilithium 5,5`-bis(tetrazole-1-oxide) • 4 H_2O (**30**). 19
Scheme 20: Reaction toward dilithium 4,6-bis(nitrimino-1,3,5-triazinan)-2-one • 3.5 H2O (**32**). 20
Scheme 21: Reaction toward picramic acid (**35**). 21
Scheme 22: Reaction toward lithium picramate sesquihydrate (**36**). 21
Scheme 23: Reaction toward lithium dinitromethanide monohydrate (**40**). 23
Scheme 24: Reaction toward 2,2,2-trinitroethyl nitrocarbamate (**43**). 26
Scheme 25: Reaction toward lithium 2,2,2-trinitroethyl nitrocarbamate monohydrate (**44**). 26
Scheme 26: Reaction toward pentaerythritol tetranitrocarbamate (**47**)..... 29
Scheme 27: Unsuccessful reaction toward tetralithium pentaerythritol tetranitrocarbamate (**48**). 29
Scheme 28: Reaction toward potassium dihydrobis(pyrazol-1-yl)borate (**49**). 30
Scheme 29: Reaction toward lithium dihydrobis(pyrazol-1-yl)borate monohydrate (**50**)..... 31
Scheme 30: Reaction toward potassium dihydrobis(3-nitropyrazol-1-yl)borate (**51**). 34
Scheme 31: Reaction toward lithium dihydrobis(3-nitropyrazol-1-yl)borate monohydrate (**52**). 36
Scheme 32: Reaction toward lithium dihydrobis(3-nitropyrazol-1-yl)borate (**53**)..... 37
Scheme 33: Reaction toward potassium dihydrobis(4-amino-3,5-dinitropyrazol-1-yl)borate (**54**). 39

Scheme 34: Reaction toward lithium dihydrobis(4-amino-3,5-dinitropyrazol-1-yl)borate (**55**). 40
Scheme 35: Reaction toward potassium dihydrobis(1,2,4-triazol-1-yl)borate (**57**)..... 42
Scheme 36: Reaction toward lithium dihydrobis(1,2,4-triazol-1-yl)borate sesquihydrate (**59**) over the free acid, namely (1H-1,2,4-triazole)dihydro(1,2,4-triazol-1-yl)borate (**58**). 44
Scheme 37: Reaction toward lithium dihydrobis(tetrazol-1-yl)borate monohydrate (**60**).... 46
Scheme 38: Reaction toward lithium dihydrobis(5-aminotetrazol-1-yl)borate monohydrate (**63**). 47
Scheme 39: Reaction toward lithium dihydrobis(5-aminotetrazol-1-yl)borate (**64**). 49

List of Tables

Table 1: Crystallographic data of lithium 3,4-dinitropyrazolate monohydrate (**6**). 8
Table 2: Crystallographic data of lithium 3,5-dinitropyrazolate trihydrate (**9**). 10
Table 3: Crystallographic data of lithium 4-amino-3,5-dinitropyrazolate sesquihydrate (**14**). 12
Table 4: Crystallographic data of lithium 3,4,5-trinitropyrazolate monohydrate. 15
Table 5: Crystallographic data of lithium picramate · 1.5 H_2O (**36**). 22
Table 6: Crystallographic data of lithium dinitromethanide monohydrate (**40**). 25
Table 7: Crystallographic data of lithium 2,2,2-trinitroethyl nitrocarbamate monohydrate (**44**). 28
Table 8: Crystallographic data of lithium dihydrobis(pyrazol-1-yl)borate monohydrate (**50**). 33
Table 9: Crystallographic data of lithium dihydrobis(3-nitropyrazol-1-yl)borate monohydrate (**52**). 39
Table 10: Crystallographic data of potassium dihydrobis(1,2,4-triazol-1-yl)borate (**57**). 43
Table 11: Crystallographic data of lithium dihydrobis(1,2,4-triazol-1-yl)borate sesquihydrate (**59**). 45
Table 12: Crystallographic data of lithium dihydrobis(tetrazol-1-yl)borate monohydrate (**60**). 47
Table 13: Crystallographic data of lithium dihydrobis(5-aminotetrazol-1-yl)borate monohydrate (**63**). 50
Table 14: Overview of the synthesized compounds, the corresponding hygroscopicity/ageing studies. 51
Table 15: Overview of the sensitivity properties of the lithium salts. 57
Table 16: Results of the toxicity measurements of the lithium salts of dihydrobis(1,2,4-triazol-1-yl)borate sesquihydrate (**59**), dihydrobis(5-aminotetrazolal-1-yl)borate (**64**), 4-amino-3,5-dinitropyrazolate sesquihydrate (**14**), 5,5-bistetrazolate dihydrate (**26**) and 5-aminotetrazolate (**20**), respectively. 61
Table 17: Composition of a chlorine-free strontium-based control AD-1[4] and of "drop-in" formulations AD-2 to AD-5 with lithium dihydrobis(1,2,4-triazol-1-yl)borate sesquihydrate (**59**), lithium dihydrobis(5-aminotetrazol-1-yl)borate (**64**), lithium 4-amino-3,5-dinitropyrazolate sesquihydrate (**14**) and lithium 5-aminotetrazolate (**20**). 64
Table 18: "Drop-in" formulations with modified system containing lithium 5-tetrazolate (**18**), lithium 5-aminotetrazolate (**20**), dilithium 5,5'-bistetrazolate dihydrate (**26**), dilithium 5,5'-bis(tetrazole-1-oxide) tetrahydrate (**30**), lithium 4-amino-3,5-dinitropyrazolate sesquihydrate (**14**), lithium dihydrobis(1,2,4-triazol-1-yl)borate sesquihydrate (**59**), lithium dihydrobis(5-aminotetrazol-1-yl)borate (**64**), respectively. 65
Table 19: Measured parameters of "drop-in" formulations with modified system containing lithium 5-tetrazolate (**18**), lithium 5-aminotetrazolate (**20**), dilithium 5,5'-

bistetrazolate dihydrate (**26**), dilithium 5,5'-bis(tetrazole-1-oxide) tetrahydrate (**30**), lithium 4-amino-3,5-dinitropyrazolate sesquihydrate (**14**), lithium dihydrobis(1,2,4-triazol-1-yl)borate sesquihydrate (**59**), lithium dihydrobis(5-aminotetrazol-1-yl)borate (**64**), respectively. 66

Table 20: Variation of the lithium content of pyrotechnical formulations containing the salts lithium 5-tetrazolate (**18**), lithium 5-aminotetrazolate (**20**), dilithium 5,5'-bistetrazolate dihydrate (**26**), lithium 4-amino-3,5-dinitropyrazolate sesquihydrate (**14**), lithium dihydrobis(5-aminotetrazol-1-yl)borate (**64**), respectively. 68

Table 21: Measured parameters of the pyrotechnical formulations containing an increased amount of the respective lithium salts: 5-tetrazolate (**18**), 5-aminotetrazolate (**20**), 5,5'-bistetrazolate dihydrate (**26**), 4-amino-3,5-dinitropyrazolate sesquihydrate (**14**), dihydrobis(5-aminotetrazol-1-yl)borate (**64**), respectively. 69

Table 22: Variation of the magnesium content of pyrotechnical formulations containing the salts lithium 5-tetrazolate (**18**), lithium 5-aminotetrazolate (**20**), dilithium 5,5'-bistetrazolate dihydrate (**26**), lithium 4-amino-3,5-dinitropyrazolate sesquihydrate (**14**), lithium dihydrobis(5-aminotetrazol-1-yl)borate (**64**), respectively. 72

Table 23: Measured parameters of the pyrotechnical formulations containing an increased amount of magnesium with the respective lithium salts: 5-tetrazolate (**18**), 5-aminotetrazolate (**20**), 5,5'-bistetrazolate dihydrate (**26**), 4-amino-3,5-dinitropyrazolate sesquihydrate (**14**), dihydrobis(5-aminotetrazol-1-yl)borate (**64**), respectively. 73

Table 24: Variation of the magnesium grain size of pyrotechnical formulations containing the salts lithium 5-aminotetrazolate (**20**), dilithium 5,5'-bistetrazolate dihydrate (**26**), lithium 4-amino-3,5-dinitropyrazolate sesquihydrate (**14**), respectively. 75

Table 25: Measured parameters of the pyrotechnical formulations containing different grain sizes of magnesium and the salts lithium 5-aminotetrazolate (**8**), dilithium 5,5'-bistetrazolate dihydrate (**9**), lithium 4-amino-3,5-dinitropyrazolate sesquihydrate (**11**), respectively. 77

Table 26: Pyrotechnical formulations containing different grain sizes of aluminum and the salts lithium 5-aminotetrazolate (**20**), dilithium 5,5'-bistetrazolate dihydrate (**26**), lithium 4-amino-3,5-dinitropyrazolate sesquihydrate (**14**), respectively. 79

Table 27: Measured parameters of the pyrotechnical formulations containing different grain sizes of aluminum and the salts lithium 5-aminotetrazolate (**20**), dilithium 5,5'-bistetrazolate dihydrate (**26**), lithium 4-amino-3,5-dinitropyrazolate sesquihydrate (**14**), respectively. 80

Table 28: Pyrotechnical formulations containing pyrotechnical additives and the salts lithium 5-aminotetrazolate (**20**), dilithium 5,5'-bistetrazolate dihydrate (**26**), lithium 4-amino-3,5-dinitropyrazolate sesquihydrate (**14**), respectively. 81

Table 29: Measured parameters of the pyrotechnical formulation containing pyrotechnical additives and the salts lithium 5-aminotetrazolate (**20**), dilithium 5,5'-bistetrazolate dihydrate (**26**), lithium 4-amino-3,5-dinitropyrazolate sesquihydrate (**14**), respectively. 83

Table 30: Compositions of the pyrotechnical formulation containing lithium 5-aminotetrazolate (**20**), dilithium 5,5`-bistetrazole dihydrate (**26**), lithium 4-amino-3,5-dinitropyrazolate sesquihydrate (**14**), lithium dihydrobis(1,2,4-triazol-1-yl)borate (**59**) and lithium dihydrobis(5-aminotetrazol-1-yl)borate monohydrate (**64**), respectively. 86
Table 31: Measured values of the pyrotechnical formulation containing lithium 5-aminotetrazolate (**20**), dilithium 5,5`-bistetrazole dihydrate (**26**), lithium 4-amino-3,5-dinitropyrazolate sesquihydrate (**14**), lithium dihydrobis(1,2,4-triazol-1-yl)borate (**59**) and lithium dihydrobis(5-aminotetrazol-1-yl)borate (**64**)..... 87
Table 32: Overview of the selected lithium salts after the pyrotechnical measurements. 89
Table 33: Chemical makeup of the red illuminant compositions..... 90
Table 34: Geometry and optical emissive output of all cluster flares..... 96
Table 35: Geometry and optical emissive output of all parachute flares. 97
Table 36: Sr-based red-light illuminant formulations of a cluster and a parachute flare..... 110
Table 37: Most promising formulations. 114
Table 38: Measured pyrotechnic values of the most promising mixtures..... 115
Table 39: Prepared formulations at DEVCOM..... 115
Table 40: Geometry and optical emissive output of all cluster flares..... 116
Table 41: Geometry and optical emissive output of all parachute flares. 117

1 Abstract

1.1 Introduction and Objective

Traditional red-light-emitting pyrotechnic formulations are based on strontium and chlorinated organic materials.[1] During the combustion highly carcinogenic polychlorinated compounds are formed.[2] Additionally, strontium is classified as potentially harmful to human health by the United States Environmental Protection Agency (U.S. EPA).[3] Therefore, the goal of the project WP19-1287 is to find a novel pyrotechnic system that will significantly reduce the environmental impact of pyrotechnics. These pyrotechnic systems are required to be free of chlorine (perchlorate), heavy metals and strontium and weight reduced. Furthermore, they should have high color purity and luminous intensity and no toxic solvents should be involved in synthesis and purification. To achieve these requirements, new lithium based pyrotechnical compositions with a high nitrogen content are tested. The lithium salt synthesis should be simple and easily up-scalable.

1.2 Technical Approach

The approach of this project was to screen for new and literature-known lithium salts that are thermally stable, insensitive to external stimuli and have no toxic characteristics. New salts should also be fully characterized and investigated. Promising lithium salts were mixed in pyrotechnical formulations, pyrotechnical parameters were measured and compared with the chlorine-free mixture produced by *Sabatini* et al.[4] Most promising salts were transferred to the cooperation partner *DEVCOM AC*, where cluster and parachute flares were prepared, burned and their performance was compared to a standard strontium formulation.

1.3 Performance and cost assessment

In the course of this project, more than 15 new lithium salts were synthesized and investigated. A considerable number of them was tested in pyrotechnic formulations. The opposing nature of spectral purity and light intensity resulted in the required parameters being attained, but not in a single formulation. Compared with a standard strontium formulation, the measured values of lithium flares at *DEVCOM* performed markedly inferior.

The expense cost of the project totaled 371,400 $ over a period of 3 years.

1.4 Implementation Issues

The reason for the poorer performance of the flares is the oxophilicity of lithium. This results in the formation of additional by-products, which have a negative influence on the coloration. Since the flares still contain additives (paper tubes), this can also influence the performance. Too high burning temperatures due to the fuel can also be a negative influence.

1.5 Publications

- The Lithium Salts of Bis(azoyl)borates as Strontium- and Chlorine-free Red Pyrotechnic Colorants. Alicia M. W. Dufter, Thomas M. Klapötke, Magdalena Rusan, and Jörg Stierstorfer, *Z. Anorg. Allg. Chem*. **2020**, *646*, 580–585.
- Comparison of Functionalized Lithium Dihydrobis(azolyl)borates with Their Corresponding Azolates as Environmentally Friendly Red Pyrotechnic Coloring Agents. Alicia M. W. Dufter, Thomas M. Klapötke, Magdalena Rusan, Alexander Schweiger and Jörg Stierstorfer, *ChemPlusChem*. **2020**, *85*, 2044–2050.
- Lithium Nitropyrazolates as Potential Red Pyrotechnic Colorants. A. M. W. Dufter-Münster, Alexander G. Harter, Thomas M. Klapötke, Elena Reinhardt, Julia Römer and Jörg Stierstorfer, *Eur. J. Inorg. Chem.* ***2022****, in press.*

2 Results and Discussion

2.1 Synthesis and characterization of new lithium compounds

In regard of the synthesis of new lithiated materials, special focus was set on nitrogen-rich representatives based on pyrazoles, triazoles or tetrazoles and the introduction of nitro groups in order to tailor the oxygen balance of the colorants to fit oxidizers. Furthermore, we aimed at an enhanced luminous intensity of resulting pyrotechnic formulations by forming multivalent lithium salts. Dihydrobis(azolyl)borates are commonly accessed by the acid-base reaction of borohydride with the desired azole ligand.[5] Due to the instability of borohydrides toward hydrolysis all samples were prepared under an atmosphere of dry argon by means of standard Schlenk techniques and solely distilled solvent was used. The reactions proceed with the release of hydrogen so that pressure compensation has to be ensured, e.g. by adding a bubble counter.

2.1.1 1*N*-Nitro-1*H*-pyrazole

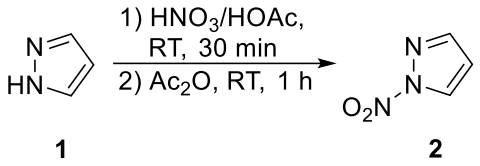

***Scheme 1**: Reaction toward 1N-Nitro-1H-pyrazole (**2**).*

Compound **1** was nitrated according to the literature-known protocol of *Bölter et al.*[6]

2.1.2 3-Nitro-1*H*-pyrazole

The literature provides two protocols for the thermal rearrangement from 1*N*-nitro-1*H*-pyrazole to 3-nitro-1*H*-pyrazole whereby the N-nitrated pyrazole is suspended in anisole[6] or dissolved in benzonitrile,[7] respectively. The method using benzonitrile was favored because in this solvent the rearrangement takes place faster.

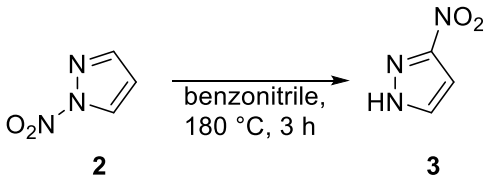

***Scheme 2**: Reaction toward 3-Nitro-1H-pyrazole (**3**).*

5.000 g 1*N*-nitropyrazole (44 mmol) were dissolved in 100 mL benzonitrile and heated at 180 °C for three hours. Upon cooling to 0 °C a precipitate was formed which was filtered off. Both the residue and the filtrate were stand before they were dried at 100 °C in an oven overnight to give a white or brown crystalline material, respectively. The overall yield of the product amounts to 82 % (4.079 g).

IR (ATR): $\tilde{\nu}$ = 3142(s), 3022(m), 2926(m), 2884(m), 1756(vw), 1676(vw), 1608(vw), 1556(s), 1511(s), 1483(s), 1438(m), 1423(m), 1379(vs), 1351(vs), 1286(m), 1249(m), 1209(s), 1090(m), 1058(m), 1047(s), 990(s), 928(m), 903(m), 903(m), 862(m), 820(vs), 794(s), 783(vs), 752(vs), 640(w), 613(m), 537(vw), 516(vw), 474(vw), 442(s) cm^{-1}. $^{14}N\{H\}$ NMR (DMSO-d_6, 25 °C): δ = -17.8 (s, *N*O_2) ppm. $^{13}C\{H\}$ NMR (DMSO-d_6, 25 °C): δ = 156.3 (s, *C*-NO_2), 132.3 (s, *C*H), 101.8 (s, *C*H) ppm. $^{1}H\{/\}$ NMR (DMSO-d_6, 25 °C): δ = 13.94 (br s, 1H, N*H*), 8.03 (d, 1H, C*H*), 7.03 (d, 1H, C*H*) ppm. EA ($C_3H_3N_3O_2$, 113.08): calcd. N 37.16, C 31.86, H 2.67 %; found N 37.29, C 31.73, H 2.62 %. DTA (5 °C min^{-1}): 174 (endothermic), 262 (endothermic) °C.

2.1.3 Lithium 3-nitropyrazolate

2.1.3.1 Procedure

The reaction of the saltification of 3-nitro-1*H*-pyrazole is shown in **Scheme 3**.

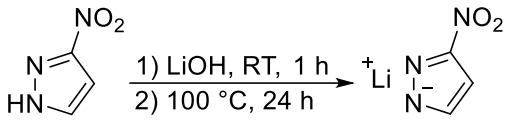

3 **4**

***Scheme 3**: Reaction toward lithium 3-nitropyrazolate (**4**).*

A suspension of 1.000 g 3-nitro-1*H*-pyrazole (9 mmol) and 0.212 g lithium hydroxide (9 mmol) in roughly 13 mL of water was stirred at room temperature for one hour before unreacted azole was filtered off and the solvent was removed from the filtrate *in vacuo*. Drying of the residue at 100 °C overnight yielded 0.802 g of a yellowish powder (76 %).

IR (ATR): $\tilde{\nu}$ = 3152(w), 3128(vw), 2568(vw), 2285(vw), 1559(vw), 1516(m), 1510(m), 1488(s), 1437(w), 1423(m), 1364(m), 1329(vs), 1241(m), 1133(vs), 1108(vs), 1056(s), 1039(s), 1003(vs), 937(s), 897(w), 881(w), 825(s), 779(s), 779(s), 753(s), 613(m), 571(m), 503(m), 446(w), 414(w) cm^{-1}. $^{7}Li\{H\}$ NMR (DMSO-d_6, 25 °C): δ = -0.8 (s, *Li*) ppm. $^{14}N\{H\}$ NMR (DMSO-d_6, 25 °C): δ = -14.2 (s, *N*O_2) ppm. $^{13}C\{H\}$ NMR (DMSO-d_6, 25 °C): δ = 157.4 (s, *C*-NO_2), 138.1 (s, *C*H), 101.0 (s, *C*H) ppm. $^{1}H\{/\}$ NMR (DMSO-d_6, 25 °C): δ = 7.39 (d, 1H, C*H*), 6.64 (d, 1H, C*H*) ppm. EA ($LiC_3H_2N_3O_2$, 119.01): calcd. N 35.31, C 30.27, H 1.70; found N 35.38, C 30.22, H 1.75 %. DTA (5 °C min^{-1}): 332 (exothermic) °C.

2.1.3.2 Ageing effects

For the aging studies, 100 mg of the tested substance was weighed out twice, each from the same batch, in two different weighing dishes. The two samples were stored open on a laboratory bench at the same room conditions. One batch was weighed each day to track the weight progression and the other batch was photographed each day to record visual changes. From the batch, which was observed photographically, a certain amount of substance (10 mg) was removed after certain periods of time and analyzed via NMR or differential thermal analysis (DTA). This type of test for hydrolysis sensitivity/ageing of salts is the same for all compounds tested in the following report, unless stated otherwise. Although, usually pyrotechnics are stored in hermetically sealed containers, the aging studies performed are still significant enough to be considered as a go/no-go result, since the processing of pyrotechnics takes place under normal atmosphere.

The hygroscopic character of this lithium salt already showed after storage at room conditions for one day by a fading of the yellow color, a significant weight gain as well as by the occurrence of an endothermic signal in the DTA curve (see **Figure 1** and **Figure 2**).

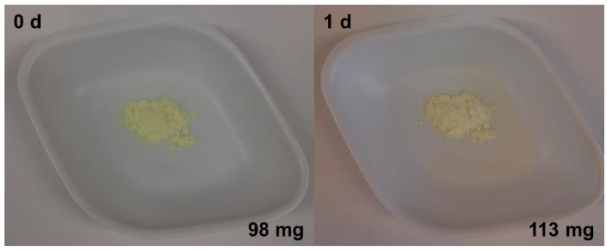

***Figure 1**: Color change and weight gain of a sample of lithium 3-nitropyrazolate after exposure to air for 0 or 1 days (from left to right).*

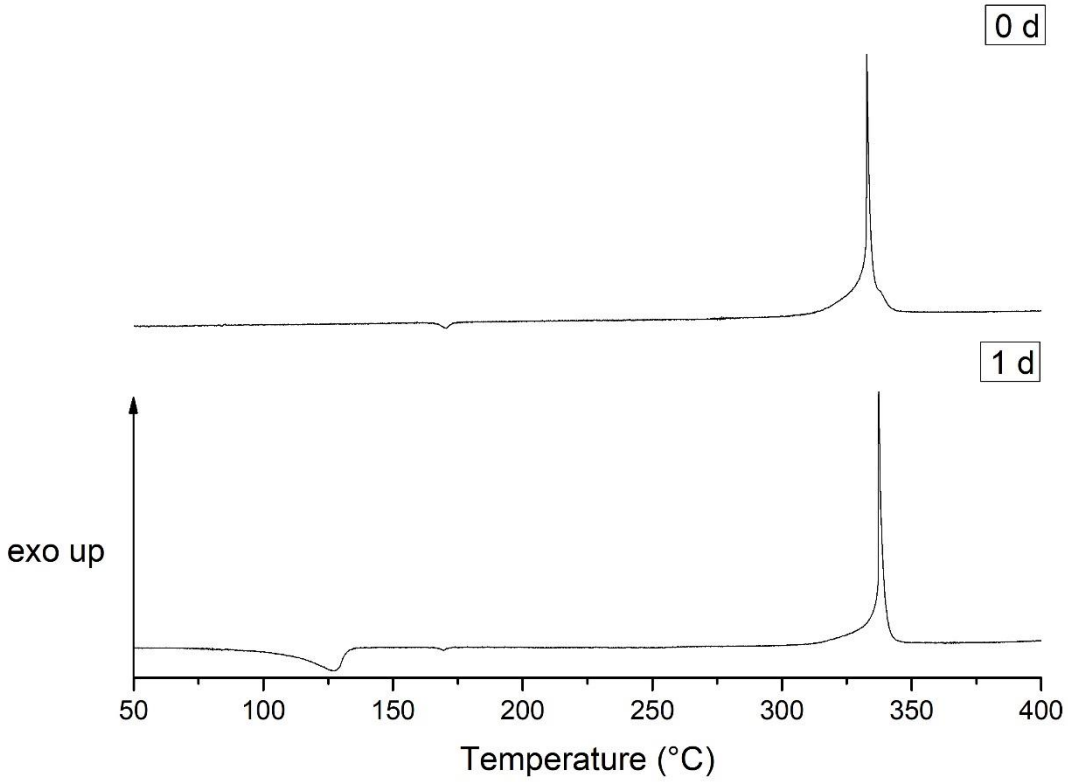

***Figure 2**: DTA curves of a freshly prepared sample of lithium 3-nitropyrazolate or after exposure to air for one day (from top to bottom).*

2.1.4 3,4-Dinitro-1*H*-pyrazole

The literature provides a protocol for the nitration of 3-nitro-1*H*-pyrazole to 3,4-dinitro-1*H*-pyrazole as well, however, no analytical data are reported (see **Scheme 4**).[6]

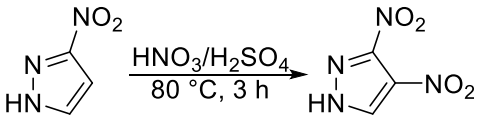

3 **5**

***Scheme 4**: Reaction toward 3,4-dinitro-1H-pyrazole (**5**).*

Fuming nitric acid (100 %, 2.2 mL) was added dropwise to a 0 °C cold solution of 3-nitro-1*H*-pyrazole (2.001 g, 18 mmol) in concentrated sulfuric acid (96 %, 3.3 mL) whereby the temperature of the nitration mixture was kept below 10 °C. Afterwards, the latter was allowed to warm to room temperature and subsequently refluxed at 80 °C for three hours before it was poured on 200 mL of ice-cold water, the aqueous solution was extracted three times with roughly 50 mL of diethyl ether each and the combined organic phases counterextracted twice with approximately 50 mL of bidistilled water each and once with 50 mL of a saturated sodium

chloride solution. After the organic layer had been dried over magnesium sulfate, it was stand for crystallisation to yield yellowish crystals (2.322 g, 83 %).

IR (ATR): $\tilde{\nu}$ = 3297(w), 3262(w), 3149(w), 3135(m), 2902(w), 1677(w), 1632(w), 1545(s), 1519(vs), 1447(m), 1414(w), 1370(s), 1340(s), 1280(s), 1235(m), 1182(w), 1154(w), 1092(m), 1064(m), 984(w), 934(w), 848(m), 805(vs), 805(vs), 755(m), 740(s), 607(m), 574(m), 505(w), 469(w), 443(w) cm^{-1}. $^{14}N\{H\}$ NMR (DMSO-d_6, 25 °C): δ = -25.7 (br s, NO_2) ppm. $^{13}C\{H\}$ NMR (DMSO-d_6, 25 °C): δ = 148.1 (s, C-NO_2), 132.7 (s, CH), 126.3 (s, C-NO_2) ppm. ^{1}H NMR (DMSO-d_6, 25 °C): δ = 14.86 (br s, 1H, NH), 9.11 (s, 1H, CH) ppm. EA ($C_3H_2N_4O_4$, 158.07): calcd. N 35.45, C 22.79, H 1.28 %; found N 34.98, C 23.12, H 1.25 %. DTA (5 °C min^{-1}): 65 (endothermic), 249 (exothermic) °C.

2.1.5 Lithium 3,4-dinitropyrazolate monohydrate

2.1.5.1 Procedure

Lithium 3,4-dinitropyrazolate monohydrate is accessible by reacting 3,4-dinitro-1*H*-pyrazole with lithium hydroxide (see **Scheme 5**).

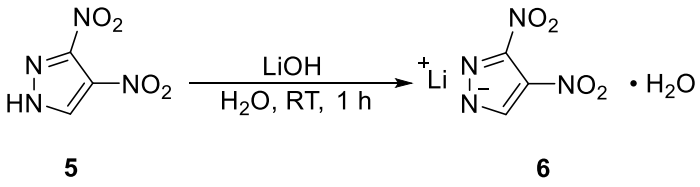

***Scheme 5**: Reaction toward lithium 3,4-dinitropyrazolate monohydrate (**6**).*

The saltification of 3,4-dinitro-1*H*-pyrazole (0.499 g, 3 mmol) with lithium hydroxide (0.077 g, 3 mmol) in roughly 5 mL of bidistilled water was allowed to proceed for one hour at room temperature before the solvent was removed *in vacuo* and the residue was recrystallized from approximately 60 mL 2-propanole. A brownish yellow solid (0.432 g, 75 %) was gained.

IR (ATR): $\tilde{\nu}$ = 3539(w), 3403(w), 3297(w), 3138(w), 1665(m), 1525(s), 1518(s), 1491(vs), 1433(m), 1397(m), 1376(vs), 1339(vs), 1286(s), 1165(s), 1118(m), 1097(m), 1085(m), 1069(m), 954(m), 937(w), 874(w), 854(s), 809(s), 809(s), 750(s), 673(w), 635(m), 609(m), 543(s), 493(s), 416(m) cm^{-1}. $^{1}H\{/\}$ NMR (DMSO-d_6, 25 °C): δ = 8.25 (s, 1H, CH), 4.02 (br s, 2H, H_2O) ppm. EA ($LiC_3H_3N_4O_5$, 182.02): calcd. N 30.78, C 20.63, H 1.66 %; found N 31.06, C 20.38, H 1.47 %. DTA (5 °C min^{-1}): 139 (endothermic), 232 (exothermic) °C. FS (100-500 µm): 240 N. IS (100-500 µm): 5 J.

2.1.5.2 Crystal structure

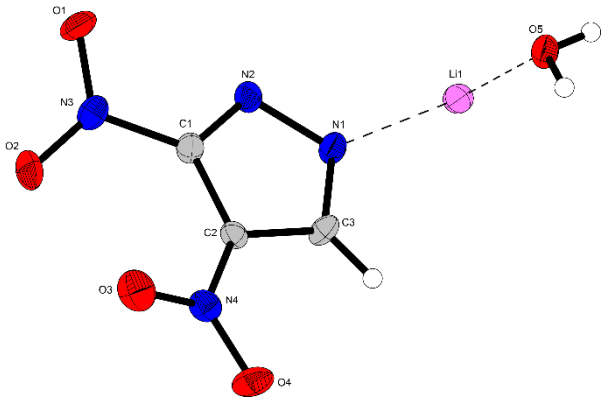

***Figure 3**: Crystal structure of lithium 3,4-dinitropyrazolate monohydrate (**6**).*

***Table 1**: Crystallographic data of lithium 3,4-dinitropyrazolate monohydrate (**6**).*

Formula	$LiC_3H_3N_4O_5$
FW [g mol^{-1}]	182.02
Crystal system	Monoclinic
Space Group	$P2_1/c$
Color / Habit	Yellowish block
Size [mm]	0.09 x 0.18 x 0.42
a [Å]	3.4643(3)
b [Å]	9.5834(6)
c [Å]	19.5933(14)
α [°]	90
β [°]	91.967(7)
γ [°]	90
V [Å^3]	650.11(8)
Z	4
$\rho_{calc.}$ [g cm^{-3}]	1.860
μ [mm^{-1}]	0.172
F(000)	368
$\lambda_{MoK\alpha}$ [Å]	0.71073
T [K]	108
θ Min–Max [°]	2.1, 24.7
Dataset	−4: 4; −11: 11; −23: 23
Reflections collected	7776
Independent refl.	1093
R_{int}	0.044
Observed reflections	973
Parameters	126
R_1 (obs)[a]	0.0776
wR_2 (all data)[b]	0.1912
GooF[c]	1.17
Resd. Dens. [e Å^{-3}]	−0.33, 0.60
Absorption correction	multi-scan

a) $R_1 = \Sigma||F_0|-|F_c||/\Sigma|F_0|$; b) $wR_2 = [\Sigma[w(F_0^2-F_c^2)^2]/\Sigma[w(F_0)^2]]^{1/2}$; $w = [\sigma c^2(F_0^2)+(xP)^2+yP]^{-1}$ and $P=(F_0^2+2F_c^2)/3$; c) GooF $= \{\Sigma[w(F_o^2-F_c^2)^2]/(n-p)\}^{1/2}$ (n = number of reflections; p = total number of parameters).

2.1.6 3,5-Dinitro-1*H*-pyrazole

The nitration of 3-nitro-1*H*-pyrazole to 1,3-dinitropyrazole and subsequent thermal rearrangement of the nitro group were performed as described in the literature (see **Scheme 6**).[6]

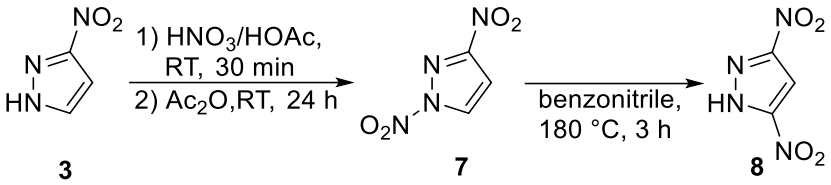

***Scheme 6**: Reaction toward 3,5-dinitro-1H-pyrazole (**8**).*

2.1.7 Lithium 3,5-dinitropyrazole monohydrate

2.1.7.1 Procedure

Lithium 3,5-dinitropyrazolate can already be found in the literature[8] but to the best of our knowledge its crystal structure was not elucidated so far. This moiety can be synthesized by the acid base reaction between the neutral compound and lithium hydroxide (see **Scheme 7**).

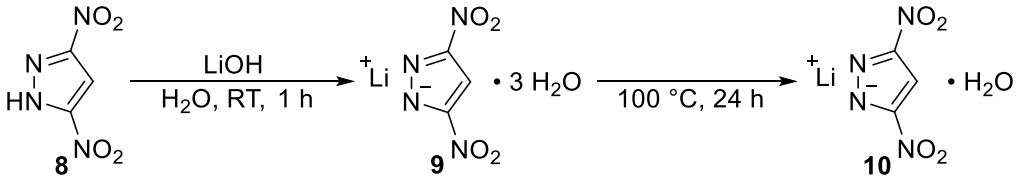

***Scheme 7**:Reaction toward lithium 3,5-dinitropyrazolate monohydrate (**10**).*

After lithium hydroxide (0.077 g, 3 mmol) had been added to a suspension of 3,5-dinitro-1*H*-pyrazole (0.501 g, 3 mmol), the reaction mixture was stirred at room temperature for one hour. Afterwards, the solution was filtered, the solvent removed from the filtrate *in vacuo* and the residue dried in an oven at 100 °C overnight to yield 0.492 g (85 %) of a yellowish powder.

IR (ATR): $\tilde{\nu}$ = 3547(m), 3458(w), 3335(w), 3201(w), 3159(m), 3145(m), 2812(vw), 2614(vw), 1651(w), 1537(s), 1513(m), 1478(s), 1445(s), 1349(vs), 1320(vs), 1284(m), 1276(m), 1202(m), 1185(m), 1075(w), 1019(m), 1000(m), 836(s), 836(s), 821(m), 750(s), 706(w), 668(w), 600(m), 591(m), 573(m), 510(w), 435(w) cm^{-1}. $^{7}Li\{H\}$ NMR (DMSO-d_6, 25 °C): δ = -1.0 (s, *Li*) ppm. $^{14}N\{H\}$ NMR (DMSO-d_6, 25 °C): δ = -16.6 (br s, *N*O_2) ppm. $^{13}C\{H\}$ NMR (DMSO-d_6, 25 °C): δ = 155.5 (s, *C*-NO_2), 98.7 (s, *C*H) ppm. $^{1}H\{/\}$ NMR (DMSO-d_6, 25 °C): δ = 7.41 (s, 1H, C*H*), 4.28 (br s, 2H, H_2O) ppm. EA ($LiC_3H_3N_4O_5$, 182.02): calcd. N 30.78, C 19.79, H 1.66 %; found N 30.03, C 19.48, H 2.11 %. DTA (5 °C min^{-1}): 77 (endothermic), 162 (endothermic), 284 (exothermic) °C. FS (100-500 µm): 192 N. IS (100-500 µm): 6 J.

2.1.7.2 Crystal structure

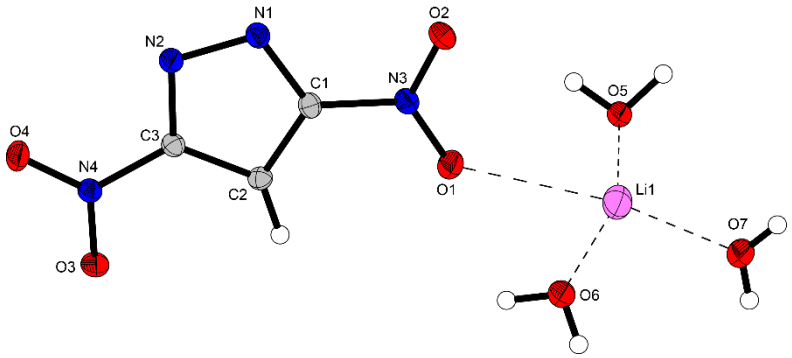

***Figure 4**: Crystal structure of lithium 3,5-dinitropyrazolate trihydrate (**9**).*

***Table 2**: Crystallographic data of lithium 3,5-dinitropyrazolate trihydrate (**9**).*

Formula	$LiC_3H_7N_4O_7$
FW [g mol^{-1}]	218.05
Crystal system	Monoclinic
Space Group	$P2_1/n$
Color / Habit	Colorless needle
Size [mm]	0.08 x 0.25 x 0.40
a [Å]	3.3560(2)
b [Å]	17.3695(9)
c [Å]	14.1549(9)
α [°]	90
β [°]	91.900(6)
γ [°]	90
V [Å^3]	824.66(8)
Z	4
$\rho_{calc.}$ [g cm^{-3}]	1.756
μ [mm^{-1}]	0.168
F(000)	448
$\lambda_{MoK\alpha}$ [Å]	0.71073
T [K]	123
θ Min–Max [°]	1.9, 32.3
Dataset	−5: 5; −25: 25; −21: 20
Reflections collected	16785
Independent refl.	2786
R_{int}	0.035
Observed reflections	2204
Parameters	160
R_1 (obs)[a]	0.0380
wR_2 (all data)[b]	0.1070
GooF[c]	1.05
Resd. Dens. [e Å^{-3}]	−0.22, 0.43
Absorption correction	multi-scan

a) $R_1 = \Sigma||F_0|-|F_c||/\Sigma|F_0|$; b) $wR_2 = [\Sigma[w(F_0^2-F_c^2)^2]/\Sigma[w(F_0)^2]]^{1/2}$; $w = [\sigma c^2(F_0^2)+(xP)^2+yP]^{-1}$ and $P=(F_0^2+2F_c^2)/3$; c) GooF = $\{\Sigma[w(F_o^2-F_c^2)^2]/(n-p)\}^{1/2}$ (n = number of reflections; p = total number of parameters).

2.1.8 4-Amino-3,5-dinitro-1*H*-pyrazole

The title compound was synthesized according to a literature-known procedure (see **Scheme 8**).[9]

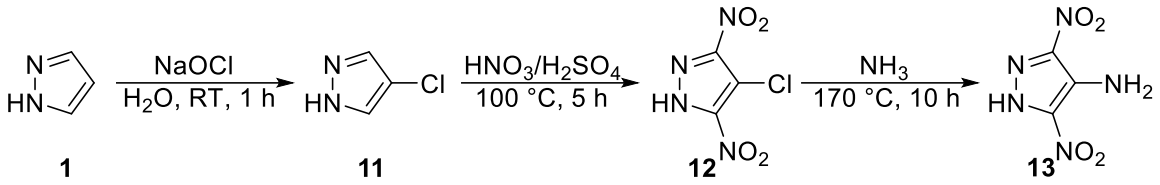

***Scheme 8**: Reaction toward 4-amino-3,5-dinitro-1H-pyrazole (**13**).*

2.1.9 Lithium 4-amino-3,5-dinitropyrazolate sesquihydrate

2.1.9.1 Procedure

This material as well was gained by deprotonation of the neutral compound by lithium hydroxide (see **Scheme 9**).

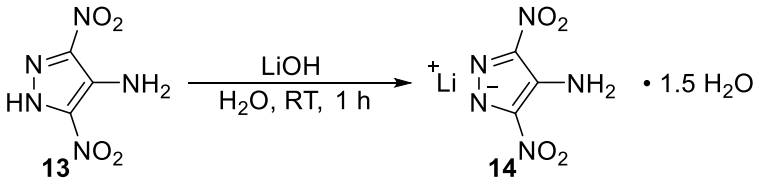

***Scheme 9**:Reaction toward lithium 4-amino-3,5-dinitropyrazolate sesquihydrate (**14**).*

A mixture of 4-amino-3,5-dinitro-1*H*-pyrazole (0.501 g, 3 mmol) and lithium hydroxide (0.068 g, 3 mmol) in roughly 5 mL of bidistilled water was reacted at room temperature for one hour. After filtering off unreacted starting material the solvent was removed from the filtrate *in vacuo* and the residue was recrystallized from approximately 5 mL of ethanol. This procedure led to an orange-yellow powder (0.311 g, 52 %).

IR (ATR): $\tilde{\nu}$ = 3517(w), 3436(m), 3324(s), 3182(m), 1639(s), 1578(w), 1509(w), 1466(s), 1427(s), 1303(vs), 1287(vs), 1257(s), 1233(s), 1208(s), 1146(m), 928(m), 842(m), 829(s), 758(m), 724(w), 674(w), 648(w), 551(w), 551(w), 528(m), 498(m), 465(w), 434(m), 427(m), 414(m) cm^{-1}. $^{7}Li\{H\}$ NMR (DMSO-d_6, 25 °C): δ = -1.0 (s, *Li*) ppm. $^{14}N\{H\}$ NMR (DMSO-d_6, 25 °C): δ = -20.4 (br s, *N*O_2) ppm. $^{13}C\{H\}$ NMR (DMSO-d_6, 25 °C): δ = 142.8 (s, *C*-NO_2), 131.5 (s, *C*-NH_2) ppm. $^{1}H\{/\}$ NMR (DMSO-d_6, 25 °C): δ = 6.68 (br s, 2H, NH_2), 3.65 (br s, 3H, H_2O) ppm. EA ($LiC_3H_5N_5O_{5.5}$, 206.04): calcd. N 33.99, C 17.49, H 2.45 %; found N 34.27, C 17.79, H 2.31 %. DTA (5 °C min^{-1}): 69 (endothermic), 132 (endothermic), 168 (exothermic) °C. FS (100-500 µm): 360 N. IS (100-500 µm): > 40 J.

2.1.9.2 Crystal structure

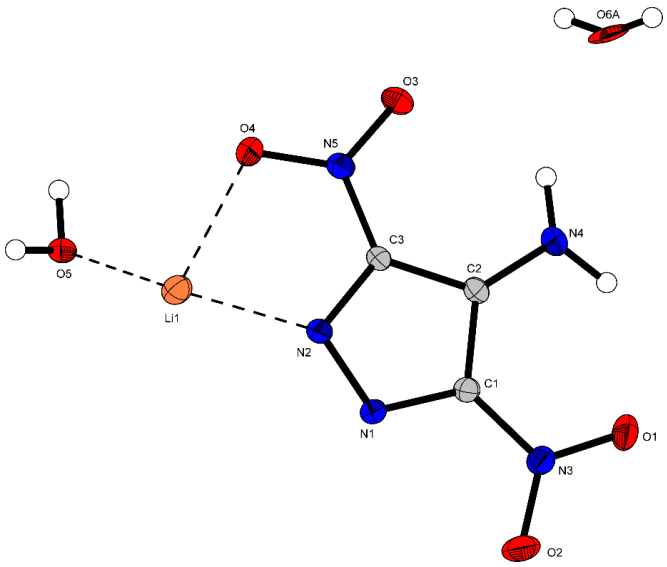

***Figure 5**: Crystal structure of lithium 4-amino-3,5-dinitropyrazolate sesquihydrate (**14**).*

***Table 3**: Crystallographic data of lithium 4-amino-3,5-dinitropyrazolate sesquihydrate (**14**).*

Formula	$LiC_3H_5N_5O_{5.5}$
FW [g mol^{-1}]	206.04
Crystal system	Triclinic
Space Group	*P*-1
Color / Habit	Yellow rod
Size [mm]	0.05 x 0.05 x 0.50
a [Å]	3.4057(2)
b [Å]	9.1857(5)
c [Å]	12.3747(7)
α [°]	87.979(4)
β [°]	86.748(4)
γ [°]	85.699(4)
V [Å^3]	385.23(4)
Z	1
$\rho_{calc.}$ [g cm^{-3}]	1.776
μ [mm^{-1}]	0.164
F(000)	210
$\lambda_{MoK\alpha}$ [Å]	0.71073
T [K]	110
θ Min–Max [°]	2.2, 32.3
Dataset	−5: 3; −13: 10; −17: 18
Reflections collected	3811
Independent refl.	2503
R_{int}	0.027
Observed reflections	1900
Parameters	162
R_1 (obs)[a]	0.0537
wR_2 (all data)[b]	0.1750
GooF[c]	1.13
Resd. Dens. [e Å^{-3}]	−0.42, 0.69
Absorption correction	multi-scan

a) $R_1 = \Sigma||F_0|-|F_c||/\Sigma|F_0|$; b) $wR_2 = [\Sigma[w(F_0^2-F_c^2)^2]/\Sigma[w(F_0)^2]]^{1/2}$; $w = [\sigma c^2(F_0^2)+(xP)^2+yP]^{-1}$ and $P=(F_0^2+2F_c^2)/3$; c) GooF = $\{\Sigma[w(F_o^2-F_c^2)^2]/(n-p)\}^{1/2}$ (n = number of reflections; p = total number of parameters).

2.1.10 3,4,5-Trinitro-1*H*-pyrazole

3,4,5-Trinitro-1*H*-pyrazole was prepared as stated in the literature (see **Scheme 10**).[10]

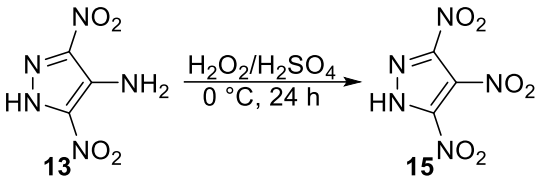

***Scheme 10**: Reaction toward 3,4,5-trinitro-1H-pyrazole (**15**).*

2.1.11 Lithium 3,4,5-trinitropyrazolate trihydrate

2.1.11.1 Procedure

Although lithium 3,4,5-trinitropyrazolate was synthesized as described in the literature[8] (see **Scheme 11**), according to elemental analysis a trihydrate instead of a tetrahydrate was obtained. Also, after the recrystallization with ethanol, the monohydrate form was found. This result suggests that several different hydrate forms might exist.

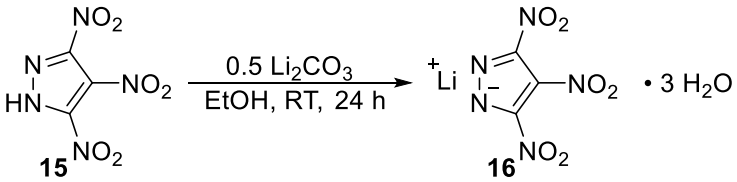

***Scheme 11**: Reaction toward lithium 3,4,5-trinitropyrazolate trihydrate (**16**).*

The metathesis reaction between 3,4,5-trinitro-1*H*-pyrazole (250 mg, 1.23 mmol) and the stoichiometric amount of lithium carbonate (45.5 mg, 0.616 mmol) in ethanol (10 mL) was allowed to proceed at room temperature overnight. Evaporation of the solvent yielded a yellow-brown solid (205 mg, 63 %).

IR (ATR): $\tilde{\nu}$ = 3621(m), 3583(m), 3515(m), 3463(w), 3427(w), 3346(m), 3211(m), 2846(w), 2759(vw), 2631(vw), 1667(m), 1628(w), 1568(w), 1541(s), 1520(vs), 1490(m), 1457(s), 1412(m), 1353(vs), 1341(s), 1325(vs), 1309(s), 1299(s), 1299(s), 1199(w), 1174(w), 1134(m), 1108(m), 1026(w), 1011(w), 849(vs), 806(m), 763(m), 749(m), 680(w), 664(vw), 607(m), 489(m), 455(m), 418(vw), 406(vw) cm^{-1}. $^{13}C\{H\}$ NMR (DMSO-d_6, 25 °C): δ = 147.4 (s, *C*-NO_2), 133.5 (s, *C*-NO_2) ppm. ^{1}H NMR (DMSO-d_6, 25 °C): δ = 3.33 (br s, 6H H_2O) ppm. EA ($LiC_3H_6N_5O_9$, 263.05): calcd. N 26.63, C 13.70, H 2.30 %; found N 25.30, C 14.09, H 2.43 %. DTA (5 °C min^{-1}): 192 (endothermic), 250 (exothermic) °C.

For the monohydrate, we found that this salt is highly hygroscopic as it can be seen from differential thermal analysis of a freshly prepared sample and one exposed to air over night (see **Figure 6**).

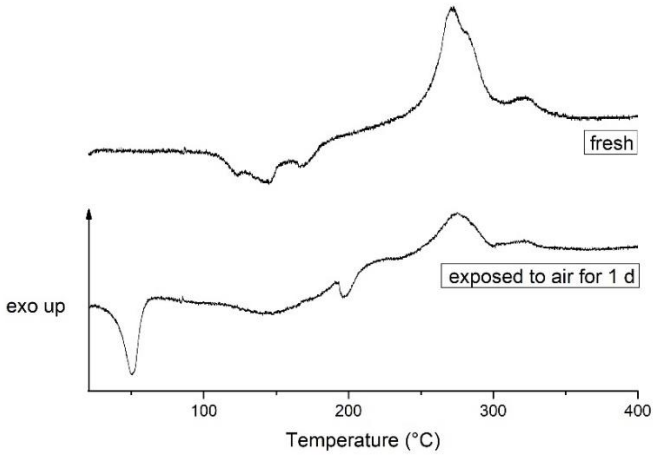

***Figure 6**: DTA plots of lithium 3,4,5-trinitropyrazolate • H_2O from top to bottom directly after synthesis and after storage at ambient conditions for one day.*

2.1.11.2 Crystal structure

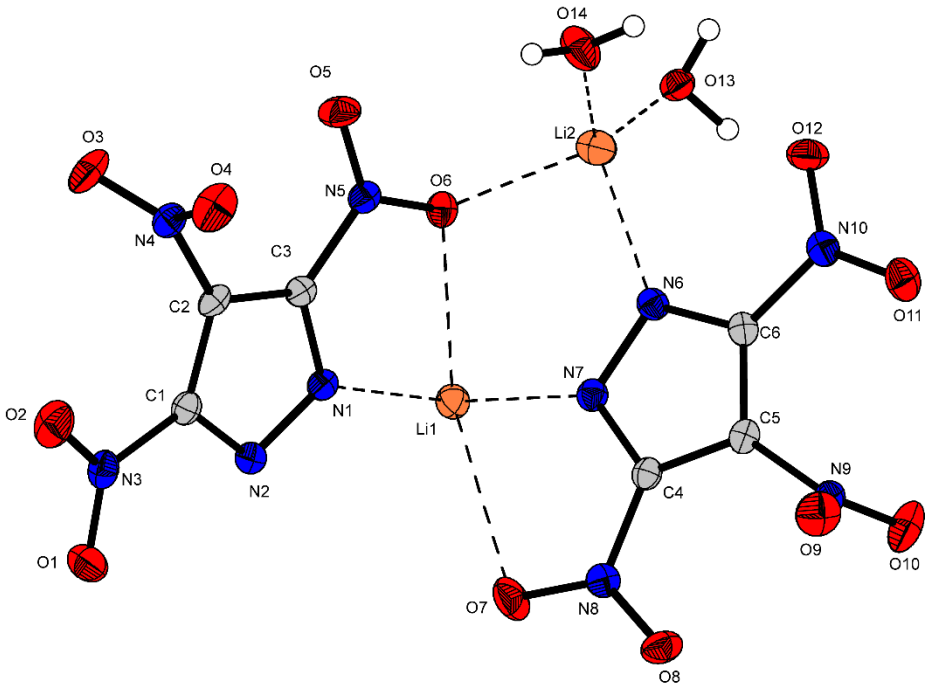

***Figure 7**: Crystal structure of lithium 3,4,5-trinitropyrazolate monohydrate.*

***Table 4**: Crystallographic data of lithium 3,4,5-trinitropyrazolate monohydrate.*

Formula	$LiC_3H_2N_5O_7$
FW [g mol^{-1}]	227.02
Crystal system	Monoclinic
Space Group	$P2_1/n$
Color / Habit	Yellow block
Size [mm]	0.34 x 0.39 x 0.63
a [Å]	9.3009(4)
b [Å]	19.8282(6)
c [Å]	9.5957(4)
α [°]	90
β [°]	114.836(5)
γ [°]	90
V [Å^3]	1605.97(13)
Z	4
$\rho_{calc.}$ [g cm^{-3}]	1.878
μ [mm^{-1}]	0.181
F(000)	912
$\lambda_{MoK\alpha}$ [Å]	0.71073
T [K]	108
θ Min–Max [°]	2.1, 26.4
Dataset	−8: 11; −24: 23; −11: 11
Reflections collected	8606
Independent refl.	3278
R_{int}	0.021
Observed reflections	2813
Parameters	303
R_1 (obs)[a]	0.0305
wR_2 (all data)[b]	0.0749
GooF[c]	1.04
Resd. Dens. [e Å^{-3}]	−0.25, 0.30
Absorption correction	multi-scan

a) $R_1 = \Sigma||F_0|-|F_c||/\Sigma|F_0|$; b) $wR_2 = [\Sigma[w(F_0^2-F_c^2)^2]/\Sigma[w(F_0)^2]]^{1/2}$; $w = [\sigma c^2(F_0^2)+(xP)^2+yP]^{-1}$ and $P=(F_0^2+2F_c^2)/3$; c) GooF = $\{\Sigma[w(F_o^2-F_c^2)^2]/(n-p)\}^{1/2}$ (n = number of reflections; p = total number of parameters).

2.1.12 Lithium tetrazolate

Lithium tetrazolate was prepared according to the literature[11] (see **Scheme 12**).

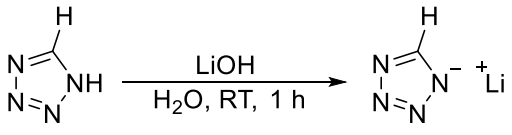

17 **18**

***Scheme 12**: Reaction toward lithium tetrazolate (**18**).*

2.1.13 Lithium 5-aminotetrazolate

The lithium salt of 5-aminotetrazole was prepared according to literature[12] (see **Scheme 13**).

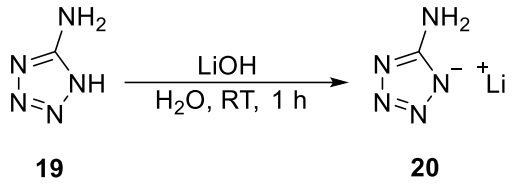

19 **20**

***Scheme 13**: Reaction toward lithium 5-aminotetrazolate (**20**).*

2.1.14 4,5-Dihydro-5-(nitrimino)-1*H*-tetrazole

This heterocycle was synthesized by a combination of the reported procedures[13,14,15] (see **Scheme 14**).

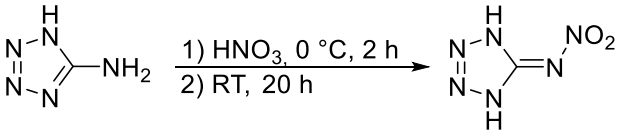

19 **21**

***Scheme 14**: Reaction toward 4,5-dihydro-5-(nitrimino)-1H-tetrazole (**21**).*

5-Amino-1*H*-tetrazole (3.40 g, 40 mmol, 1 eq.) was added in small portions to ice-cooled HNO_3 (100 %, 12 mL, 288 mmol, 7 eq.) and the suspension was stirred for two hours at 0 °C. After the ice bath had been removed, the nitration mixture was stirred for further 20 hours at room temperature. Afterwards it was poured onto ice (20 mL). The resulting solution was neutralized with calcium hydroxide keeping the temperature below 10 °C before it was heated at 80 °C for 30 minutes. Calcium 5-nitraminotetrazolate pentahydrate (3.87 g, 15 mmol) was filtered off, suspended in water (25 mL) and half-concentrated hydrochloric acid (18.5 %, 10 mL) was added. The reaction mixture was heated at 100 °C until all reactants dissolved and the cool solution was evaporated to dryness. The residue was recrystallized from water (50 mL) and ether (50 mL) to yield 4,5-dihydro-5-(nitrimino)-1*H*-tetrazole (2.60 g, 20 mmol, 50 %) as yellowish solid.

IR (ATR): $\tilde{\nu}$ = 3205(w), 3074(w), 2929(m), 2861(m), 2787(m), 2671(m), 2156(w), 2145(w), 1707(w), 1606(s), 1500(s), 1459(m), 1450(m), 1404(m), 1378(m), 1308(vs), 1218(vs), 1131(m), 1051(s), 1019(s), 993(s), 876(s), 778(s), 778(s), 752(m), 705(s), 645(s), 476(s), 405(w) cm^{-1}. $^{14}N\{H\}$ NMR (DMSO-d_6, 25 °C): δ = 23.7 (br s, NO_2) ppm. $^{13}C\{H\}$ NMR (DMSO-d_6, 25 °C): δ = 152.7 (s, *C*-N) ppm. EA ($CH_2N_6O_2$, 130.02): calcd. N 64.61, C 9.23, H 1.55 %; found N 63.64, C 9.55, H 1.80 %. DTA (5 °C min^{-1}): 60 (endothermic), 120 (exothermic) °C.

2.1.15 Lithium 5-nitriminotetrazolate monohydrate

The lithium salt of 4,5-dihydro-5-(nitrimino)-1*H*-tetrazole was prepared according to the literature[16] (see **Scheme 15**), however, lithium hydroxide was used as lithium source instead of lithium carbonate. Furthermore, *Vasiliev* et al. do not provide any analytical data for the title compound other than a crystal structure.

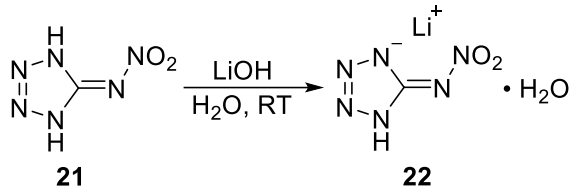

***Scheme 15**: Reaction toward lithium 5-nitriminotetrazolate · H_2O (**22**).*

4,5-Dihydro-5-(nitrimino)-1*H*-tetrazole (131 mg, 1 mmol, 1 eq.) was dissolved in water (5 mL), lithium hydroxide (24 mg, 1 mmol, 1 eq.) was added and the reaction mixture was stirred at ambient temperature until complete dissolution. The solution was transferred to a crystallization bowl to yield lithium 5-nitriminotetrazolate · H_2O (144 mg, 1 mmol, 93 %) as yellowish solid.

IR (ATR): $\tilde{\nu}$ = 3453(m), 3204(m), 3008(m), 2153(w), 1700(w), 1560(s), 1447(s), 1366(s), 1335(vs), 1239(s), 1158(m), 1101(m), 1056(vs), 1034(s), 1007(s), 886(w), 846(s), 783(m), 769(s), 740(s), 663(m), 544(s), 492(m), 492(m), 417(m) cm^{-1}. ^{7}Li NMR (DMSO-d_6, 25 °C): δ = -1.0 (s, *Li*) ppm. ^{14}N NMR (DMSO-d_6, 25 °C): δ = -26.7 (br s, *N*O_2) ppm. ^{13}C{H} NMR (DMSO-d_6, 25 °C): δ = 157.8 (s, *C*-N) ppm. ^{1}H NMR (DMSO-d_6, 25 °C): δ = 3.38 (br s, 2H, *H*$_2$O) ppm. EA ($CH_3N_6O_3Li$, 154.04): calcd. N 54.57, C 7.80, H 1.96 %; found N 54.40, C 7.84, H 1.90 %. DTA (5 °C min^{-1}): 164 (endothermic), 240 (exothermic) °C.

2.1.16 Dilithium 5,5`-bistetrazolate dihydrate

2.1.16.1 Synthesis approach 1

In the first synthesis approach we tried to prepare the title compound via the neutral compound. Therefor we used a combination of two reported procedures[17,18] (see **Scheme 16**).

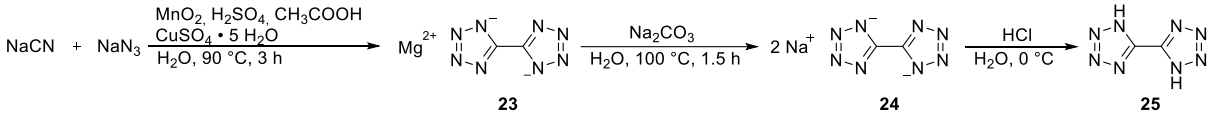

***Scheme 16**: Synthesis toward the neutral compound 5,5`-bistetrazole (**25**).*

Manganese dioxide (10.9 g, 125 mmol) was added to a mixture of sodium azide (13.0 g, 200 mmol) and sodium cyanide (9.99 g, 204 mmol) in water (120 mL), which was stirred and cooled by an ice bath. The resulting suspension was mixed with a solution of concentrated sulfuric acid (10.9 mL, 203 mmol), glacial acetic acid (15.3 mL, 268 mmol) and copper(II) sulfate pentahydrate (0.325 g, 1.30 mmol) in water (50 mL) maintaining a temperature of 20 to 30 °C. After heating to 90 °C over one hour and holding the temperature between 90 and 95 °C for 3 hours, the mixture was cooled to room temperature and manganese 5,5'-bistetrazolate was filtered off. The metathesis reaction between the latter and sodium carbonate (15.6 g, 147 mmol) in water (200 mL) was allowed to proceed for 1.5 hours under boiling, before manganese carbonate was filtered off and washed with hot water (200 mL). The filtrate was neutralized with concentrated hydrochloric acid (18 mL). The volume of the solution was reduced to a maximum of 150 mL and cooled to 0 °C and the thus formed precipitate was filtered off and recrystallized from water to yield 5,5'-bis-1*H*-tetrazole (12.0 g, 43 %) in the form of white flakes.

The following reaction towards the lithium salt was prepared according to the literature[19] (see **Scheme 17**), however the described work-up does not lead to a sufficiently pure product. The reason for the insufficient purity was the sodium chloride as impurity from the previous neutralization of the sodium salt with hydrochloric acid, which could not be removed during salinization with lithium hydroxide.

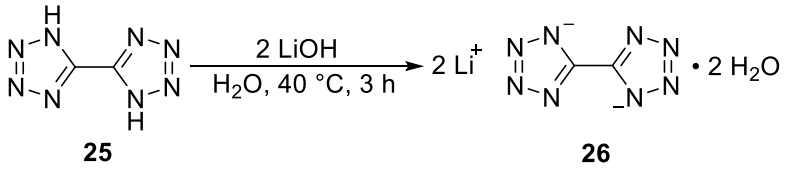

***Scheme 17**: Reaction toward dilithium 5,5'-bistetrazolate dihydrate (**26**).*

2.1.16.2 Synthesis approach 2

The resulting problem in the previous synthetical approach could be solved by converting disodium 5,5`-bistetrazolate to the respective diammonium salt. The latter was used as starting material to form the lithium salt (see **Scheme 18**).

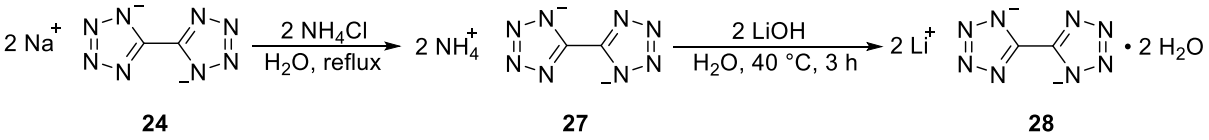

24 **27** **28**

***Scheme 18**: Reaction toward dilithium 5,5`-bistetrazole dihydrate (**26**) over the respective diammonium salt (**27**).*

A solution of ammonium chloride (32.10 g, 0.6 mol, 1 eq.) in water (150 mL) was added to a suspension of disodium bistetrazolate (109.20 g, 0.6 mol, 1 eq.) in hot water (200 mL). The resulting reaction mixture was cooled in a freezer at 4 °C overnight. The formed solid was filtered off and washed with a small amount of cold water (50 mL) and ethanol (300 mL) to yield diammonium 5,5`-bistetrazolate (33.81 g, 0.2 mol) as white solid. After the addition of diammonium 5,5`-bistetrazolate (2.00 g, 12 mmol, 1 eq.) to a solution of lithium hydroxide (0.56 g, 23 mmol, 2 eq.) in water (50 mL), the reaction was heated at 40 °C under nitrogen flow for three hours. Afterwards, the solvent was allowed to evaporate and dilithium 5,5`-bistetrazole · 2 H_2O (2.08 g, 11 mmol, 96 %) was obtained as greenish solid.

IR (ATR): $\tilde{\nu}$ = 3101(m), 1344(s), 1317(m), 1213(s), 1169(m), 1066(m), 1033(s), 798(s), 731(s), 715(vs), 476(m), 462(m) cm^{-1}.^{7}Li NMR (DMSO-d_6, 25 °C): δ = -0.4 (s) ppm. ^{13}C{H} NMR (DMSO-d_6, 25 °C): δ = 155.6 (s, *C*-N) ppm. ^{1}H NMR (DMSO-d_6, 25 °C): δ = 3.44 (br s, 4H, H_2O) ppm. EA ($C_2H_4N_8O_2Li_2$, 185.99): calcd. N 60.25, C 12.92, H 2.17 %; found N 60.67, C 12.79, H 2.23 %. DTA (5°C min^{-1}): 187 °C (endothermic), 444 °C (exothermic). FS (< 100 µm): > 360 N. IS (< 100 µm): > 40 J.

2.1.17 Dilithium 5,5`-bis(tetrazole-1-oxide) tetrahydrate

The target moiety was synthesized according to literature[20], but its low purity did not allow for measuring the combustion parameters. For this reason, lithium carbonate was used as a base instead of lithium hydroxide, whereby highly pure dilithium 5,5'-bis(tetrazole-1-oxide) • 4 H_2O could be obtained (see **Scheme 19**).

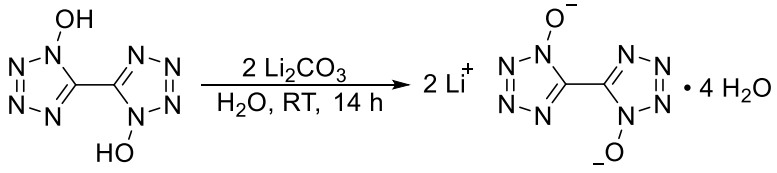

29 **30**

***Scheme 19**: Reaction toward dilithium 5,5`-bis(tetrazole-1-oxide) • 4 H_2O (**30**).*

5,5`-bis(tetrazole-1-oxide) (0.51 g, 3 mmol, 1 eq.) was dissolved in water (7 mL). After the acid base reaction with lithium carbonate (0.24 g, 3 mmol, 1 eq.) had been allowed to proceed for 14 hours at room temperature, the solvent was evaporated. Dilithium 5,5`-bis(tetrazole-1-oxide) · 4 H_2O (0.68 g, 3 mmol, 89 %) was obtained in the form of colorless crystals.

IR (ATR): $\tilde{\nu}$ = 3535(m), 3292(s), 1664(m), 1430(vs), 1416(vs), 1367(s), 1241(s), 1180(s), 1063(m), 1008(m), 859(m), 740(m), 700(w), 611(w), 497(m), 475(m), 416(s) cm^{-1}. ^{7}Li NMR (DMSO-d_6, 25 °C): δ = -0.4 (s) ppm. ^{13}C{H} NMR (DMSO-d_6, 25 °C): δ = 134.7 (s, *C*-N) ppm. ^{1}H NMR (DMSO-d_6, 25 °C): δ = 3.37 (br s, 8H, H_2O) ppm. EA ($C_2H_8N_8O_6Li_2$, 254.02): calcd. N 44.11, C 9.46, H 3.17 %; found N 43.99, C 9.27, H 3.09 %. DTA (5°C min^{-1}): 107 °C (endothermic), 179 °C (endothermic), 327 °C (exothermic), 366°C (exothermic). FS (< 100 µm): > 360 N. IS (< 100 µm): > 40 J.

2.1.18 Dilithium 4,6-bis(nitrimino-1,3,5-triazinan)-2-one • 3.5 H_2O

The neutral compound of the titled lithium salt was prepared according to literature[21]. The following acid base reaction of 4,6-bis(nitrimino-1,3,5-triazinan)-2-one (250 mg, 1 mmol, 1 eq.) with lithium carbonate (85 mg, 1 mmol, 1 eq.) in hot water (5 mL) was allowed to proceed until no more release of carbon dioxide was observed. Dilithium 4,6-bis(nitrimino-1,3,5-triazinan)-2-one · 3.5 H_2O was obtained as white powder in quantitative yield (336 mg, 1 mmol, 100 %) (see **Scheme 20**).

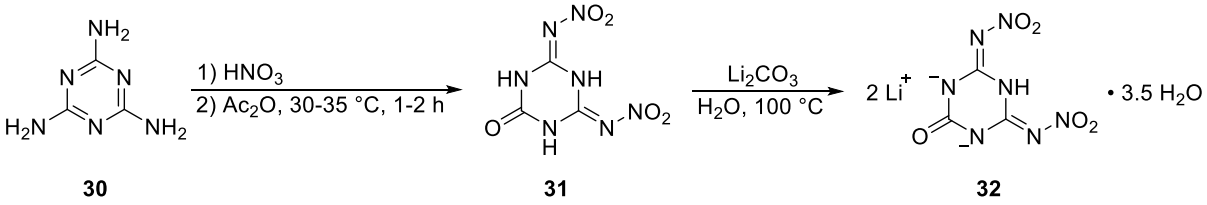

Scheme 20: *Reaction toward dilithium 4,6-bis(nitrimino-1,3,5-triazinan)-2-one • 3.5 H2O (**32**).*

IR (ATR): $\tilde{\nu}$ = 3181 (m), 1741 (w), 1657 (m), 1532 (s), 1447 (m), 1391 (m), 1269 (s), 1237 (vs), 1178 (vs), 1147 (vs), 1061 (s), 1026 (s), 950 (m), 814 (m), 785 (s), 774 (s), 717 (s), 622 (s), 530 (s), 463 (vs), 446 (vs), 443 (vs), 412 (vs) cm^{-1}. ^{7}Li NMR (DMSO-d_6, 25 °C): δ = 1.9 (s, *Li*) ppm. ^{14}N NMR (DMSO-d_6, 25 °C): δ = -10.3 (br s, NO_2) ppm. ^{13}C{H} NMR (DMSO-d_6, 25 °C): δ = 157.1 (s, *C*=O) ppm. ^{1}H NMR (DMSO-d_6, 25 °C): δ = 10.95 (br s, 1H, N*H*), 3.41 (br s, 7H, H_2O) ppm. EA ($C_3H_8N_7O_{8.5}Li_2$, 292.02): calcd. N 33.58, C 12.34, H 2.76 %; found N 32.86, C 12.11, H 2.84 %. DTA (5 °C min^{-1}): 59 (endothermic), 101 (endothermic), 123 (endothermic), 189 (endothermic), 220 (exothermic) °C.

Although the elemental analysis suggests a value of 3.5 water, this number could not be confirmed because no crystal structure could be obtained.

2.1.19 Lithium picramate sesquihydrate

2.1.19.1 Procedure

Picramic acid was obtained by synthesizing the sodium salt according to literature[22] and subsequent acidification (see **Scheme 21**).

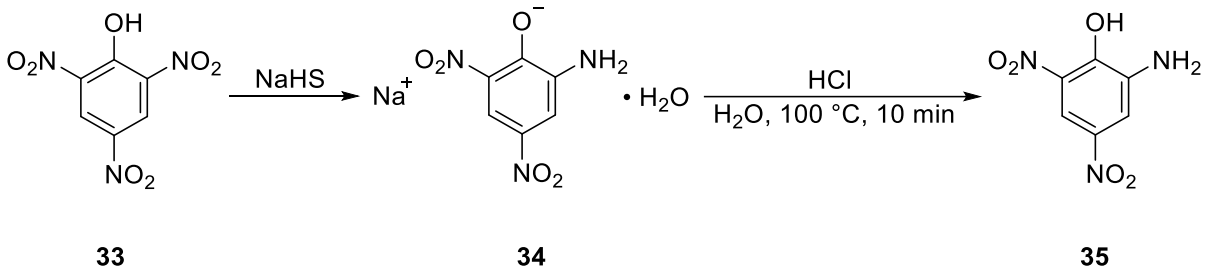

***Scheme 21**: Reaction toward picramic acid (**35**).*

An aqueous solution (200 mL) of sodium picramate monohydrate (1.00 g, 4 mmol, 1 eq.) was heated to 100 °C and acidified with hydrochloric acid (2M, 10 mL). After stirring for 10 minutes, the mixture was extracted three times with toluene (200 mL each) and the combined organic phases were dried over magnesium sulfate. The solvent was removed *in vacuo* to obtain picramic acid (0.68 g, 3 mmol, 82 %) as a red solid.

IR (ATR): $\tilde{\nu}$ = 3375 (m), 3121 (w), 3106 (m), 2925 (w), 1783 (w), 1739 (w), 1634 (w), 1615 (m), 1594 (m), 1549 (s), 1512 (s), 1440 (m), 1402 (w),1331 (vs), 1300 (vs), 1231 (s), 1139 (s), 1108 (s), 1063 (s), 993 (s), 933 (m), 894 (m), 879 (s), 854 (m), 814 (m), 804 (m), 770 (m), 735 (m), 709 (s), 668 (s) cm^{-1}. EA ($C_6H_5N_3O_5$, 199.12): calcd. N 21.10, C 36.19, H 2.53 %; found N 20.91, C 35.96, H 2.52 %. DTA (5°C min^{-1}): 175 °C (endothermic), 217 °C (exothermic). FS (< 100 µm): > 360 N. IS (< 100 µm): > 40 J. ESD (< 100 µm): 840 mJ.

The following acid-base reaction toward the titled compound is shown in **Scheme 22**.[23]

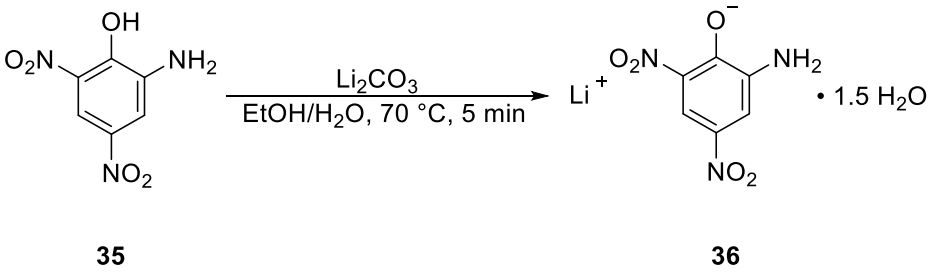

***Scheme 22**: Reaction toward lithium picramate sesquihydrate (**36**).*

Under heating at 70 °C, picramic acid (100 mg, 0.5 mmol, 1 eq.) was dissolved in ethanol (10 mL) and stirred for 5 minutes. An aqueous solution (10 mL) of lithium carbonate (19 mg, 0.3 mmol, 1 eq.) was slowly added, it was further stirred for 5 minutes and the reaction mixture left on air for crystallization. The alkali picramate was obtained as red single crystals (84 mg, 0.4 mmol, 72 %).

IR (ATR): $\tilde{\nu}$ = 3544 (w), 3457 (m), 3450 (m), 3411 (m), 3374 (m), 3315 (m), 3270 (m), 3260 (m), 3099 (m), 3082 (m), 1742 (vw), 1651 (w), 1591 (m), 1538 (s), 1532 (s), 1478 (s), 1425 (m), 1350 (s), 1319 (s), 1279 (vs), 1251 (vs), 1194 (s), 1145 (m), 1145 (m), 1077 (m), 996 (w), 938 (w), 895 (m), 871 (m), 824 (w), 804 (w) cm^{-1}. EA ($C_6H_7N_3O_{6.5}Li$, 232.08): calcd. N 18.11, C 31.05, H 3.04 %; found N 17.89, C 30.99, H 2.88 %. DTA (5 °C min^{-1}): 105 °C (endothermic), 295 °C (exothermic). FS (< 100 µm): > 360 N. IS (< 100 µm): > 40 J. ESD (< 100 µm): 1080 mJ.

2.1.19.2 Crystal structure

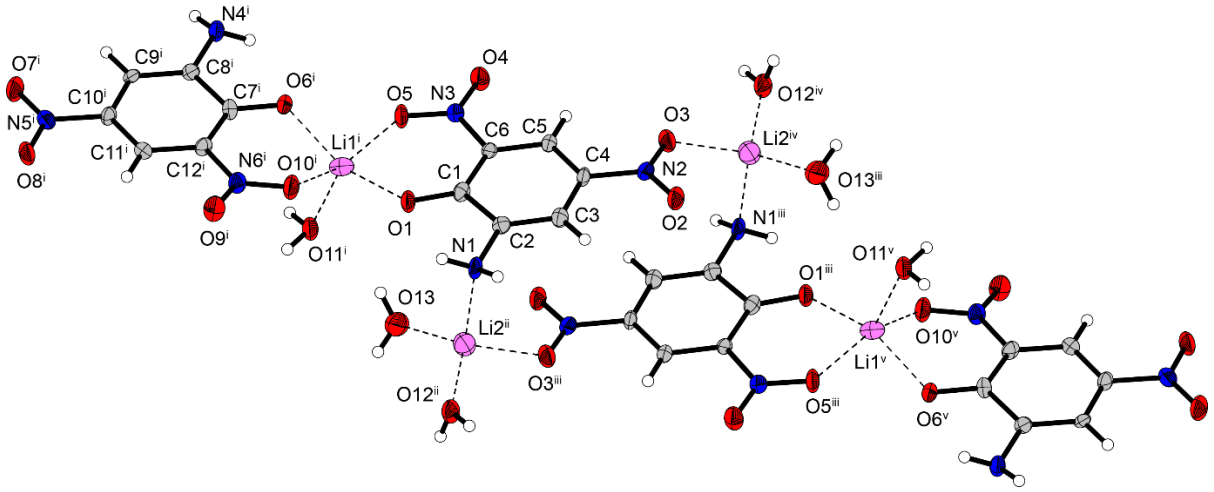

***Figure 8**: Dimer of lithium picramate · 1.5 H_2O (**36**).*

***Table 5**: Crystallographic data of lithium picramate · 1.5 H_2O (**36**).*

Formula	$C_6H_7N_3O_{6.5}Li$
FW [g mol^{-1}]	232.08
Crystal system	Triclinic
Space Group	*P*-1
Color / Habit	Orange platelet
Size [mm]	0.03 x 0.24 x 0.44
a [Å]	8.6881(13)
b [Å]	9.7990(15)
c [Å]	11.4482(18)
α [°]	81.600(13)
β [°]	69.628(15)
γ [°]	85.143(12)
V [$Å^3$]	903.3(3)
Z	2
$\rho_{calc.}$ [g cm^{-3}]	1.707
μ [mm^{-1}]	0.153
F(000)	176
$\lambda_{MoK\alpha}$ [Å]	0.71073
T [K]	121
θ Min–Max [°]	3.5, 26.4
Dataset	−10: 10; −10: 12; −14: 14

Reflections collected	5015
Independent refl.	3623
R_{int}	0.043
Observed reflections	3623
Parameters	338
R_1 (obs)[a]	0.0672
wR_2 (all data)[b]	0.1405
GooF[c]	0.98
Resd. Dens. [e Å^{-3}]	−0.32, 0.34
Absorption correction	multi-scan

a) $R_1 = \Sigma||F_0|-|F_c||/\Sigma|F_0|$; b) $wR_2 = [\Sigma[w(F_0^2-F_c^2)^2]/\Sigma[w(F_0)^2]]^{1/2}$; $w = [\sigma c^2(F_0^2)+(xP)^2+yP]^{-1}$ and $P=(F_0^2+2F_c^2)/3$; c) GooF = $\{\Sigma[w(F_o^2-F_c^2)^2]/(n-p)\}^{1/2}$ (n = number of reflections; p = total number of parameters).

2.1.20 Lithium dinitromethanide monohydrate

2.1.20.1 Procedure

The reaction toward compound **38** was implemented from a literature procedure with minor modifications.[24]

Fuming nitric acid (1.44 mol, 60 mL) was added into a mixture of barbituric acid (25.6 g, 0.2 mol) dissolved in 96% sulfuric acid (120 mL), while the temperature was kept below 20 °C. The resulting reaction mixture was then heated to 45 °C. The resulting precipitate was filtered, washed with trifluoroacetic acid and dried over night to yield 5,5`-dinitrobarbituric acid (40.13 g, 0.184 mol, 92%). 5,5`-Dinitrobarbituric acid (40.13 g, 0.184 mol) was added to water 200 mL and a 100 mL solution of KOH (26 g, 0.46 mol) under ice cooling. The reaction mixture was allowed to warm to ambient temperature and was stirred for 1 h. A yellow precipitate formed. The solid was filtered off, washed with cold water and was dried. The potassium salt of (2,2`-dinitroacetyl)urea (yellow crystals, 27.68 g, 0.120 mol) was obtained in 60% yield. The latter was added to 250 mL of a potassium hydroxide (27.7 g, 0.48 mol) solution. The resulting solution was stirred for 2 h at 80 °C. The reaction was cooled to 0 °C and the yellow crystals were filtered off and washed with 10 mL cold water and dried to give the pure potassium dinitromethanide (11.23 g, 0.078 mol, 65%). The analytical values were as stated in the literature.[24]

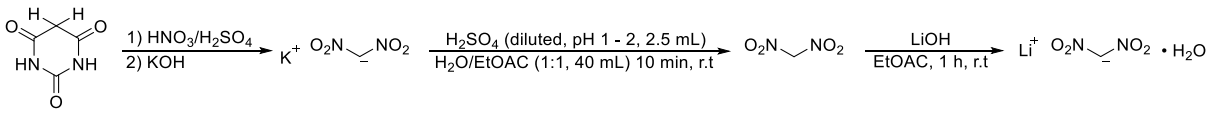

37 **38** **39** **40**

***Scheme 23**: Reaction toward lithium dinitromethanide monohydrate (**40**).*

The synthesis towards the neutral compound was reproduced from literature.[25]

Compound **38** (2.00 g, 13.88 mmol) was dissolved in a mixture of 20 mL of water and 20 mL of ethyl acetate. Diluted sulfuric acid (2.5 mL aqueous solution containing 0.8 mL of 96% sulfuric acid) was added to obtain pH 1-2. The solution was stirred for 10 min. The layers were separated and the aqueous phase was extracted 3 times with 20 mL of ethyl acetate. The

combined organic phases were washed with water to obtain a neutral solution. For further synthesis we assume a complete conversion.
Lithium hydroxide (110.6 mg, 4.62 mmol, 1 eq.) was dissolved in 10 mL of methanol. The resulting solution was added to a solution of dinitromethane (490 mg, 4.62 mmol,1 eq) in 25 mL ethyl acetate. The resulting mixture was stirred for 1 h at room temperature. The solvent was removed *in vacuo* and gave crystals suitable for X-ray diffraction. However, it was not possible to characterize the substance completely, since there was always a spontaneous decomposition of the salt after an indefinite time. One possible reason is that it loses the water of crystallization by drying at room temperature, which contributes to the stability of the molecule.

2.1.20.2 Crystal structure

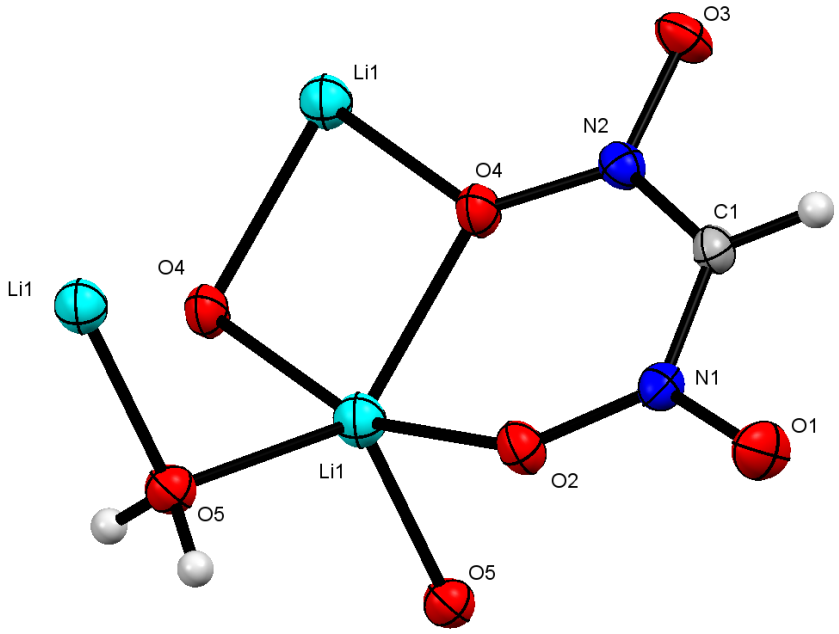

***Figure 9**: Crystal structure of lithium dinitromethanide monohydrate (**40**).*

***Table 6**: Crystallographic data of lithium dinitromethanide monohydrate (**40**).*

Formula	C H3 Li N2 O5
FW [g mol^{-1}]	129.99
Crystal system	monoclinic
Space group	P2_1/n
Color / Habit	yellowish/plate
Size [mm]	0.5 x 0.5 x 0.05
a [Å]	3.3549(5)
b [Å]	17.520(2)
c [Å]	7.8168(11)
α [°]	90
β [°]	99.494(13)
γ [°]	90
V [Å^3]	453.16(11)
Z	4
$\rho_{calc.}$ [g cm^{-3}]	1.905
μ [mm^{-1}]	0.192
F(000)	264
$\lambda_{MoK\alpha}$ [Å]	0.71073
T [K]	102
θ Min-Max [°]	2.325, 26.358
Dataset	-3: 4; -21: 19;-9: 9
Reflections collected	3012
Independent refl.	927
R_{int}	0.0224
Observed reflections	775
Parameters	94
R_1 (obs)[a]	0.0292
wR_2 (all data)[b]	0.0778
S [c]	1.035
Resd. dens [e Å^{-3}]	-0.182, 0.205
Device type	'Xcalibur, Sapphire3'
Solution	'SHELXT 2018/2 (Sheldrick, 2018)'
Refinement	'SHELXT 2018/2 (Sheldrick, 2018)'
Absorption correction	multiscan
CCDC	-

[a]$R_1 = \Sigma||F_0|-|F_c||/\Sigma|F_0|$; [b]$wR_2 = [\Sigma[w(F_0^2-F_c^2)^2]/\Sigma[w(F_0)^2]]^{1/2}$; $w = [\sigma c^2(F_0^2)+(xP)^2+yP]^{-1}$ and $P=(F_0^2+2F_c^2)/3$; [c]$S = \{\Sigma[w(F_o^2-F_c^2)^2]/(n-p)\}^{1/2}$ (n = number of reflections; p = total number of parameters).

2.1.21 Lithium 2,2,2-trinitroethyl nitrocarbamate monohydrate

2.1.21.1 Procedure

2,2,2-Trinitroethyl nitrocarbamate was synthesized according to literature procedures[26,27] (see **Scheme 24**).

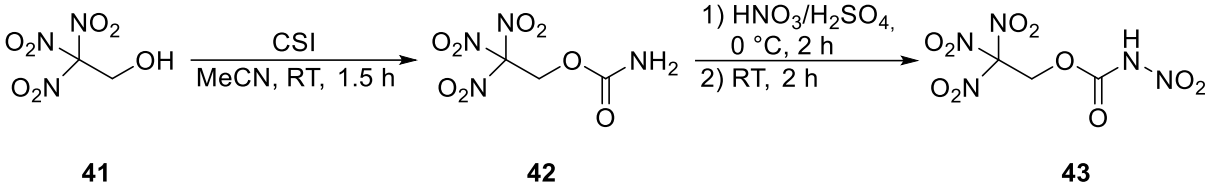

41 **42** **43**

***Scheme 24**: Reaction toward 2,2,2-trinitroethyl nitrocarbamate (**43**).*

For the following acid-base reaction lithium hydroxide was used as the lithium donating species (see **Scheme 25**).

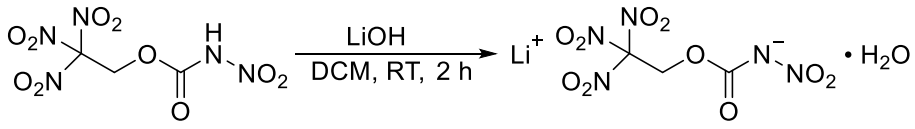

43 **44**

***Scheme 25**: Reaction toward lithium 2,2,2-trinitroethyl nitrocarbamate monohydrate (**44**).*

2,2,2-Trinitroethyl nitrocarbamate (100 mg, 0.37 mmol) was dissolved in dichloromethane and lithium hydroxide monohydrate (15.5 mg, 0.37 mmol) was slowly added. Whilst the reaction mixture was stirred for two hours at room temperature, a yellow solid precipitated. The solid was filtered and dried on air to yield lithium 2,2,2-trinitroethyl nitrocarbamate • H_2O quantitatively.

IR (ATR): $\tilde{\nu}$ = 3629 (w), 3502 (w), 1699 (s), 1590 (w), 1460 (m), 1435 (m), 1390 (m), 1358 (w), 1305 (m), 1237 (s), 1129 (s), 1095 (m), 983 (w), 892 (w), 857 (w), 819 (m), 788 (m), 769 (m), 655 (w), 551(w), 478 (w), 442 (w), 413 (w) cm^{-1}. $^{14}N\{H\}$ NMR (D_2O, 25 °C): δ = −9.9 (NO_2), −33.8 ($C(NO_2)_3$) ppm. $^{13}C\{H\}$ NMR (D_2O, 25 °C): δ = 158.7 (*C*O), 124.0 ($C(NO_2)_3$), 61.1 (CH_2) ppm. ^{1}H NMR (D_2O, 25 °C): δ = 5.70 (s, 2H, CH_2) ppm. EA ($C_3H_4N_5O_{11}Li$, 293.03): calcd. N 23.90, C 12.30, H 1.38 %; found N 23.45, C 12.53, H 1.48 %.

2.1.21.2 Crystal structure

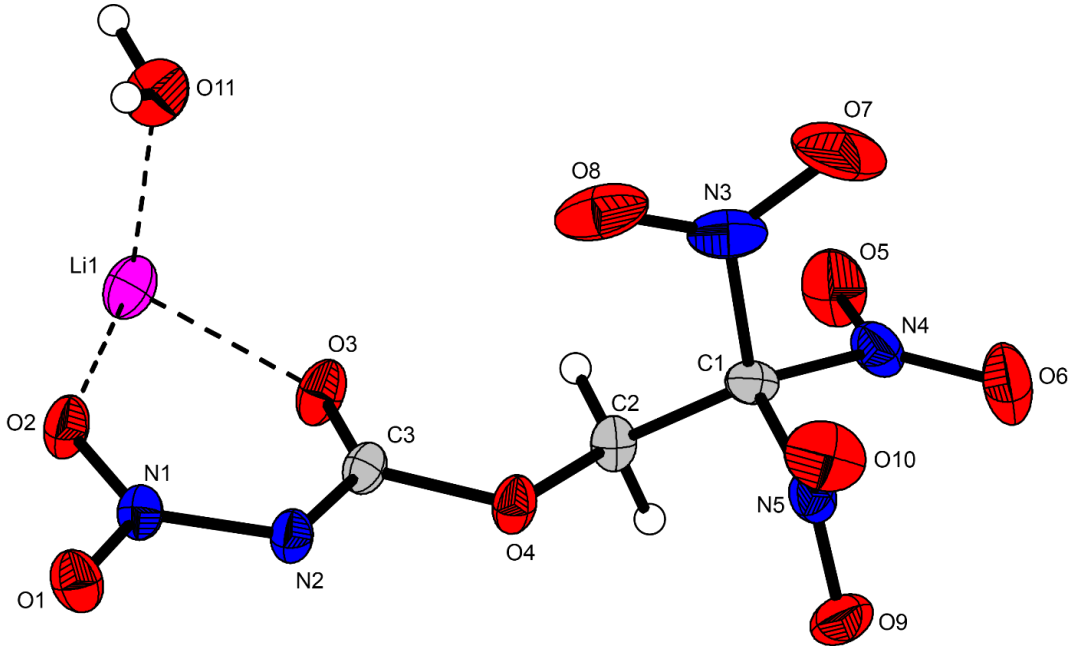

***Figure 10**: Crystal structure of lithium 2,2,2-trinitroethyl nitrocarbamate monohydrate (**44**).*

***Table 7**: Crystallographic data of lithium 2,2,2-trinitroethyl nitrocarbamate monohydrate (**44**).*

Formula	C3 H4 Li N5 O11
FW [g mol^{-1}]	293.05
Crystal system	orthorhombic
Space group	Pbca (No. 61)
Color / Habit	colorless/block
Size [mm]	0.05 x 0.20 x 0.25
a [Å]	6.3781(4)
b [Å]	10.1200(5)
c [Å]	33.7553(19)
α [°]	90
β [°]	90
γ [°]	90
V [Å^3]	2178.8(2)
Z	8
$\rho_{calc.}$ [g cm^{-3}]	1.787
μ [mm^{-1}]	0.182
F(000)	1184
$\lambda_{MoK\alpha}$ [Å]	0.71073
T [K]	103
θ Min-Max [°]	2.4, 26.4
Dataset	-7: 7 ; -12: 12 ; -42: 42
Reflections collected	30202
Independent refl.	2208
R_{int}	0.074
Observed reflections	1663
Parameters	197
R_1 (obs)[a]	0.0493
wR_2 (all data)[b]	0.1198
S [c]	1.04
Resd. dens [e Å^{-3}]	-0.30, 0.42
Device type	'Xcalibur, Sapphire3'
Solution	'SHELXT 2018/2 (Sheldrick, 2018)'
Refinement	'SHELXT 2018/2 (Sheldrick, 2018)'
Absorption correction	multiscan
CCDC	-

[a]$R_1 = \Sigma||F_0|-|F_c||/\Sigma|F_0|$; [b]$wR_2 = [\Sigma[w(F_0^2-F_c^2)^2]/\Sigma[w(F_0)^2]]^{1/2}$; $w = [\sigma c^2(F_0^2)+(xP)^2+yP]^{-1}$ and $P=(F_0^2+2F_c^2)/3$; [c]$S = \{\Sigma[w(F_o^2-F_c^2)^2]/(n-p)\}^{1/2}$ (n = number of reflections; p = total number of parameters).

2.1.22 Tetralithium pentaerythritol tetranitrocarbamate

In order to improve the spectral purity, we tried to increase the amount of lithium in the respective salts. Therefor we tried to synthesize the titled lithium salt for investigation. The precursors were successfully prepared according to literature[28] (see **Scheme 26**).

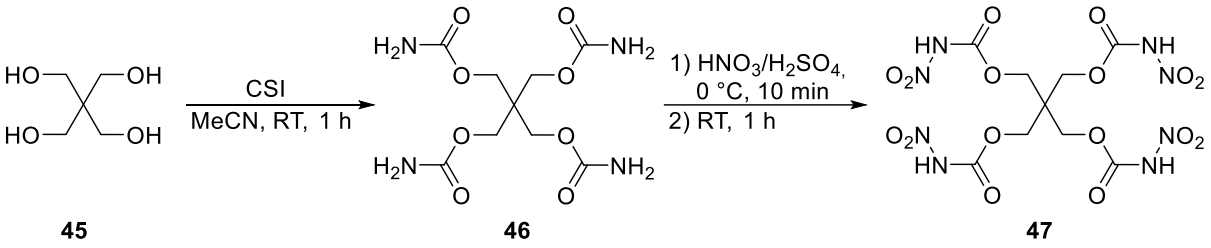

***Scheme 26**:Reaction toward pentaerythritol tetranitrocarbamate (**47**).*

The lithium salt of pentaerythritol tetranitrocarbamate was prepared according to literature[29] (see **Scheme 27**). However, synthesis in several approaches was not successful. The title molecule could not be produced completely clean. Likewise, the water content could not be accurately determined because no crystal structure could be grown.

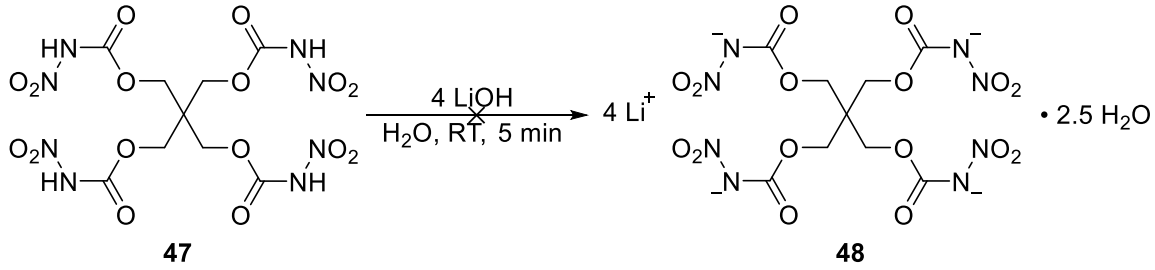

***Scheme 27**: Unsuccessful reaction toward tetralithium pentaerythritol tetranitrocarbamate (**48**).*

Even several purification steps and multiple recrystallizations failed to remove the impurity. Therefore, further work with this molecule was ruled out.

2.1.23 Potassium dihydrobis(pyrazol-1-yl)borate

2.1.23.1 Synthesis optimization

Trofimenko published a procedure for potassium dihydrobis(pyrazol-1-yl)borate whereby four equivalents of 1*H*-pyrazole are molten at 90 °C and allowed to react with one equivalent of potassium borohydride for 20 hours at temperatures between 90 and 115 °C.[5] In order to further delimit the given temperature range, the Lewis acid-base reaction of potassium borohydride with 1*H*-pyrazole was conducted at different temperatures and the reaction progress tracked by recording ^{1}H-coupled ^{11}B NMR spectra of the crude products after washing with toluene. Keeping the temperature constant after the melting process led to significant amounts of intermediate trihydro(pyrazol-1-yl)borate left behind which is recognizable in the NMR spectrum by a quartet at about −20 ppm next to the lower field-shifted broad triplet provoked by dihydrobis(pyrazol-1-yl)borate. The intensity of this signal is

greatly diminished in the NMR spectrum of a sample heated to 110 °C, however the high field-shifted quintet at approximately −40 ppm assignable to the borohydride anion did not disappear. Since at a reaction temperature of 110 °C 1*H*-pyrazole was observed to start evaporating and trace amounts of higher substituted hydrotris(pyrazol-1-yl)borate causing a doublet at approximately −1 ppm were detected, the problem of remaining starting material was approached by extending the reaction time rather than further increasing the temperature. Even if under these conditions no full conversion of starting material to the desired compound was achieved and the signal for the tris-substituted borate was slightly enhanced, the yield was considerably increased (47 vs. 78 %) (see **Figure 11**).

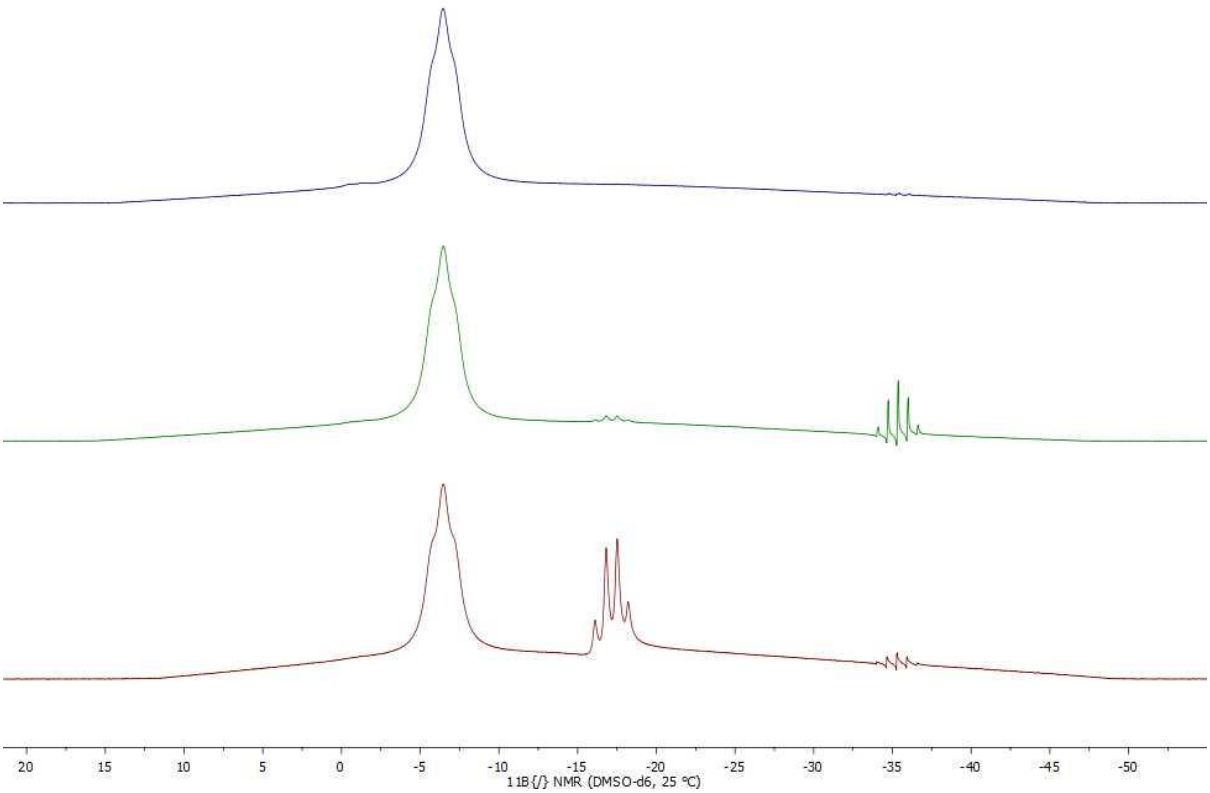

***Figure 11**: ^{1}H-coupled ^{11}B NMR spectra of samples prepared using different reaction temperatures and times: red curve – 90 °C, 22.5 hours; green curve – 110 °C, 20.5 hours; blue curve – 110 °C, 40.25 hours.*

2.1.23.2 Procedure

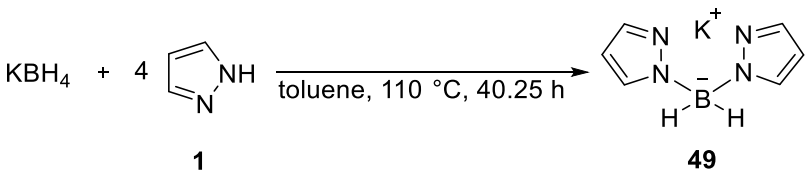

***Scheme 28**: Reaction toward potassium dihydrobis(pyrazol-1-yl)borate (**49**).*

6.712 g 1*H*-pyrazole (99 mmol) in a mixture with 1.329 g potassium borohydride (25 mmol) were molten at 90 °C before the starting materials were reacted at 110 °C for 40.25 hours.

After 25 mL of toluene had been added and the solution had cooled down to room temperature, the solid was collected, washed with 50 mL of 100 °C hot toluene first and then with an additional 50 mL of toluene to remove unreacted 1*H*-pyrazole. Air-drying gave the target salt (3.558 g, 78 %) impurified by trace amounts of potassium hydrotris(pyrazol-1-yl)borate in the form of a white powder.

IR (ATR): $\tilde{\nu}$ = 2432 (w), 2401 (w), 2286 (vw), 2269 (w), 1741 (vw), 1623 (vw), 1571 (vw), 1551 (vw), 1496 (m), 1417 (w), 1388 (m), 1285 (m), 1256 (w), 1191 (m), 1185 (m), 1143 (m), 1081 (m), 1048 (s), 1010 (w), 954 (m), 918 (w), 895 (w), 879 (m), 879 (m), 858 (m), 836 (w), 765 (vs), 723 (m), 673 (w), 662 (w), 643 (vs) cm^{-1}. $^{11}B\{/\}$ NMR (DMSO-d_6, 25 °C): δ = −7.0 (br s, BH_2) ppm. $^{13}C\{H\}$ NMR (DMSO-d_6, 25 °C): δ = 137.9 (*C*H), 133.6 (*C*H), 102.6 (*C*H) ppm. $^{1}H\{/\}$ NMR (DMSO-d_6, 25 °C): δ = 7.44 (br s, 2H, C*H*), 7.33 (br s, 2H, C*H*), 6.02 (br s, 2H, C*H*), 3.69 (br s, 2H, BH_2) ppm. EA ($C_6H_8N_4BK$, 186.07): calcd. N 30.11, C 38.73, H 4.33 %; found N 29.87, C 38.48, H 4.37 %. DTA (5 °C min^{-1}): 169 (endothermic), 297 (exothermic) °C.

2.1.24 Lithium dihydrobis(pyrazol-1-yl)borate monohydrate

2.1.24.1 Procedure

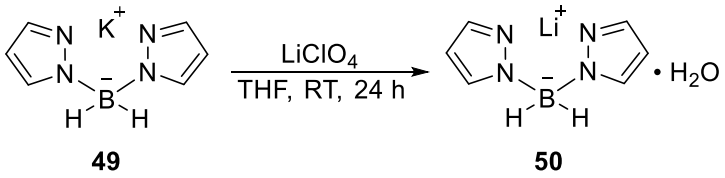

49 **50**

***Scheme 29**: Reaction toward lithium dihydrobis(pyrazol-1-yl)borate monohydrate (**50**).*

A solution of 0.999 g potassium dihydrobis(pyrazol-1-yl)borate with minor impurity by the higher substituted borate species (5 mmol) and 0.573 g lithium perchlorate (5 mmol) in 50 mL tetrahydrofurane was stirred at room temperature for 24 hours whereby potassium perchlorate precipitated. The by-product was filtered off and the solvent was allowed to evaporate from the filtrate whereupon the crude product containing the decomposition products tetrahydroxyborate and 1*H*-pyrazole along with the lithium salts of the two borate species present was obtained as a white powder. A crystalline analytical sample was gained by washing with 10 mL of benzene and toluene each in order to remove lithium hydrotris(pyrazol-1-yl)borate and the azole, respectively, and by extracting the target salt with 10 mL of dichloromethane. As soon as the solvent was evaporated, a crystal was mounted in Kel-F oil and measured shortly after.

2.1.24.2 Aging Effects

Apart from the suspected hygroscopicity of crystalline potassium dihydrobis(1,2,4-triazol-1-yl)borate, lithium dihydrobis(pyrazol-1-yl)borate monohydrate was the only investigated

moiety subject to ageing effects. The crude product obtained directly after removal of the solvent *in vacuo* already contained 20 % of 1*H*-pyrazole visible by a triplet at 6.26 ppm and a doublet at 7.61 ppm with an integral ratio of 1:2 in the ^{1}H NMR (see **Figure 12**). The intensity of the doublet signal increased by 10 % per day of storage at ambient conditions until after exposure to air for four days half of the target salt was decomposed. This result explains why previous attempts to access lithium dihydrobis(pyrazol-1-yl)borate starting from lithium borohydride and 1*H*-pyrazole were not successful.

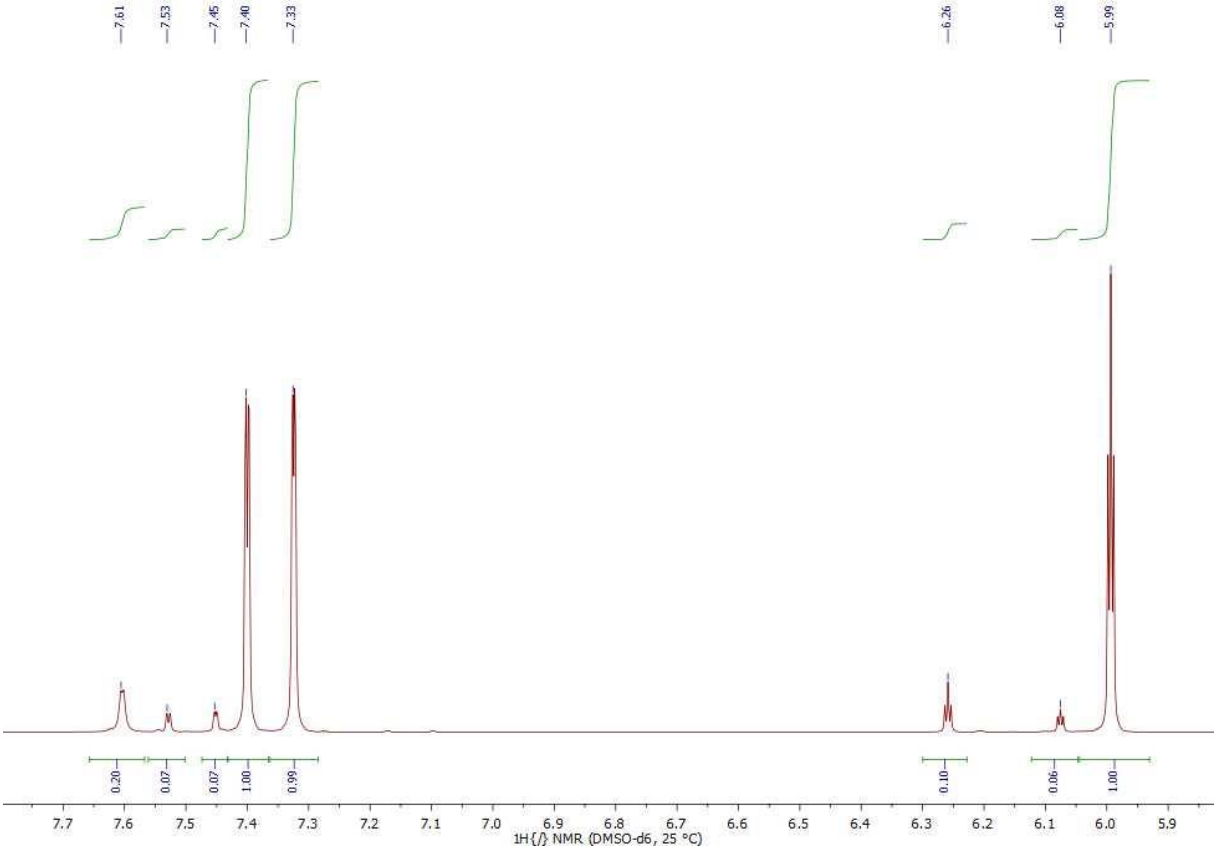

***Figure 12**: ^{1}H NMR spectrum of a freshly prepared sample of lithium dihydrobis(pyrazol-1-yl)borate monohydrate (**50**).*

Another triplet signal and two doublet signals occurring in the lower field with respect to the product signals can be assigned to the tris-substituted borate anion that was present in trace amounts in the sample of potassium dihydrobis(pyrazol-1-yl)borate serving as starting material.

2.1.24.3 Crystal structure

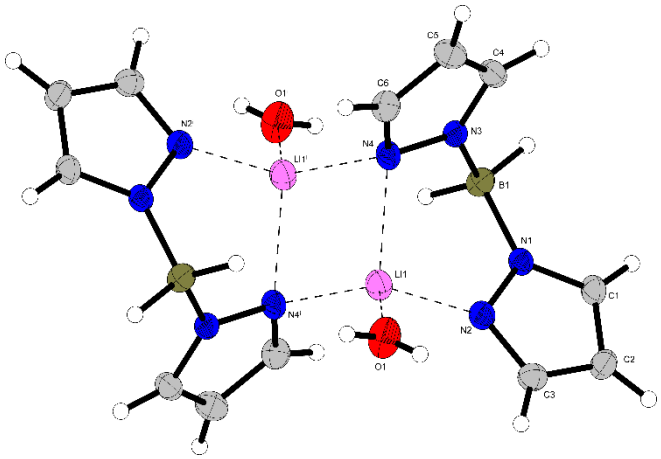

***Figure 13**: Crystal structure of lithium dihydrobis(pyrazol-1-yl)borate monohydrate (**50**).*

***Table 8**: Crystallographic data of lithium dihydrobis(pyrazol-1-yl)borate monohydrate (**50**).*

Formula	$C_6H_{10}BLiN_4O$
FW [g mol^{-1}]	171.93
Crystal system	Monoclinic
Space Group	$P2_1/n$
Color / Habit	Brownish block
Size [mm]	0.10 x 0.35 x 0.40
a [Å]	8.1502(4)
b [Å]	7.1232(3)
c [Å]	15.3774(6)
α [°]	90
β [°]	93.256(4)
γ [°]	90
V [Å^3]	891.30(7)
Z	4
$\rho_{calc.}$ [g cm^{-3}]	1.281
μ [mm^{-1}]	0.088
F(000)	360
$\lambda_{MoK\alpha}$ [Å]	0.71073
T [K]	143
θ Min–Max [°]	3.8, 26.4
Dataset	−10: 10; −8: 7; −11: 19
Reflections collected	6865
Independent refl.	1817
R_{int}	0.028
Observed reflections	1537
Parameters	134
R_1 (obs)[a]	0.0350
wR_2 (all data)[b]	0.0896
GooF[c]	1.05
Resd. Dens. [e Å^{-3}]	−0.17, 0.20
Absorption correction	multi-scan
CCDC	1917116

a) $R_1 = \Sigma||F_0|-|F_c||/\Sigma|F_0|$; b) $wR_2 = [\Sigma[w(F_0^2-F_c^2)^2]/\Sigma[w(F_0)^2]]^{1/2}$; $w = [\sigma c^2(F_0^2)+(xP)^2+yP]^{-1}$ and $P=(F_0^2+2F_c^2)/3$; c) GooF = $\{\Sigma[w(F_o^2-F_c^2)^2]/(n-p)\}^{1/2}$ (n = number of reflections; p = total number of parameters).

2.1.25 Potassium dihydrobis(3-nitropyrazol-1-yl)borate

2.1.25.1 Procedure

Regarding that the reaction between the two starting materials leads to the formation of hydrogen gas and that the reaction rate is significantly increased at elevated temperature, combining potassium tetrahydroborate with the heterocycle at room temperature appeared to be safer. Since the corresponding borate salt carrying 1*H*-1,2,4-triazole as ligand was accessible by refluxing the reaction mixture in acetonitrile for six days[30] and due to the similar pKa values of triazole[31] and nitropyrazole,[32] we expected a temperature of 80 °C to be sufficient for overcoming the reaction barrier. In this way, anisole was replaced by easier removable acetonitrile. Additionally, isolating 3-nitro-1*H*-pyrazole before reacting it with potassium borohydride allows for a higher degree of control over the stoichiometry.

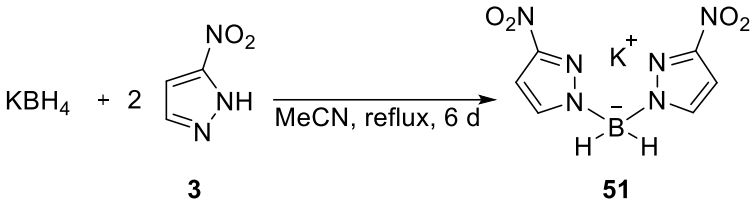

***Scheme 30**: Reaction toward potassium dihydrobis(3-nitropyrazol-1-yl)borate (**51**).*

A solution of 0.366 g potassium borohydride (7 mmol) and 1.534 g 3-nitro-1*H*-pyrazole (14 mmol) in roughly 2 mL of anhydrous acetonitrile which was prepared under ice cooling was stirred at room temperature until ease of hydrogen formation and subsequently refluxed over six nights. After the slurry had been filtrated, the residue was washed twice with approximately 5 mL ethanol each, recrystallized from 16 mL of methanol and was dried at 100 °C in an oven overnight. The target salt was obtained in 33 % yield (0.619 g) in the form of brownish crystals.

IR (ATR): $\tilde{\nu}$ = 3146(w), 3129(w), 2452(w), 2428(m), 2385(w), 2287(w), 2269(w), 1769(vw), 1670(vw), 1551(w), 1528(m), 1521(m), 1490(m), 1478(s), 1440(m), 1392(m), 1381(s), 1362(s), 1301(m), 1231(s), 1206(m), 1142(vs), 1055(s), 1055(s), 1006(m), 989(m), 913(w), 899(m), 886(w), 830(s), 822(m), 785(s), 754(vs), 728(m), 677(w), 662(m), 643(m), 616(m), 540(w), 451(w), 440(w), 407(vw) cm^{-1}. $^{11}B\{/\}$ NMR (DMSO-d_6, 25 °C): δ = -5.5 (br s, BH_2) ppm. $^{14}N\{H\}$ NMR (DMSO-d_6, 25 °C): δ = -18.4 (br s, NO_2) ppm. $^{13}C\{H\}$ NMR (DMSO-d_6, 25 °C): δ = 156.6 (s, *C*-NO_2), 137.1 (s, *C*H), 101.4 (s, *C*H) ppm. $^{1}H\{/\}$ NMR (DMSO-d_6, 25 °C): δ = 7.62 (d, 2H, C*H*), 6.78 (d, 2H, C*H*), 3.60 (br s, 2H, BH_2) ppm. EA ($KBC_6H_6N_6O_4$, 276.06): calcd. N 30.44, C 26.11, H 2.19 %; found N 30.36, C 25.90, H 2.11 %. DTA (5 °C min^{-1}): 244 (exothermic) °C.

2.1.25.2 Ageing effects

During work-up of the title compound we observed that it gets a greenish color when exposed to air. In order to find an explanation for this behavior we performed a stability test: two

samples were stored at ambient conditions and their changes in weight and composition according to ^{1}H NMR spectroscopy were tracked after exposure times of one, seven and 14 days, respectively.

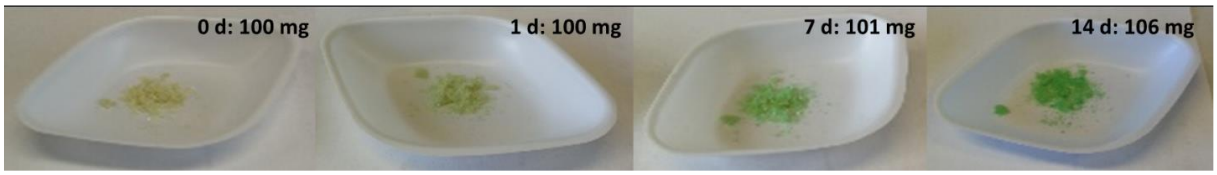

***Figure 14**: Change in color and weight of a sample of potassium dihydrobis(3-nitropyrazol-1-yl)borate (**51**) after exposure to air for one, seven and 14 days, respectively.*

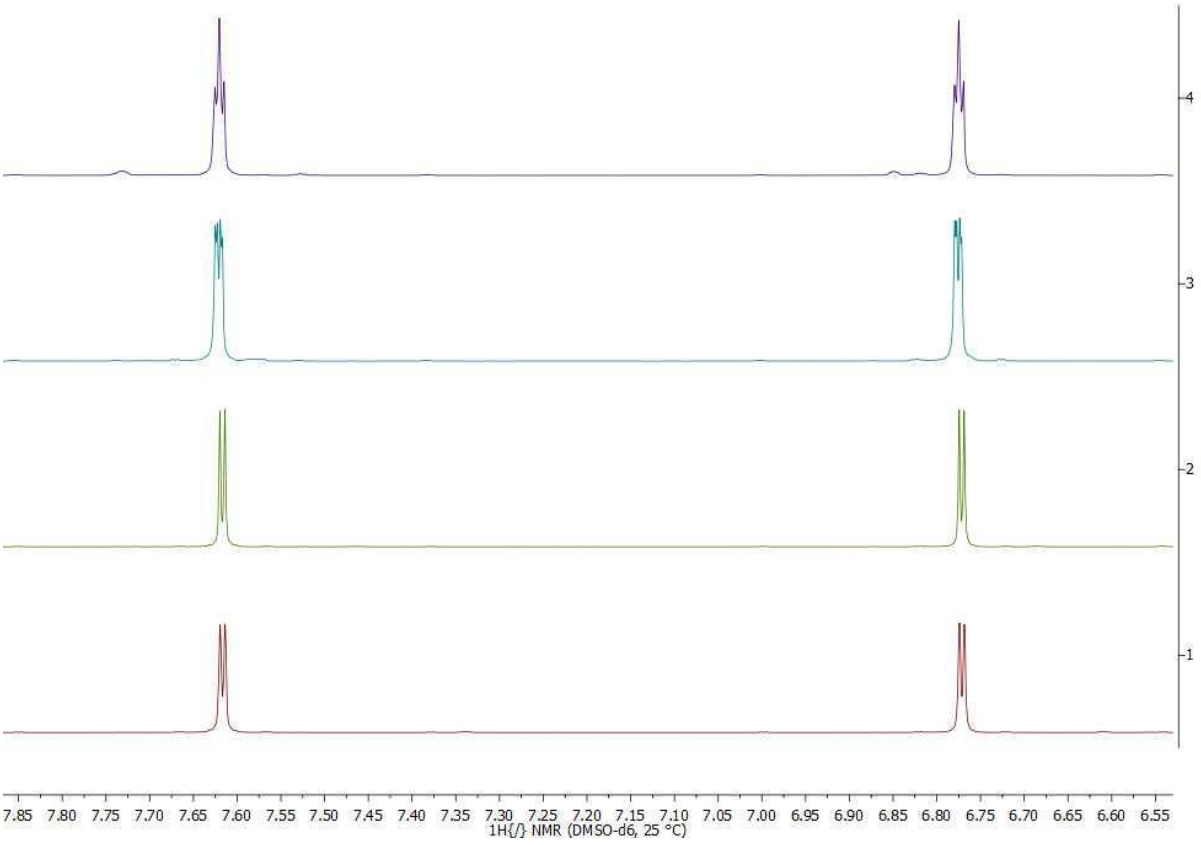

***Figure 15**: ^{1}H NMR spectra of a sample of potassium dihydrobis(3-nitropyrazol-1-yl)borate (**51**) after exposure to air directly after reaction (red graph), for one day (green graph), after seven days (blue graph) and after 14 days (violet graph).*

Potassium dihydrobis(3-nitropyrazol-1-yl)borate (**51**) already changes its color from yellowish to slightly greenish after storage at ambient conditions for one day although a mass increase beyond the error of the weighing device and the presence of 3-nitro-1*H*-pyrazole occurring as decomposition product could only be found after two weeks. These results indicate that trace amounts of decomposition product suffice for causing a visible change in color.

2.1.26 Lithium dihydrobis(3-nitropyrazol-1-yl)borate

2.1.26.1 Procedure

The titled compound is accessible via the metathesis reaction between compound **51** and lithium perchlorate (see **Scheme 31**).

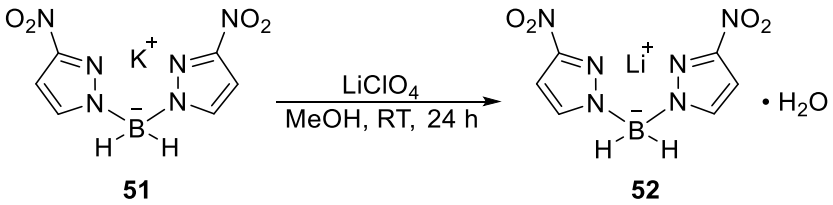

51 **52**

***Scheme 31**: Reaction toward lithium dihydrobis(3-nitropyrazol-1-yl)borate monohydrate (**52**).*

The metathesis reaction between 0.998 g potassium dihydrobis(3-nitropyrazol-1-yl)borate (4 mmol) and 0.385 g lithium perchlorate (4 mmol) in roughly 50 mL of methanol was allowed to proceed for 24 hours at room temperature. After potassium perchlorate had been filtered off, the solvent was removed from the filtrate *in vacuo*. Recrystallization of the residue from 5 mL of ethyl acetate and drying at 100 °C overnight gave 0.472 g of a light brown powder (50 %).

IR (ATR): $\tilde{\nu}$ = 3608(w), 3497(w), 3164(w), 3151(w), 3131(w), 2469(w), 2419(w), 1602(w), 1558(w), 1533(m), 1494(vs), 1456(w), 1447(w), 1392(m), 1359(vs), 1299(m), 1237(s), 1206(w), 1193(w), 1154(s), 1134(vs), 1068(s), 1059(s), 1059(s), 1010(m), 1001(m), 987(w), 976(w), 882(m), 828(s), 797(m), 786(s), 753(s), 723(m), 658(m), 639(w), 613(w), 548(w), 481(m), 453(m), 418(w) cm^{-1}. $^{7}Li\{H\}$ NMR (DMSO-d_6, 25 °C): δ = -1.0 (s, *Li*) ppm. $^{11}B\{/\}$ NMR (DMSO-d_6, 25 °C): δ = -6.0 (br s, *B*H_2) ppm. $^{14}N\{H\}$ NMR (DMSO-d_6, 25 °C): δ = -16.4 (br s, *N*O_2) ppm. $^{13}C\{H\}$ NMR (DMSO-d_6, 25 °C): δ = 156.6 (s, *C*-NO_2), 137.1 (s, *C*H), 101.4 (s, *C*H) ppm. $^{1}H\{/\}$ NMR (DMSO-d_6, 25 °C): δ = 7.62 (d, 2H, C*H*), 6.78 (d, 2H, C*H*), 3.60 (br s, 2H, BH_2), 3.37 (br s, 2H, H_2O) ppm. EA ($LiBC_6H_8N_6O_5$, 261.92): calcd. N 32.09, C 27.52, H 3.08 %; found N 32.15, C 27.69, H 2.82 %. DTA (5 °C min^{-1}): 93 (endothermic), 196 (exothermic) °C.

Additionally, it was found that the monohydrate can be dried at 100 °C over two nights to give the water-free form (see **Figure 16** and **Scheme 32**).

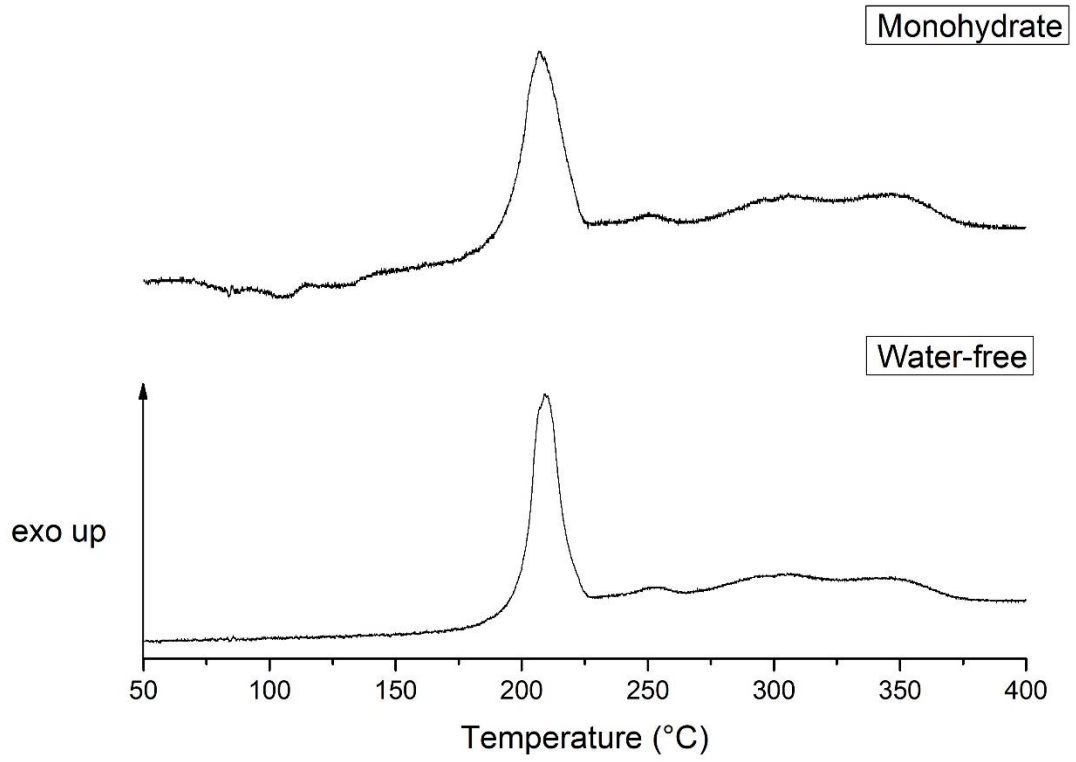

***Figure 16**: DTA curves of lithium dihydrobis(3-nitropyrazol-1-yl)borate monohydrate (**52**) and lithium dihydrobis(3-nitropyrazol-1-yl)borate (**53**) (top to bottom).*

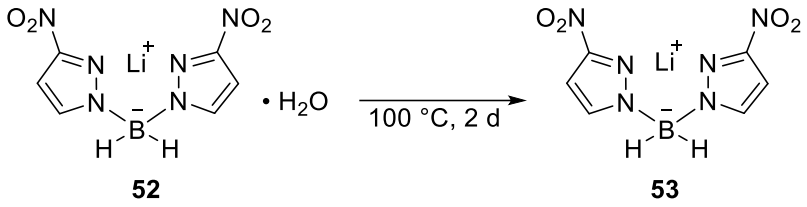

***Scheme 32**: Reaction toward lithium dihydrobis(3-nitropyrazol-1-yl)borate (**53**).*

After the crude product of the reaction between 1.002 g potassium dihydrobis(3-nitropyrazol-1-yl)borate (4 mmol) and 0.387 g lithium perchlorate (4 mmol) in 50 mL methanol had been recrystallized from 5 mL ethyl acetate, the crystals were dried at 100 °C over two nights to yield 0.590 g (67 %) of a light brown material.

IR (ATR): $\tilde{\nu}$ = 3182(vw), 3169(vw), 3149(w), 3126(w), 2480(w), 2421(w), 1561(w), 1541(m), 1529(m), 1495(s), 1486(s), 1448(w), 1360(vs), 1299(w), 1231(s), 1187(w), 1179(m), 1168(m), 1159(m), 1151(s), 1136(vs), 1124(vs), 1063(s), 1063(s), 1011(m), 982(w), 903(w), 884(w), 871(w), 842(m), 827(s), 800(m), 787(s), 753(vs), 720(m), 710(m), 666(w), 656(m), 634(m), 622(w), 611(w), 550(w), 466(w), 450(w) cm^{-1}. $^{7}Li\{H\}$ NMR (DMSO-d_6, 25 °C): δ = -1.1 (s, *Li*) ppm. $^{11}B\{/\}$ NMR (DMSO-d_6, 25 °C): δ = -6.0 (br s, BH_2) ppm. $^{14}N\{H\}$ NMR (DMSO-d_6, 25 °C): δ = -18.8 (br s, NO_2) ppm. $^{13}C\{H\}$ NMR (DMSO-d_6, 25 °C): δ = 156.6 (s, *C*-NO_2), 137.1 (s, *C*H), 101.4 (s, *C*H) ppm. $^{1}H\{/\}$ NMR (DMSO-d_6, 25 °C): δ = 7.62 (d, 2H, C*H*), 6.77 (d, 2H, C*H*), 3.60 (br s, 2H, BH_2) ppm. EA ($LiBC_6H_6N_6O_4$, 243.90): calcd. N 34.46, C 29.55, H 2.48 %; found N 34.22, C 29.12, H

2.49 %. DTA (5 °C min^{-1}): 200 (exothermic) °C. FS (100-500 µm): 144 N. IS (< 100 µm): 2 J. ESD (100-500 µm): 0.42 J.

2.1.26.2 Ageing effects

Although a sample of lithium dihydrobis(3-nitropyrazol-1-yl)borate already significantly changed its color after one week of exposure to air (see **Figure 17**), no weight gain beyond the measurement uncertainty or change in composition by ^{1}H NMR and ^{1}H-coupled ^{11}B NMR experiments were detected.

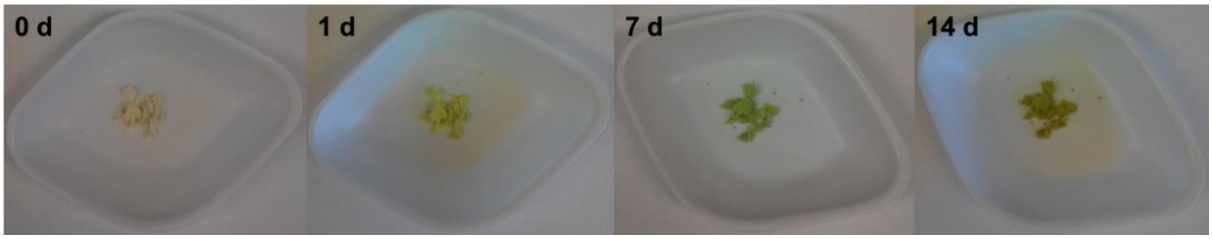

***Figure 17**: Color change of a sample of lithium dihydrobis(3-nitropyrazol-1-yl)borate (**53**) after exposure to air for 0, 1, 7 or 14 days (from left to right).*

2.1.26.3 Crystal structure

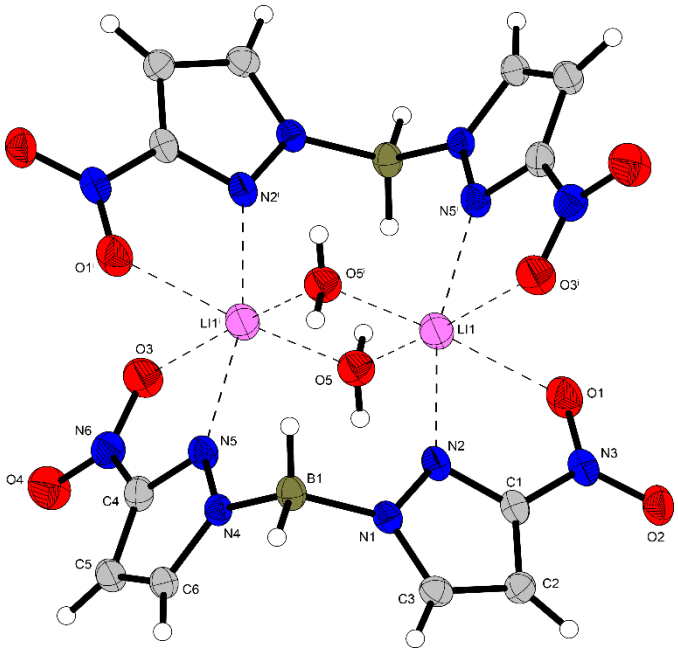

***Figure 18**: Dimer of lithium dihydrobis(3-nitropyrazol-1-yl)borate monohydrate (**52**).*

***Table 9**: Crystallographic data of lithium dihydrobis(3-nitropyrazol-1-yl)borate monohydrate (**52**).*

Formula	$LiBC_6H_8N_6O_5$
FW [g mol^{-1}]	261.92
Crystal system	Monoclinic
Space Group	$P2_1/n$
Color / Habit	Colorless block
Size [mm]	0.20 x 0.25 x 0.30
a [Å]	10.2635(4)
b [Å]	11.1377(4)
c [Å]	10.3316(4)
α [°]	90
β [°]	103.434(4)
γ [°]	90
V [Å^3]	1148.71(8)
Z	2
$\rho_{calc.}$ [g cm^{-3}]	1.515
μ [mm^{-1}]	0.126
F(000)	536
$\lambda_{MoK\alpha}$ [Å]	0.71073
T [K]	143
θ Min–Max [°]	2.5, 26.4
Dataset	−12: 12; −13: 13; −12: 12
Reflections collected	17362
Independent refl.	2340
R_{int}	0.032
Observed reflections	1983
Parameters	188
R_1 (obs)[a]	0.0365
wR_2 (all data)[b]	0.0973
GooF[c]	1.07
Resd. Dens. [e Å^{-3}]	−0.18, 0.33
Absorption correction	multi-scan
CCDC	1998250

a) $R_1 = \Sigma||F_0|-|F_c||/\Sigma|F_0|$; b) $wR_2 = [\Sigma[w(F_0^2-F_c^2)^2]/\Sigma[w(F_0)^2]]^{1/2}$; $w = [\sigma c^2(F_0^2)+(xP)^2+yP]^{-1}$ and $P=(F_0^2+2F_c^2)/3$; c) GooF $= \{\Sigma[w(F_o^2-F_c^2)^2]/(n-p)\}^{1/2}$ (n = number of reflections; p = total number of parameters).

2.1.27 Potassium dihydrobis(4-amino-3,5-dinitropyrazol-1-yl)borate

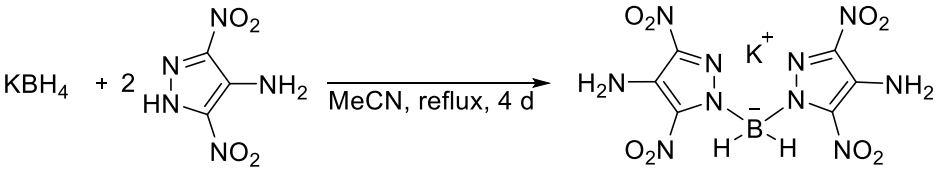

13 **54**

***Scheme 33**: Reaction toward potassium dihydrobis(4-amino-3,5-dinitropyrazol-1-yl)borate (**54**).*

A reaction mixture of 0.908 g (17 mmol) potassium borohydride, 5.825 g 4-amino-3,5-dinitro-1*H*-pyrazole (34 mmol) and roughly 9 mL of anhydrous acetonitrile was prepared under ice cooling and first stand and then stirred at room temperature until the exothermic release of hydrogen gas had eased up. After the suspension had been refluxed for four days, the cake was collected on filter paper and subsequently grinded. By adding approximately 88 mL of glacial acetic acid, stirring the suspension for 30 minutes, filtering off the solid and washing it

three times with about 30 mL of ethyl acetate each and once with roughly 5 mL of acetone, hydrolyzed boric acid, dissociated ligand and intermediate trihydro(4-amino-3,5-dinitropyrazol-1-yl)borate were removed. This procedure afforded 2.831 g (42 %) of an intensively yellow colored powder.

IR (ATR): $\tilde{\nu}$ = 3477(w), 3456(w), 3343(m), 2494(w), 2463(w), 1632(s), 1569(vw), 1494(m), 1462(s), 1439(s), 1378(w), 1310(vs), 1274(vs), 1212(s), 1151(m), 1128(s), 1036(m), 1004(s), 895(w), 883(m), 864(m), 827(m), 773(m), 773(m), 756(m), 751(s), 692(vw), 669(w), 642(vw), 619(w), 571(w), 527(m), 502(m), 484(s), 419(w) cm^{-1}. $^{11}B\{/\}$ NMR (DMSO-d_6, 25 °C): δ = -1.9 (br s, BH_2) ppm. $^{14}N\{H\}$ NMR (DMSO-d_6, 25 °C): δ = -19.6 (br s, NO_2) ppm. $^{13}C\{H\}$ NMR (DMSO-d_6, 25 °C): δ = 141.1 (s, C-NO_2), 135.8 (s, C-NO_2), 130.6 (s, C-NH_2) ppm. $^{1}H\{/\}$ NMR (DMSO-d_6, 25 °C): δ = 6.94 (br s, 4H, NH_2), 3.84 (br s, 2H, BH_2) ppm. EA ($KBC_6H_6N_{10}O_8$, 396.08): calcd. N 35.36, C 18.20, H 1.53 %; found N 35.68, C 18.88, H 1.78 %. DTA (5 °C min^{-1}): 159 (endothermic, followed by exothermic signal) °C.

2.1.28 Lithium dihydrobis(4-amino-3,5-dinitropyrazol-1-yl)borate

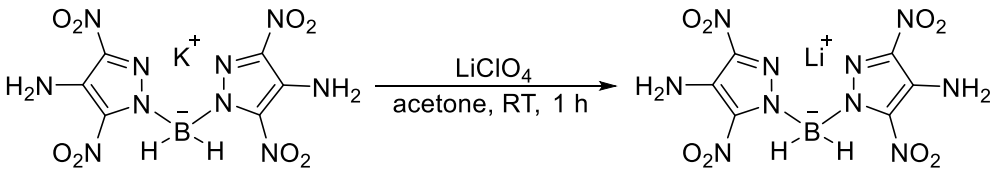

54 **55**

***Scheme 34**: Reaction toward lithium dihydrobis(4-amino-3,5-dinitropyrazol-1-yl)borate (**55**).*

The metathesis reaction between 0.998 g (3 mmol) potassium dihydrobis(4-amino-3,5-dinitropyrazol-1-yl)borate and 0.268 g (3 mmol) lithium perchlorate in roughly 50 mL of acetone was allowed to proceed for 1 hour before the suspension was filtered and the filtrate was dried *in vacuo*. The crude product thus obtained was already partially hydrolysed to boric acid and the substituent.

2.1.29 Potassium dihydrobis(1,2,4-triazol-1-yl)borate

2.1.29.1 Synthesis optimization

Since to the best of our knowledge the crystal structure of potassium dihydrobis(1,2,4-triazol-1-yl)borate has not been determined so far, the synthesis of this moiety was investigated further. Potassium dihydrobis(1,2,4-triazol-1-yl)borate is reported to be accessible by refluxing a solution of one equivalent potassium tetrahydroborate and two equivalents 1*H*-1,2,4-triazole in acetonitrile for four days[5d,e] but following this procedure yielded trihydro(1,2,4-triazol-1-yl)borate with trace amounts of borohydride. While in regard of the starting material a complete consumption was achieved by extending the reaction time by

one day, the mono-substituted borate still was not fully converted. This was the case, however, when the samples were reacted over one more day (see **Figure 19**).

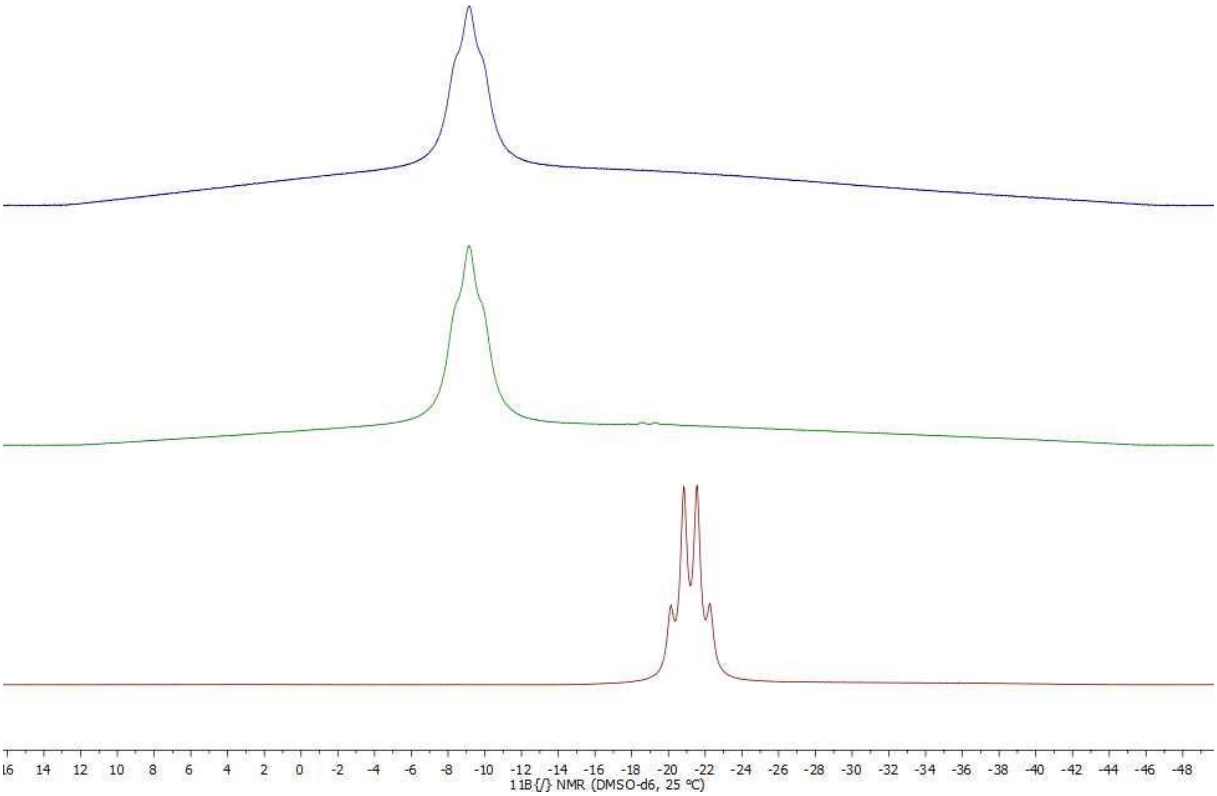

***Figure 19**: ^{1}H-coupled ^{11}B NMR spectra of samples prepared using different reaction times at constant concentrations ([KBH_4] = 1.63–2.68 mol L^{-1}, [$C_2H_3N_3$] = 3.26–5.36 mol L^{-1}).*

Doubling the concentrations of potassium borohydride and 1*H*-1,2,4-triazole in acetonitrile significantly raised the yield obtained (25 vs. 67 %) whereas further increasing the saturations resulted in a mixture. The latter provoked two overlapping quartets in the ^{1}H-coupled ^{11}B NMR spectrum along with the triplet from dihydrobis(1,2,4-triazol-1-yl)borate and a singlet at approximately 5 ppm assignable to tetrahydroxoborate. While the lower field-shifted quartet signal from trihydro(1,2,4-triazol-1-yl)borate had already been observed in the previous study, the second quartet can be attributed to trihydro(1,2,4-triazol-4-yl)borate (see **Figure 20**).

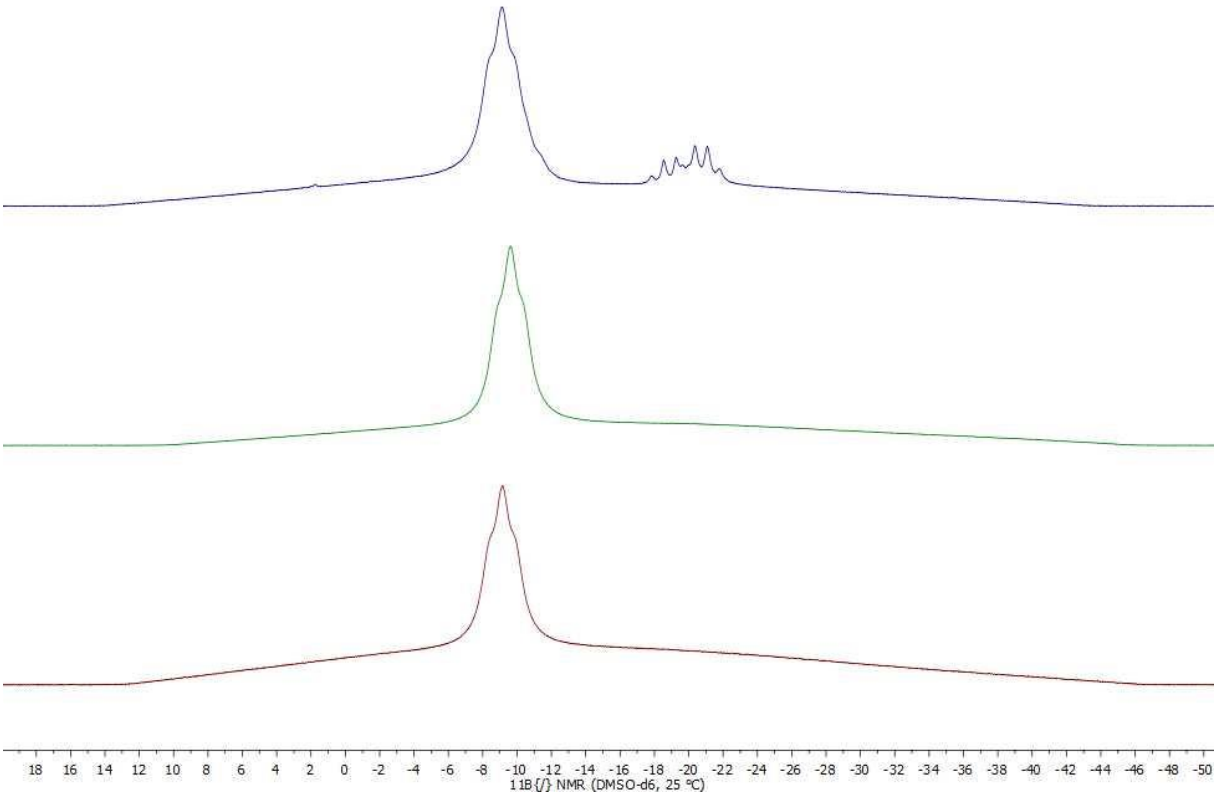

***Figure 20**: ^{1}H-coupled ^{11}B NMR spectra of samples prepared using different concentrations at a constant reaction time of six days: red curve – $[KBH_4]$ = 2.25 mol L^{-1}, $[C_2H_3N_3]$ = 4.51 mol L^{-1}; green curve – $[KBH_4]$ = 4.64 mol L^{-1}, $[C_2H_3N_3]$ = 9.28 mol L^{-1}; blue curve – $[KBH_4]$ = 10.06 mol L^{-1}, $[C_2H_3N_3]$ = 20.12 mol L^{-1}.*

2.1.29.2 Procedure

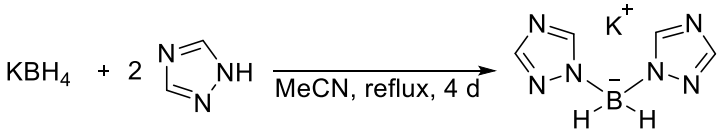

56 **57**

***Scheme 35**: Reaction toward potassium dihydrobis(1,2,4-triazol-1-yl)borate (**57**).*

The target salt (3.494 g, 67 %) was gained in the form of a white powder by refluxing a solution of 1.502 g potassium borohydride (28 mmol) and 3.847 g 1*H*-1,2,4-triazole (56 mmol) in 6 mL of distilled acetonitrile over six nights, filtering off the solid and washing it with 24 mL of acetonitrile. Single crystals suitable for X-ray diffraction were grown from an aqueous solution.

IR (ATR): $\tilde{\nu}$ = 3123 (w), 3108 (w), 2438 (w), 2410 (m), 2384 (w), 2370 (w), 2356 (w), 2345 (w), 2294 (w), 2283 (w), 2272 (w), 2179 (vw), 1787 (vw), 1768 (vw), 1758 (w), 1747 (w), 1569 (vw), 1500 (s), 1411 (w), 1342 (vw), 1313 (m), 1266 (s), 1208 (m), 1208 (m), 1177 (s), 1155 (vs), 1129 (s), 1123 (s), 1023 (s), 991 (w), 963 (m) cm^{-1}. $^{11}B\{/\}$ NMR (DMSO-d_6, 25 °C): δ = −9.6 (br t, BH_2) ppm. $^{13}C\{H\}$ NMR (DMSO-d_6, 25 °C): δ = 151.1 (*C*H), 147.5 (*C*H) ppm. $^{1}H\{/\}$ NMR (DMSO-d_6, 25 °C): δ = 8.00 (s, 2H, C*H*), 7.69 (s, 2H, C*H*), 3.65 (br s, 2H, BH_2), 3.43 (br s, 2H, H_2O) ppm.

EA ($C_4H_6N_6BK$, 188.04): calcd. N 44.69, C 25.55, H 3.22 %; found N 44.65, C 25.55, H 2.99 %. DTA (5 °C min^{-1}): 247 °C (endothermic, followed by exothermic signal).

2.1.29.3 Crystal structure

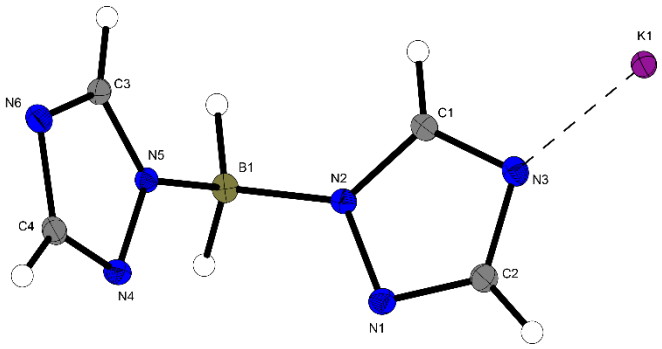

***Figure 21**: Molecular unit of potassium dihydrobis(1,2,4-triazol-1-yl)borate (**57**).*

***Table 10**: Crystallographic data of potassium dihydrobis(1,2,4-triazol-1-yl)borate (**57**).*

Formula	$C_4H_6BKN_6$
FW [g mol^{-1}]	188.06
Crystal system	Orthorhombic
Space Group	$P2_12_12_1$
Color / Habit	Colorless block
Size [mm]	0.10 x 0.15 x 0.15
a [Å]	5.7966(3)
b [Å]	6.9027(3)
c [Å]	20.2527(8)
α [°]	90
β [°]	90
γ [°]	90
V [$Å^3$]	810.36(6)
Z	4
$\rho_{calc.}$ [g cm^{-3}]	1.541
μ [mm^{-1}]	0.604
F(000)	384
$\lambda_{MoK\alpha}$ [Å]	0.71073
T [K]	128
θ Min–Max [°]	3.6, 26.4
Dataset	−7: 6; −8: 7; −25: 25
Reflections collected	6484
Independent refl.	1658
R_{int}	0.033
Observed reflections	1566
Parameters	118
R_1 (obs)[a]	0.0253
wR_2 (all data)[b]	0.0610
GooF[c]	1.04
Resd. Dens. [e $Å^{-3}$]	−0.17, 0.21
Absorption correction	multi-scan
CCDC	1917118

a) $R_1 = \Sigma||F_0|-|F_c||/\Sigma|F_0|$; b) $wR_2 = [\Sigma[w(F_0^2-F_c^2)^2]/\Sigma[w(F_0)^2]]^{1/2}$; $w = [\sigma c^2(F_0^2)+(xP)^2+yP]^{-1}$ and $P=(F_0^2+2F_c^2)/3$; c) GooF = $\{\Sigma[w(F_o^2-F_c^2)^2]/(n-p)\}^{1/2}$ (n = number of reflections; p = total number of parameters).

2.1.30 Lithium dihydrobis(1,2,4-triazol-1-yl)borate sesquihydrate

2.1.30.1 Procedure

To obtain the titled lithium salt, compound **57** was reacted to the corresponding free acid with glacial acetic acid as described in the literature[5d,e], namely (1*H*-1,2,4-triazole)dihydro(1,2,4-triazol-1-yl)borate (**58**) (see **Scheme 36**).

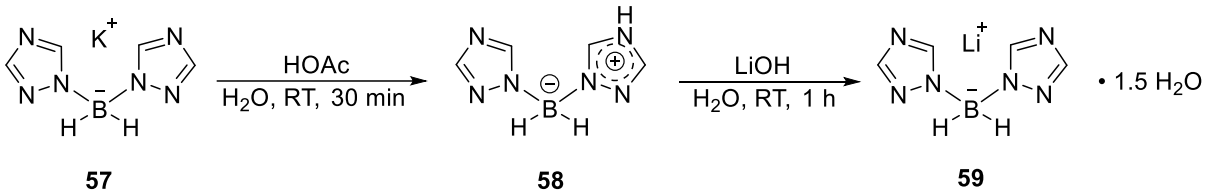

***Scheme 36**: Reaction toward lithium dihydrobis(1,2,4-triazol-1-yl)borate sesquihydrate (**59**) over the free acid, namely (1H-1,2,4-triazole)dihydro(1,2,4-triazol-1-yl)borate (**58**).*

The acid-base reaction between 0.748 g lithium hydroxide (31 mmol) and 4.683 g (1*H*-1,2,4-triazole)dihydro(1,2,4-triazol-1-yl)borane (31 mmol) in 50 mL of bidistilled water was allowed to proceed for one hour. When the solvent had completely evaporated, 5.107 g of colorless crystals (89 %) were obtained.

IR (ATR): $\tilde{\nu}$ = 3606 (w), 3560 (w), 3128 (m), 2421 (m), 2403 (m), 2376 (m), 2348 (m), 2306 (w), 2271 (w), 1767 (vw), 1650 (w), 1573 (vw), 1509 (s), 1421 (w), 1313 (m), 1276 (s), 1219 (w), 1191 (w), 1170 (m), 1146 (vs), 1044 (m), 1030 (s), 998 (w), 973 (s), 901 (w), 870 (m), 817 (m), 732 (m), 722 (s), 673 (vs), 637 (s), 619 (m), 481 (w) cm^{-1}. $^{11}B\{/\}$ NMR (DMSO-d_6, 25 °C): δ = −9.5 (br s, BH_2) ppm. $^{13}C\{H\}$ NMR (DMSO-d_6, 25 °C): δ = 151.3 (*C*H), 147.8 (*C*H) ppm. $^{1}H\{/\}$ NMR (DMSO-d_6, 25 °C): δ = 8.07 (s, 2H, C*H*), 7.74 (s, 2H, C*H*), 3.93 (s, 2H, H_2O), 3.55 (br s, 2H, BH_2) ppm. EA ($C_4H_9N_6O_{1.5}BLi$, 182.91): calcd. N 45.95, C 26.27, H 4.96 %; found N 45.68, C 26.24, H 4.82 %. DTA (5 °C min^{-1}): 94 (endothermic), 119 (endothermic), 317 (exothermic) °C. IS (100–500 µm): > 40 J. FS (100–500 µm): > 360 N. ESD (100–500 µm): > 1.5 J.

2.1.30.2 Crystal structure

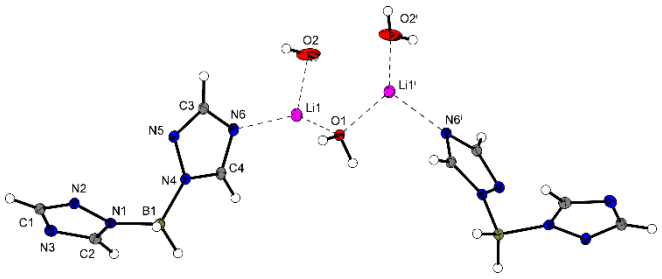

***Figure 22**: Crystal structure of lithium dihydrobis(1,2,4-triazol-1-yl)borate sesquihydrate (**59**).*

***Table 11**: Crystallographic data of lithium dihydrobis(1,2,4-triazol-1-yl)borate sesquihydrate (**59**).*

Formula	$C_8H_{18}B_2Li_2N_{12}O_3$
FW [g mol^{-1}]	365.84
Crystal system	Orthorhombic
Space Group	*Pbcn*
Color / Habit	Colorless needle
Size [mm]	0.25 x 0.40 x 0.50
a [Å]	18.3290(5)
b [Å]	7.0134(2)
c [Å]	13.4938(5)
α [°]	90
β [°]	90
γ [°]	90
V [Å^3]	1734.61(9)
Z	4
$\rho_{calc.}$ [g cm^{-3}]	1.401
μ [mm^{-1}]	0.105
F(000)	760
$\lambda_{MoK\alpha}$ [Å]	0.71073
T [K]	128
θ Min–Max [°]	4.3, 26.0
Dataset	−22: 22; −8: 7; −16: 16
Reflections collected	12386
Independent refl.	1704
R_{int}	0.022
Observed reflections	1539
Parameters	143
R_1 (obs)[a]	0.0306
wR_2 (all data)[b]	0.0794
GooF[c]	1.05
Resd. Dens. [e Å^{-3}]	−0.24, 0.18
Absorption correction	multi-scan
CCDC	1917117

a) $R_1 = \Sigma||F_0|-|F_c||/\Sigma|F_0|$; b) $wR_2 = [\Sigma[w(F_0^2-F_c^2)^2]/\Sigma[w(F_0)^2]]^{1/2}$; $w = [\sigma c^2(F_0^2)+(xP)^2+yP]^{-1}$ and $P=(F_0^2+2F_c^2)/3$; c) GooF = $\{\Sigma[w(F_o^2-F_c^2)^2]/(n-p)\}^{1/2}$ (n = number of reflections; p = total number of parameters).

2.1.31 Lithium dihydrobis(tetrazol-1-yl)borate monohydrate

2.1.31.1 Procedure

Potassium dihydrobis(tetrazol-1-yl)borate has been shown to be viable by heating a solution of potassium borohydride and two equivalents of 1*H*-tetrazole in N,N-dimethylacetamide at 100 °C for two hours.[5c] Compared to potassium the smaller lithium cation is a harder Lewis acid and should form a more reactive adduct with the soft Lewis base borohydride. Therefore, we considered a temperature of 80 °C to be sufficient for overcoming the activation energy barrier for the reaction between lithium borohydride and the heterocycle. This allowed us to replace dimethylacetamide by less toxic and easier removable acetonitrile. Lithium dihydrobis(tetrazol-1-yl)borate monohydrate was formed under these reaction conditions but the presence of boric acid and tetrahydroxoborate in the crude product after washing with undistilled solvent suggests an incomplete conversion of the starting materials. Additionally, the deprotonation of 1*H*-tetrazole upon contact with moisture complicates the work-up and impedes the yield.

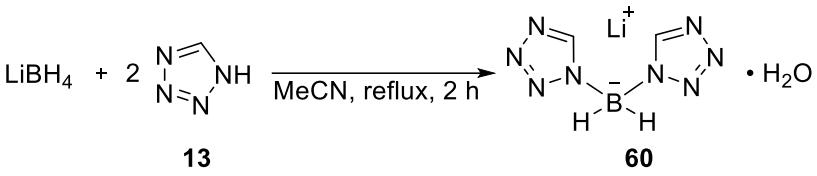

***Scheme 37**: Reaction toward lithium dihydrobis(tetrazol-1-yl)borate monohydrate (**60**).*

6 mL of anhydrous acetonitrile were slowly added to a mixture of 2.870 g 1*H*-tetrazole (41 mmol) and 0.446 g lithium tetrahydroborate (20 mmol) and the latter was kept under an argon atmosphere until the strongly exothermic release of hydrogen had eased up and equipping the flask with a bubble counter provided sufficient gas exchange. Once no more hydrogen was formed, the reaction mixture was refluxed for two hours. The cooled solution was filtrated and the solid was washed with 12 mL of acetonitrile in order to remove unconverted azole. Lithium dihydrobis(tetrazol-1-yl)borate (1.146 g, 32 %) in the form of a white powder was isolated from the crude product containing lithium tetrazolate impurity by extracting it three times with 50 mL of 2-propanole each and allowing the solvent to volatilize. Colorless crystals suitable for crystal structure analysis were grown from an acetonitrile solution.

IR (ATR): $\tilde{\nu}$ = 3473(m), 3387(m), 3286(w), 3245(w), 3149(m), 2470(m), 2447(m), 2307(vw), 2273(vw), 1783(vw), 1672(w), 1627(w), 1573(vw), 1476(m), 1399(vw), 1368(w), 1267(w), 1194(m), 1157(s), 1121(vs), 1055(m), 1036(w), 1005(s), 1005(s), 985(w), 908(w), 897(m), 866(w), 745(w), 712(m), 699(m) cm^{-1}. $^{11}B\{/\}$ NMR (DMSO-d_6, 25 °C): δ = −11.1 (br t, BH_2) ppm. $^{13}C\{H\}$ NMR (DMSO-d_6, 25 °C): δ = 147.3 (*C*H) ppm. $^{1}H\{/\}$ NMR (DMSO-d_6, 25 °C): δ = 8.84 (s, 2H, C*H*), 3.83 (br s, 2H, BH_2), 3.48 (br s, 2H, H_2O) ppm. EA ($C_2H_6N_8OBLi$, 175.88): calcd. N 63.71, C 13.66, H 3.44 %; found N 62.91, C 14.24, H 3.17 %. DTA (5 °C min^{-1}): 133 (endothermic, followed by exothermic signal), 213 (exothermic) °C. IS (grain size < 100 µm): 10 J. FS (grain size < 100 µm): > 360 N. ESD (grain size < 100 µm): 0.20 J.

2.1.31.2 Crystal structure

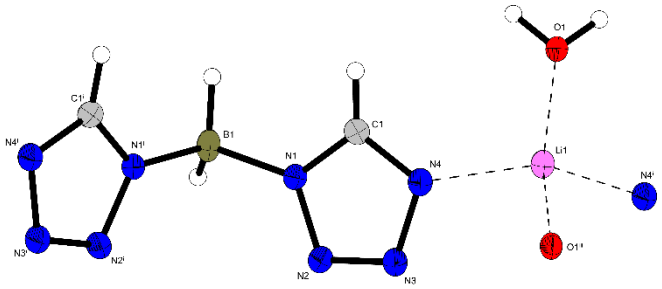

***Figure 23**: Advanced molecular unit of lithium dihydrobis(tetrazol-1-yl)borate monohydrate (**60**).*

***Table 12**: Crystallographic data of lithium dihydrobis(tetrazol-1-yl)borate monohydrate (**60**).*

Formula	$C_2H_6BLiN_8O$
FW [g mol^{-1}]	175.90
Crystal system	Orthorhombic
Space Group	$Cmc2_1$
Color / Habit	Colorless block
Size [mm]	0.03 x 0.04 x 0.08
a [Å]	9.6405(6)
b [Å]	16.9943(13)
c [Å]	5.4760(4)
α [°]	90
β [°]	90
γ [°]	90
V [Å^3]	897.15(11)
Z	4
$\rho_{calc.}$ [g cm^{-3}]	1.302
μ [mm^{-1}]	0.100
F(000)	360
$\lambda_{MoK\alpha}$ [Å]	0.71073
T [K]	110
θ Min–Max [°]	4.2, 25.4
Dataset	−11: 11; −20: 20; −6: 6
Reflections collected	5713
Independent refl.	877
R_{int}	0.033
Observed reflections	841
Parameters	75
R_1 (obs)[a]	0.0250
wR_2 (all data)[b]	0.0590
GooF[c]	1.15
Resd. Dens. [e Å^{-3}]	−0.16, 0.15
Absorption correction	multi-scan
CCDC	1917115

a) $R_1 = \Sigma||F_0|-|F_c||/\Sigma|F_0|$; b) $wR_2 = [\Sigma[w(F_0^2-F_c^2)^2]/\Sigma[w(F_0)^2]]^{1/2}$; $w = [\sigma c^2(F_0^2)+(xP)^2+yP]^{-1}$ and $P=(F_0^2+2F_c^2)/3$; c) GooF = $\{\Sigma[w(F_o^2-F_c^2)^2]/(n-p)\}^{1/2}$ (n = number of reflections; p = total number of parameters).

2.1.32 Lithium dihydrobis(5-aminotetrazol-1-yl)borate monohydrate

2.1.32.1 Procedure

The synthesis of lithium dihydrobis(5-aminotetrazol-1-yl)borate by the Lewis acid base reaction of potassium borohydride with stoichiometric amounts of 5-amino-1*H*-tetrazole, subsequent acidification with glacial acetic acid, final saltification with lithium hydroxide and drying at 100 °C overnight is described (see **Scheme 38** and **Scheme 39**).

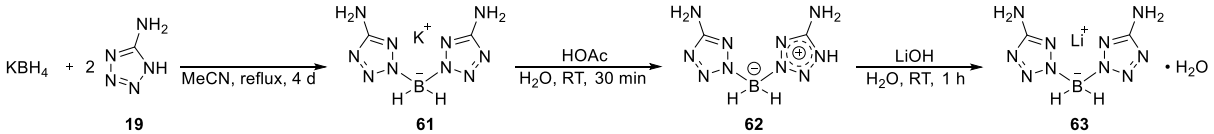

***Scheme 38**: Reaction toward lithium dihydrobis(5-aminotetrazol-1-yl)borate monohydrate (**63**).*

10 mL of anhydrous acetonitrile were added to 1.116 g potassium borohydride (21 mmol) and 3.518 g 5-amino-1*H*-tetrazole (41 mmol) and the reaction mixture was first left undisturbed

and then stirred at room temperature until the release of hydrogen had dropped. Subsequently, the Lewis acid base reaction between the two starting materials was allowed to proceed for fours days under reflux whereby a precipitate was formed. The latter (4.561 g) was filtered off, suspended in roughly 9 mL of bidistilled water and acidified with the same volume of glacial acetic acid. After the suspension had been stirred for 30 minutes, the resulting solid was filtered off and washed three times with approximately 9 mL of water each. Finally, the crude free acid (2.835 g) was suspended in roughly 50 mL water, neutralized with lithium hydroxide (0.358 g, 15 mmol) and the suspension was stirred at room temperature for one hour. Filtering off unreacted intermediate and removing the solvent from the filtrate *in vacuo* afforded 2.443 g (79 %) of a white powder.

IR (ATR): $\tilde{\nu}$ = 3497(w), 3399(m), 3365(w), 3334(m), 3195(w), 2784(w), 2484(m), 2420(m), 1610(s), 1552(s), 1488(m), 1462(m), 1308(m), 1221(w), 1173(w), 1151(m), 1117(vs), 1052(w), 1037(w), 1023(w), 904(m), 876(w), 864(m), 864(m), 807(m), 774(m), 753(s), 728(s), 704(m), 637(vs), 505(w), 459(m), 438(m), 407(m) cm^{-1}. $^{7}Li\{H\}$ NMR (DMSO-d_6, 25 °C): δ = -1.0 (s, *Li*) ppm. $^{11}B\{/\}$ NMR (DMSO-d_6, 25 °C): δ = -13.8 (br s, *B*H_2) ppm. $^{13}C\{H\}$ NMR (DMSO-d_6, 25 °C): δ = 159.2 (s, *C*-NH_2) ppm. $^{1}H\{/\}$ NMR (DMSO-d_6, 25 °C): δ = 5.60 (br s, 4H, N*H*$_2$), 3.57 (br s, 2H, *H*$_2$O), 3.30 (br s, 2H, B*H*$_2$) ppm. EA ($LiBC_2H_8N_{10}O$, 205.91): calcd. N 68.02, C 11.67, H 3.91 %; found N 67.35, C 12.21, H 3.69 %. DTA (5 °C min^{-1}): 117 (endothermic), 290 (exothermic) °C.

DTA experiments revealed that this salt loses its crystal water upon drying at 100 °C overnight (see **Figure 24**).

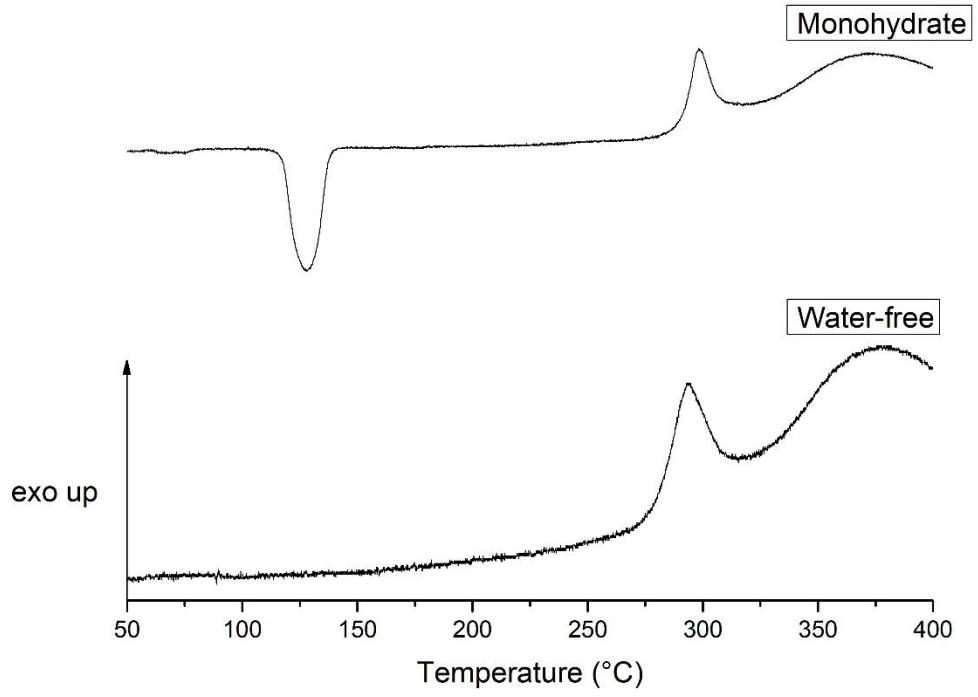

***Figure 24**: DTA curves of lithium dihydrobis(5-aminotetrazol-1-yl)borate monohydrate (**63**) and lithium dihydrobis(5-aminotetrazol-1-yl)borate (**64**) (top to bottom).*

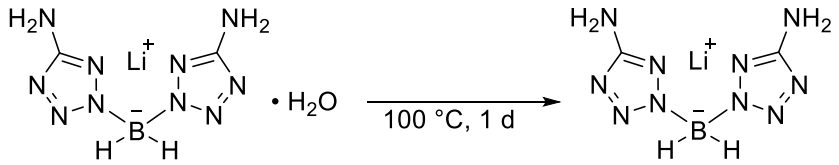

***Scheme 39**: Reaction toward lithium dihydrobis(5-aminotetrazol-1-yl)borate (**64**).*

10 mL of anhydrous acetonitrile were added to 1.116 g potassium borohydride (21 mmol) and 3.518 g 5-amino-1*H*-tetrazole (41 mmol) and the reaction mixture was first left undisturbed and then stirred at room temperature until the release of hydrogen had dropped. Subsequently, the Lewis acid base reaction between the two starting materials was allowed to proceed for fours days under reflux whereby a precipitate was formed. The latter (4.561 g) was filtered off, suspended in roughly 9 mL of bidistilled water and acidified with the same volume of glacial acetic acid. After the suspension had been stirred for 30 minutes, the resulting solid was filtered off and washed three times with approximately 9 mL of water each. Finally, the crude free acid (2.835 g) was suspended in roughly 50 mL water, neutralized with lithium hydroxide (0.358 g, 15 mmol) and the suspension was stirred at room temperature for one hour. Filtering off unreacted intermediate, removing the solvent from the filtrate *in vacuo* and drying in an oven at 100 °C overnight afforded 2.140 g (76 %) of a white powder.

IR (ATR): $\tilde{\nu}$ = 3474(w), 3442(w), 3409(w), 3379(m), 3291(w), 3213(w), 3169(w), 2457(w), 2417(w), 1621(vs), 1560(s), 1465(m), 1303(m), 1238(m), 1221(w), 1205(w), 1183(m), 1146(s), 1099(s), 1062(m), 1034(w), 876(w), 780(m), 780(m), 762(w), 751(w), 674(m), 660(s), 631(m), 501(m), 460(w), 442(w), 431(w), 418(w) cm^{-1}. ^{7}Li{H} NMR (DMSO-d_6, 25 °C): δ = -1.0 (s, *Li*) ppm. ^{11}B{/} NMR (DMSO-d_6, 25 °C): δ = -14.5 (br s, *B*H_2) ppm. ^{13}C{H} NMR (DMSO-d_6, 25 °C): δ = 159.2 (s, *C*-NH_2) ppm. ^{1}H{/} NMR (DMSO-d_6, 25 °C): δ = 5.60 (br s, 4H, NH_2), 3.34 (br s, 2H, BH_2) ppm. EA ($LiBC_2H_6N_{10}$, 187.89): calcd. N 74.55, C 12.78, H 3.22 %; found N 73.64, C 13.06, H 2.87 %. DTA (5 °C min^{-1}): 280 (exothermic) °C. FS (100-500 µm): > 360 N. IS (100-500 µm): > 40 J. ESD (100-500 µm): 1 J.

2.1.32.2 Ageing effects

A sample of the title compound exposed to air for two weeks did not undergo any change in weight beyond the measurement uncertainty or in composition according to ^{1}H NMR and ^{1}H-coupled ^{11}B NMR. Therefore, this lithium salt can be considered stable at ambient conditions.

2.1.32.3 Crystal structure

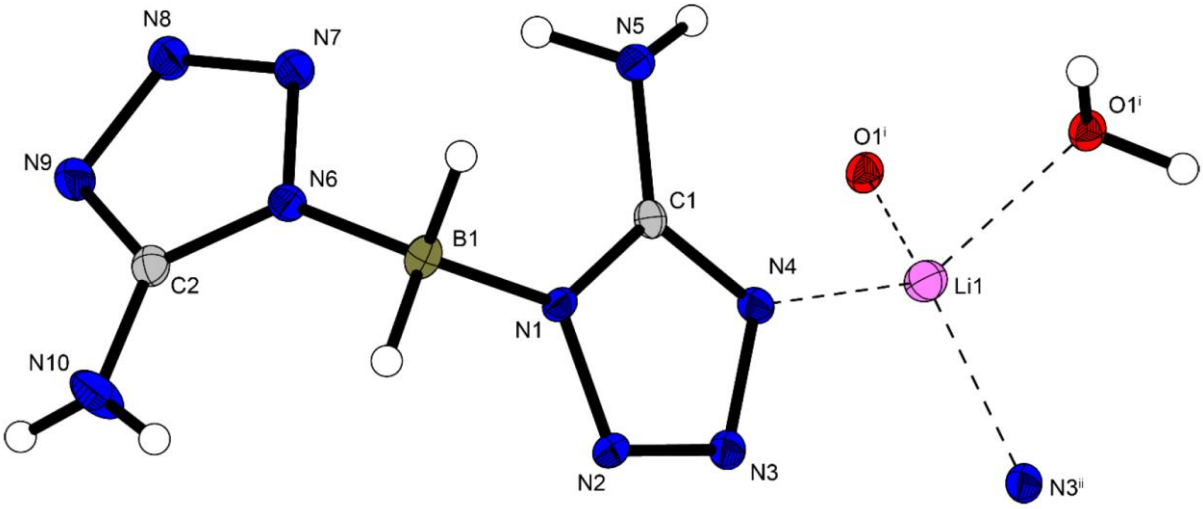

***Figure 25**: Crystal structure of lithium dihydrobis(5-aminotetrazol-1-yl)borate monohydrate (**63**).*

***Table 13**: Crystallographic data of lithium dihydrobis(5-aminotetrazol-1-yl)borate monohydrate (**63**).*

Formula	$LiBC_2H_8N_{10}O$
FW [g mol^{-1}]	205.91
Crystal system	Monoclinic
Space Group	$P2_1/n$
Color / Habit	Colorless needle
Size [mm]	0.05 x 0.05 x 0.45
a [Å]	6.3152(4)
b [Å]	20.3193(12)
c [Å]	6.7114(5)
α [°]	90
β [°]	95.274(6)
γ [°]	90
V [Å^3]	857.56(10)
Z	4
$\rho_{calc.}$ [g cm^{-3}]	1.595
μ [mm^{-1}]	0.124
F(000)	424
$\lambda_{MoK\alpha}$ [Å]	0.71073
T [K]	113
θ Min–Max [°]	3.4, 26.4
Dataset	−7: 7; −25: 25; −7: 8
Reflections collected	6205
Independent refl.	1746
R_{int}	0.049
Observed reflections	1338
Parameters	168
R_1 (obs)[a]	0.0429
wR_2 (all data)[b]	0.0972
GooF[c]	1.04
Resd. Dens. [e Å^{-3}]	−0.22, 0.26
Absorption correction	multi-scan
CCDC	1998249

a) $R_1 = \Sigma||F_0|-|F_c||/\Sigma|F_0|$; b) $wR_2 = [\Sigma[w(F_0^2-F_c^2)^2]/\Sigma[w(F_0)^2]]^{1/2}$; $w = [\sigma c^2(F_0^2)+(xP)^2+yP]^{-1}$ and $P=(F_0^2+2F_c^2)/3$; c) GooF = $\{\Sigma[w(F_o^2-F_c^2)^2]/(n-p)\}^{1/2}$ (n = number of reflections; p = total number of parameters).

2.1.33 Overview of all lithium salts

In the following section, an overview in the form of a table is provided to clarify the synthesis results and address the hygroscopic behavior/ageing studies, which are considered a go/no-go criteria for the following testing of the materials as pyrotechnical colorants.

***Table 14**: Overview of the synthesized compounds, the corresponding hygroscopicity/ageing studies.*

Compound name (number)	Molecular formula	Molecular Mass	Ageing/hygroscopicity behavior	Go/no-go
4	$C_3H_2LiN_3O_2$	119.03	Hygroscopic behavior	X
6	$C_3H_3LiN_4O_5$	182.02	No ageing / hygroscopicity visible	✓
10	$C_3H_3LiN_4O_5$	182.02	No ageing / hygroscopicity visible	✓
14	$C_3H_5LiN_5O_{5.5}$	206.04	No ageing / hygroscopicity visible	✓
16	$C_3H_8LiN_5O_7$	233.07	Hygroscopic behavior	X
18	$CHLiN_4$	75.99	No ageing / hygroscopicity visible	✓
20	CH_2LiN_5	91.00	No ageing / hygroscopicity visible	✓
22	$CH_3LiN_6O_3$	154.01	No ageing / hygroscopicity visible	✓
26	$C_2H_4Li_2N_8O_2$	185.99	No ageing / hygroscopicity visible	✓
30	$C_2H_8Li_2N_8O_6$	254.02	No ageing / hygroscopicity visible	✓
32	$C_3H_8Li_2N_7O_{8.5}$	292.02	No ageing / hygroscopicity visible	✓
36	$C_6H_7LiN_3O_{6.5}$	232.08	No ageing / hygroscopicity visible	✓
40	$CH_3LiN_2O_5$	129.98	Ageing studies were not performed due to spontaneous decomposition	
44	$C_3H_4LiN_5O_{11}$	293.03	No ageing / hygroscopicity visible	✓
48	$C_9H_{13}Li_4N_8O_{18.5}$	557.00	Product was not pure enough for ageing studies	

50	$C_6H_{10}BLiN_4O$	171.92	Direct decomposition was detected	X
52	$C_6H_8BLiN_6O_5$	261.92	No ageing / hygroscopicity visible	✓
53	$C_6H_6BLiN_6O_4$	243.90	Color change visible but no change in NMR or weight gain	✓
55	$C_6H_6BLiN_{10}O_8$	363.93	Already partially hydrolysed to boric acid	X
59	$C_4H_9BLiN_6O_{1.5}$	182.91	No ageing / hygroscopicity visible	✓
60	$C_2H_6BLiN_8O$	175.88	No ageing / hygroscopicity visible	✓
63	$C_2H_8BLiN_{10}O$	205.91	Was dried to yield salt **64**	X
64	$C_2H_6BLiN_{10}$	187.89	No ageing / hygroscopicity visible	✓

Out of the 23 reported lithium salts which are considered as potential replacements for strontium only six are not stable, due to different reasons (ageing, stability and hygroscopicity). The majority of the lithium salts showed no effects and were additionally tested for other go/no-go criteria. Nevertheless, the ratio of stable and unstable lithium salts here supports a go.

2.2 Selection process

2.2.1 Sensitivity measurements

Impact sensitivity was tested using a BAM standardized (Bundesanstalt für Materialforschung und -prüfung) drop hammer. Friction sensitivity measurements were performed using a BAM standardized friction tester. In addition, all substances were tested for hazard to electrostatic discharge using an OZM Electric Spark Tester XSpark10[33]. In all three procedures, sensitivities were determined using the 1 out of 6 method to evaluate the no-fire level.

Sensitivity measurements were performed according to the standards of the German Federal Institute for Materials Research (BAM) using the 1 out of 6 method. The "UN Recommendations on the Transport of Dangerous Goods", as well as the respective NATO STANAGs, served as a template.[34,35,36] Measuring devices (drop hammer, friction tester) manufactured in accordance with BAM regulations were used for the performance. These are described in the respective STANAG, as well as in the UN Recommendation. The ESD test was performed according to the BAM method (1 out of 6 determination), but there is no BAM standard for the equipment. The 1 out of 6 method generally runs according to the following principle: A test is performed with the highest applicable frictional force or energy. If this test is positive, the force or energy (depending on the test method) is reduced to the next lower level and tested again there. If the test is negative, testing continues at the same level until six negative tests have been reached. If one of these tests is positive, the energy/force is reduced according to the previously described procedure. If all 6 tests are negative the test series is finished and the energy/force at which the last positive test was observed is noted.

At an energy of 40 J, a negative test was initially observed, so further tests were performed at the same energy. However, since the second test was positive, the energy was reduced to the next lower level (35 J). Since here the first test resulted in an explosion, it was reduced to 30 J energy. Here, six tests in a row were negative, and the test series ended. The substance has an impact sensitivity of 35 J at the grain size tested. In addition to an explosion, decomposition is also considered a positive reaction for the drop hammer.[35,37]

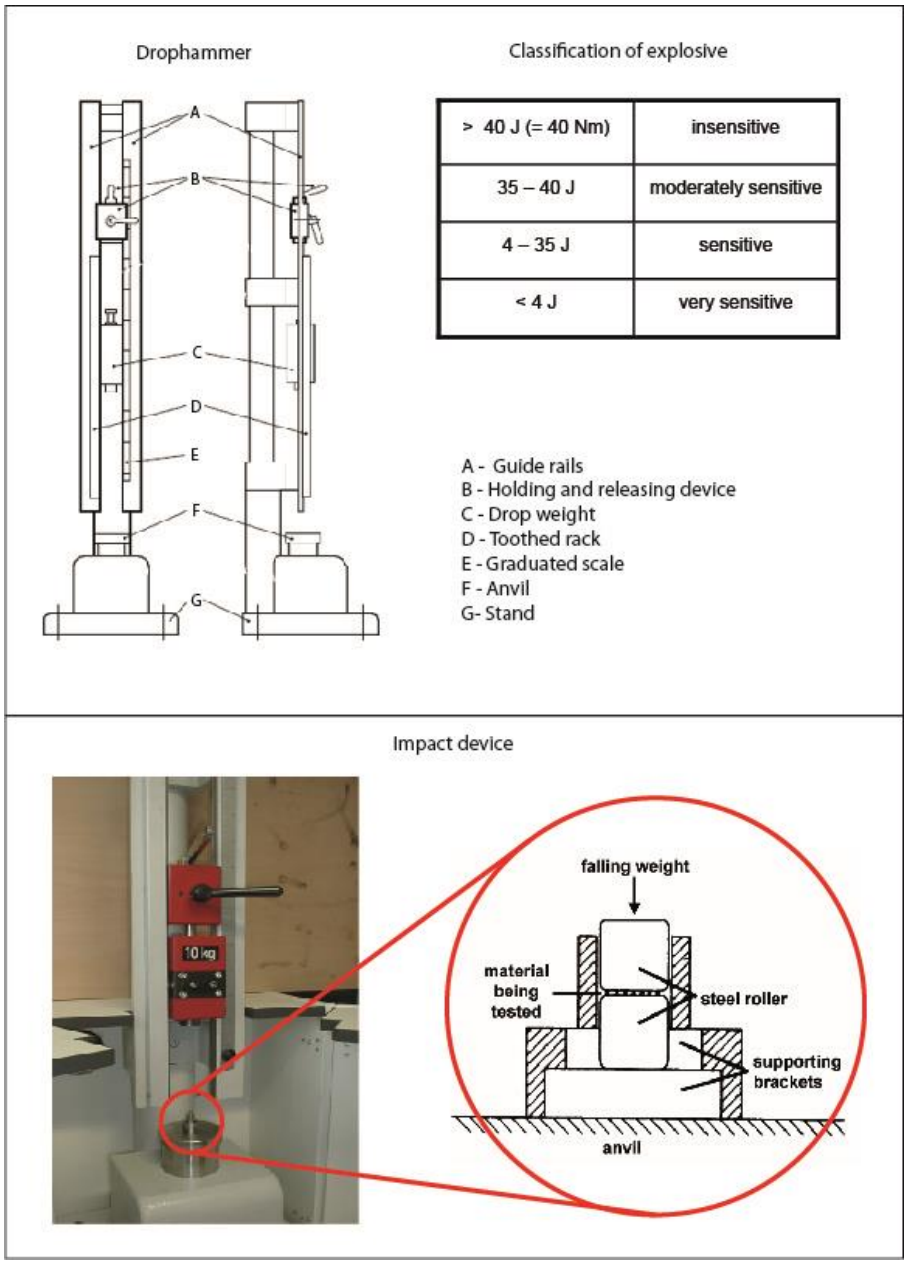

***Figure 26**: BAM Fallhammer tester with impact device and classification chart.*[34]

The friction tests are carried out in the same way as the impact sensitivity measurements. However, it should be noted that only audible, visual decomposition, i.e. detonation, flying sparks, deflagration and very severe decomposition, is considered a positive test. An odor development or color change of the sample is not sufficient.[36,38]

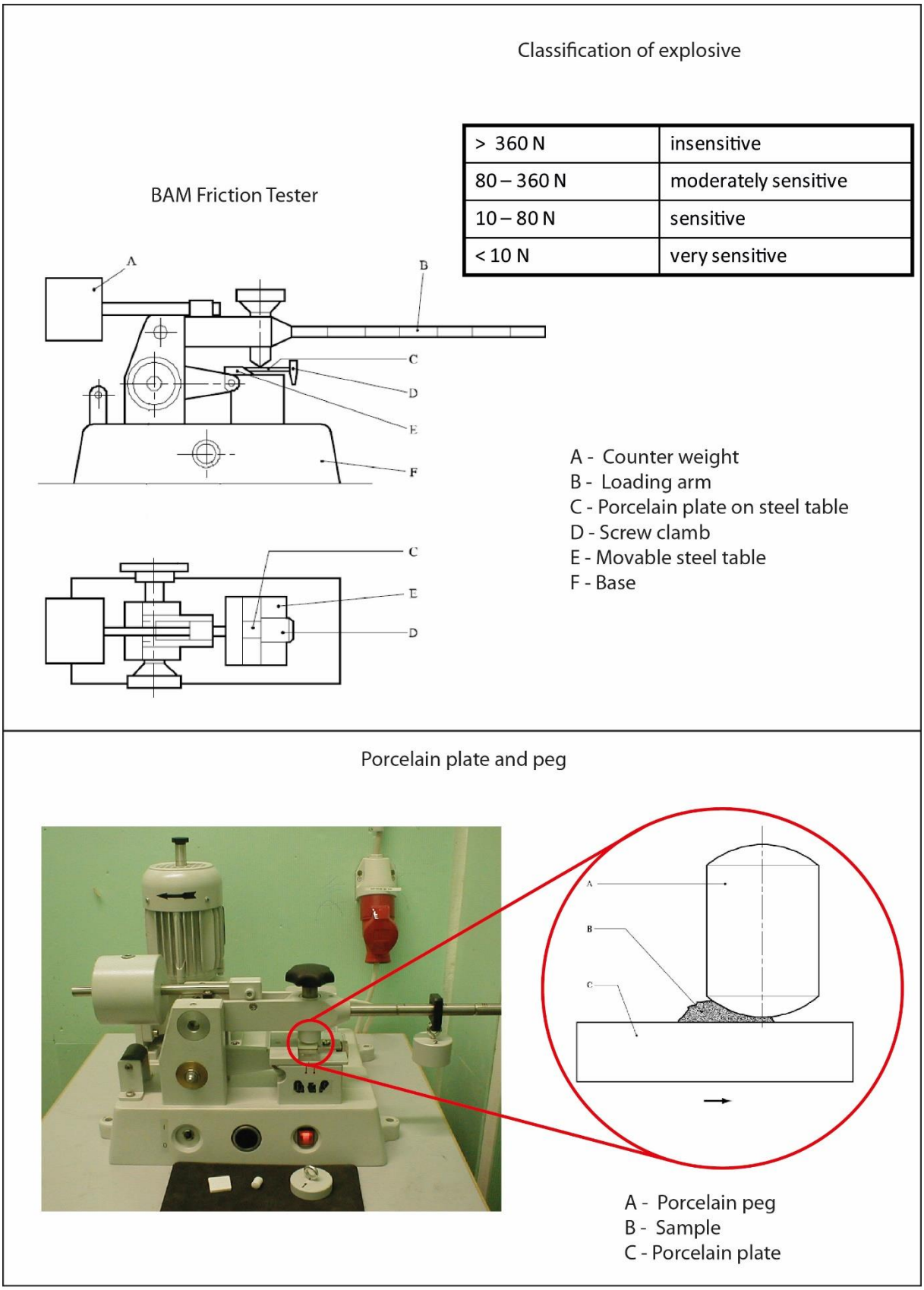

***Figure 27**: BAM friction tester with porcelain plate, peg and classification chart.*[34]

To determine the sensitivity to electrostatic discharge, the same procedure was followed as described in the example for the drop hammer. The criteria for a positive reaction are analogous to those for the drop hammer.

Figure 28: *OZM Electric Spark Tester XSpark10 for measuring the electrostatic discharge.*

In all cases where it was possible, the decomposition temperatures were also determined. This was done via differential thermal analysis (DTA). All sensitivity parameters already known from literature were also determined. A summary of these data is shown in **Table 15**. For the use of lithium salts, we have chosen compounds that are particularly thermally stable and insensitive to external stimuli.

Figure 29*: Differential thermal analysis device (DTA) for determination of decomposition temperatures.*

For this reason the salts lithium 4-amino-3,5-dinitropyrazolate sesquihydrate (**14**), lithium tetrazolate (**18**), lithium 5-aminotetrazolate (**20**), dilithium 5,5`-bistetrazolate dihydrate (**26**), dilithium 5,5`-bis(tetrazole-1-oxide) tetrahydrate (**30**), lithium picramate sesquihydrate (**36**), lithium dihydrobis(1,2,4-triazol-1-yl)borate sesquihydrate (**59**) and lithium dihydrobis(5-aminotetrazol-1-yl)borate (**64**) were interesting for further investigation.

For a few other salts such as lithium dinitromethanide monohydrate (**40**) and lithium dihydrobis(4-amino-3,5-dinitropyrazol-1-yl)borate (**55**), no exact values could be measured because these salts were not stable enough. Especially with salt **40**, spontaneous

decomposition occurred every time it was prepared, which made it almost impossible to work with.

Table 15: Overview of the sensitivity properties of the lithium salts.

Compound	T_{dec} [°C]	FS [N]	IS [J]	ESD [mJ]	Go/no-go
4	332	-	-	-	X
6	232	240	5	-	X
10	284	192	6	-	X
14	168	360	> 40	-	✓
16[8]	274 (Tetrahydrate)	96 (Tetrahydrate)	40 (Tetrahydrate)	200 (Tetrahydrate)	X
18[11]	380	> 360	> 100	-	✓
20[12]	196 (m.p.)	> 360	> 75	-	✓
22	240	-	-	-	X
26	444	> 360	> 40	-	✓
30	327	> 360	> 40	-	✓
32	220	-	-	-	X
36	295	> 360	> 40	1080	✓
40	-	-	-	-	X
44	-	-	-	-	X
48[29]	186	360	> 20	1500	X
50	-	-	-	-	X
52	196	-	-	-	X
53	200	144	2	420	X
55	-	-	-	-	X
59	317	> 360	> 40	> 1500	✓
60	213	> 360	10	200	X
63	290	-	-	-	X
64	280	> 360	> 40	1000	✓

However, these were not the only selection criteria. Although relatively good results were obtained with the borate salts lithium dihydrobis(1,2,4-triazol-1-yl)borate sesquihydrate (**59**) and lithium dihydrobis(5-aminotetrazol-1-yl)borate (**64**) in the later mixtures, further testing of the salts was not performed. There were several reasons for this. On the one hand, the reaction to form the potassium analogs produces a relatively large amount of hydrogen, and the upscale of this reaction cannot be completed on the university facilities. on the other hand, there was another toxicological reason for not working further with these compounds. During

the burnup of these salts B_2O_3 is formed, which, along with boric acid, which is also a side product of the combustion are considered a cancerogenic substance.[39] Salts **18** and **30** were not investigated in the toxicity measurements due their bad performance in the pyrotechnical formulations, which can be seen in the later chapters. Salts **14** and **36** were also not considered further, as they are considered toxic. for salt **14**, a separate toxicity measurement was carried out at the LMU. This result is presented in chapter 2.2.2. The further selection was made by pyrotechnic mixtures and their measured data. These are listed in the following chapter. Although some lithium salts are eliminated by this selection criterion, some salts still fulfill an insensitivity to external stimuli, so this can still be considered a GO.

2.2.2 Toxicity measurement

2.2.2.1 Principle of toxicology measurement

Toxicity measurements were performed for the lithium salts that made it to the narrow selection. The measurement was performed according to the instructions by HACH LANGE GmbH (Düsseldorf, Germany) for the luminescent bacteria inhibition test ("Leuchtbakterientest LCK482"). For the measurement, liquid dried bacteria of the species *Aliivibrio fischeri* (strain number NRRL-B-11177) by HACH LANGE GmbH (Düsseldorf, Germany) were used. At the beginning of each measurement, a 2 % sodium chloride stock solution was produced. The tested substances were weighed out to a specific weight and then dissolved into the stock solution. Substances with low solubility were first dissolved in acetone and then diluted within the 2 % sodium chloride solution to obtain a 1 % acetone solution.[40] A 1 % acetone solution showed an insignificant effect on the bacteria.[41] After complete solvation and setting the pH value to 6–8 the solution was filled up to a final volume of 25 ml.

Afterwards a dilution series which ranged from 1:1.5 to 1:16 was prepared following DIN 38412, L341.

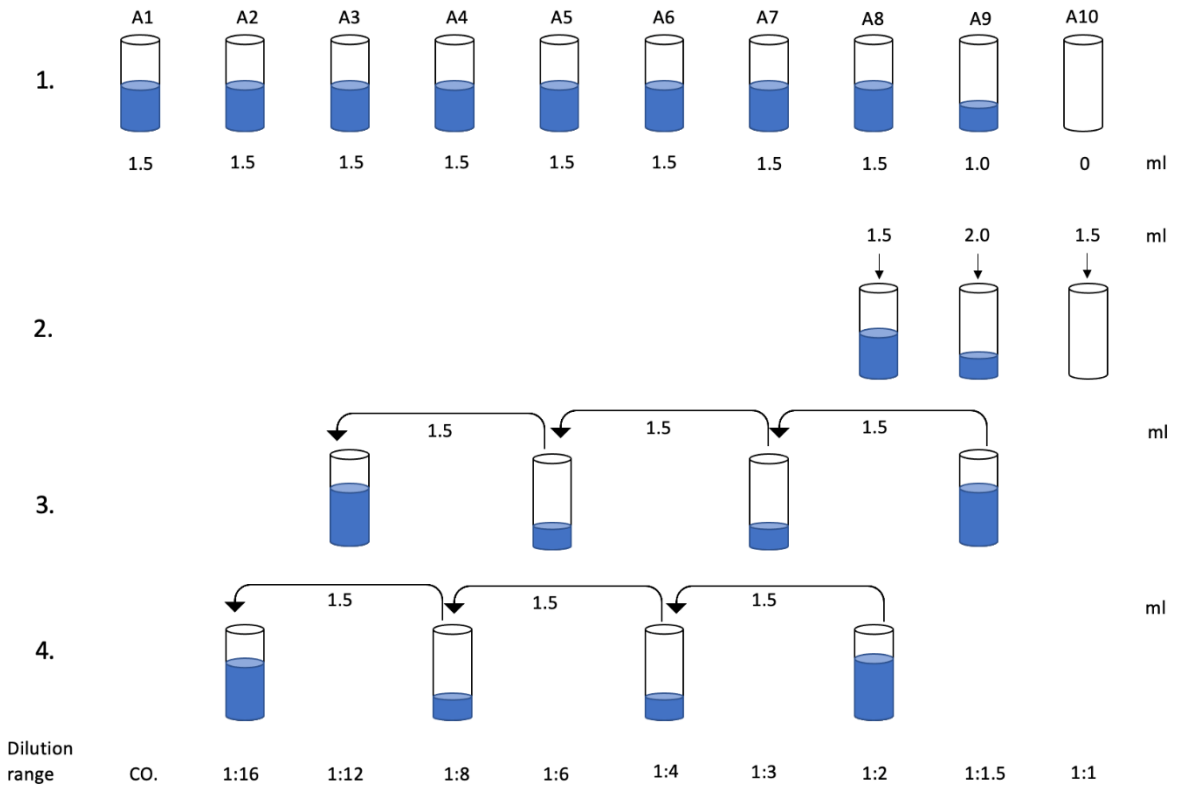

***Figure 30**: Scheme of the dilution series, adapted from HACH LANGE GmbH (Düsseldorf, Germany).*

A1–A8 were each filled with 1.5 ml of the sodium chloride stock solution, A9 with 1 ml and A10 remained empty. Thereafter a certain volume of the tested substance was filled into A8, A9 and A10. A8 and A10 obtained 1.5 ml, while A9 obtained 2.0 ml. This was used afterwards to prepare the dilution series. From A9 1.5 ml were filled into A7 and mixed, continuing with filling 1.5 ml of A7 into A5 and mixing, repeating until A3. The same was done with A8, A6, A4 and A2. A1 only obtained the sodium chloride stock solution and was used as nontoxic control, while A10 was not further diluted. The cuvettes were then placed into the LUMIStox 300 measuring device obtained from HACH LANGE GmbH (Düsseldorf, Germany).

The next step was to reactivate the bacteria. Therefore 12 ml of the reactivation solution were filled into a centrifuge tube. Before adding the reactivation solution, the frozen bacteria were incubated for 2 min in a water bath at room temperature. Afterwards 0.5 ml of the reactivation solution were filled to the bacteria and incubated for 15 min at 15°C. After incubation, the reactivated bacteria were pipetted into the remnant reactivation solution and 0.5 ml of the liquid were pipetted into 20 cuvettes. These 20 cuvettes were then incubated for 13 min at 15°C.

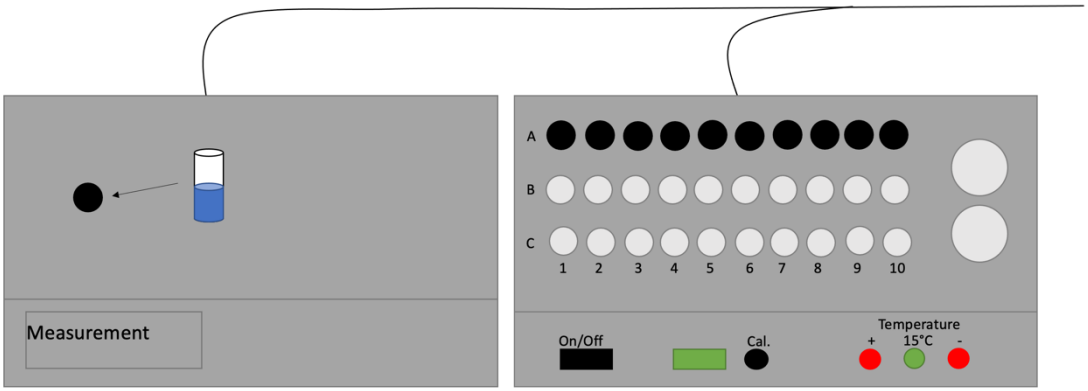

***Figure 31**. Demonstration of the LUMIStox 300. Row A contained the substance diluted in a range from 1:1 to 1:16, Row B and C contained each 0.5 ml of the reactivated bacteria in sodium chloride stock solution.*

For the measurement, the bioluminescence of each sample was measured at the beginning. After each measurement, 0.5 ml of the substance were added. This led to a total dilution range from 1:2 to 1:32 in rows B and C. The samples were then incubated, and the inhibition of the bioluminescence was measured after 15 min and 30 min.

To calculate the inhibition of the bioluminescence, the following formulas were given by HACH LANGE GmbH (Düsseldorf, Germany).

$$fK = \frac{I_t}{I_0} \tag{1}$$

fK is the time correction factor, determined from the measurement, I_0 is defined as the initial bioluminescence. I_t is the luminescence of the control at a specific time.

With *fK*, the corrected bioluminescence I_{ct} can be calculated by using this formula:

$$I_{ct} = fK * I_0 \tag{2}$$

This leads to the calculation of the inhibition, which can be determined by application of formula 3:

$$\%\ Ht = \frac{(I_{ct} - I_t) * 100}{I_{ct}} \tag{3}$$

The EC_{50} value is obtained by the following equation:

$$\Gamma = \%\frac{Ht}{100 - \%Ht} \quad (4)$$

Γ is the gamma-value, calculated by %Ht.

2.2.2.2 Results of the toxicity measurement

For all substances, the EC_{50} was calculated after 15 and 30 minutes of incubation. Compounds with an EC_{50} value lower than 0.10 g/L are classified as very toxic (++), compounds with an EC_{50} value between 0.10 g/L and 1.00 g/L are declared as toxic (+) and EC_{50} values above 1.00 g/L are classified as non-toxic (-).[41]

***Table 16**: Results of the toxicity measurements of the lithium salts of dihydrobis(1,2,4-triazol-1-yl)borate sesquihydrate (**59**), dihydrobis(5-aminotetrazolal-1-yl)borate (**64**), 4-amino-3,5-dinitropyrazolate sesquihydrate (**14**), 5,5-bistetrazolate dihydrate (**26**) and 5-aminotetrazolate (**20**), respectively.*

	59	**63**	**14**	**26**	**20**
EC_{50} (15min) [g/L]	3.87	-	0.41	3.991.	5.129
EC_{50} (30 min) [g/L]	4.75	-	0.41.	1.577	5.685
Toxicity level	**-**	**++**	**+**	**-**	**-**

The lithium salts of 5,5-bistetrazolate, 5-aminotetrazolate and dihydrobis(1,2,4-triazol-1-yl)borate sesquihydrate are considered as non-toxic, whereas, the salt lithium 4-amino-3,5-dinitropyrazole sesquihydrate is considered toxic and the salt lithium dihydrobis(5-aminotetrazol-1-yl)borate can be considered as very toxic. For the latter no values could be determined, because the inhibition rate of the salt was too high.

2.3 Pyrotechnical measurements

In order to evaluate the performance of the lithium salts, they were mixed into pyrotechnical formulations and the optical performance was analyzed, therefor the preparation of the pellets for the pyrotechnical measurements was executed as it is described in the following paragraph. However not all new synthesized lithium salts were considered as possible replacements for strontium, as these salts are not stable enough, showed a hygroscopic behavior or are too sensitive to be used in pyrotechnical formulations. For that stated reason, we made a preselection and chose the most promising ones. During the preparation of the mixtures, there was a clear trend for the performance of the respective salts, which is why more and more salts were eliminated in the course of the mixing process. This was also discussed in section 2.2 of this report, however the toxicological data and the performances of the salts were obtained only during the course of performing mixtures, which is why there was always a reduction of salts in between. According to the previous elimination procedure and the data we had available at the time, following salts were processed into pyro mixtures for investigation, lithium tetrazolate (**18**), ithium 5-aminotetrazolate (**20**), dilithium 5,5`-bistetrazolate dihydrate (**26**), dilithium 5,5`-bis(tetrazole-1-oxide) tetrahydrate (**30**), lithium dihydrobis(1,2,4-triazol-1-yl)borate sesquihydrate (**59**) and lithium dihydrobis(5-aminotetrazol-1-yl)borate (**64**).

For the processing of the pyrotechnical mixtures all constituents of the compositions had been weighed out according to their weight percentages with a deviation of 2 mg and had been hand-blended to homogeneous mixtures. For the mixtures containing the epoxy binder system, the solutions of Epon 813 and Versamid 140 in ethyl acetate with concentrations in the range of 20 or 10 g L^{-1}, respectively, were added resulting in a weight percent ratio of 80:20. The slurries thus obtained were blended approximately every ten minutes, until the solvent completely evaporated. Subsequently, the mixtures were cured at 60 °C over night and blended again to fine powders. For the mixtures containing the nitrocellulose binder, a 10 wt% solution of nitrocellulose in acetone was added. The resulting gum-like mass was kneaded, until the solvent had completely evaporated.

Portions of 500 mg with a deviation of 2 mg had been weighed out, before they were pressed to pellets in one increment at a consolidation dead load of 3 t with a dwell time of roughly 10 s. The latter were ignited by the tip of a sparkler and their combustions recorded with a digital DCR-HC37E video camera from Sony. The dominant wavelengths, spectral purities, and luminous intensities were measured over the full burn of the pellets with the aid of a HR2000+ES spectrometer with an ILX 511B linear silicon CCD-array detector (range 190 to 1100 nm) provided with software from OCEAN OPTICS. The distance between the detector of the spectrometer and the sample was calibrated to 1.000 m and the acquisition time was set to 20 ms. The dominant wavelengths as well as the color purities were evaluated based on the 1931 CIE method using illuminant C as the white reference point. Average values of all emissive parameters were gained by taking multiple samples into account, respectively.

2.3.1 Drop-in formulations

For the drop-in formulations we calculated the oxygen balance Ω_{CO2} of a compound with the sum formula $C_aH_bN_cO_d$ says whether its full burn to CO_2, H_2O, and N_2 will generate or require oxygen.[42] It can be calculated according to the following equation.

$$\Omega_{CO2} = \frac{(d - 2a - \frac{b}{2})}{M} \times 1600$$

Considering that lithium combusts to Li_2O[43] and boron to B_2O_3[44], respectively, stable and less sensitive moieties **14**, **20**, **59**, and **64** all have negative oxygen balances. As a consequence, the latter were employed as both colorants and reducing agents in "drop-in" formulations of a chlorine-free strontium-based pyrotechnic composition **AD-1**[4] (see **Table 1**). Strontium nitrate was replaced by its ammonium analogue and, since magnesium unfavorably increases the flame temperature[45] and its oxidation product incandesces, the amount of this fuel was reduced. The percentage of binder in mixtures containing lithium salts **14**, **20** or **64** was increased due to their hygroscopicity. All of the investigated test formulations burned with a red flame.

***Table 17**: Composition of a chlorine-free strontium-based control AD-1[4] and of "drop-in" formulations AD-2 to AD-5 with lithium dihydrobis(1,2,4-triazol-1-yl)borate sesquihydrate (**59**), lithium dihydrobis(5-aminotetrazol-1-yl)borate (**64**), lithium 4-amino-3,5-dinitropyrazolate sesquihydrate (**14**) and lithium 5-aminotetrazolate (**20**).*

Formulation	***$Sr(NO_3)_3$*** **[wt%]**	***Mg 50/100*** **[wt%][a]**	***NH_4NO_3*** **[wt%]**	***CH_3N_5*** **[wt%]**	***59*** **[wt%]**	***64*** **[wt%]**	***14*** **[wt%]**	***20*** **[wt%]**	***Epon/Versamid*** **[wt%]**
AD-1	48	33	-	12	-	-	-	-	7
AD-2	-	12	48	-	33	-	-	-	7
AD-3	-	12	48	-	-	30	-	-	10
AD-4	-	12	48	-	-	-	30	-	10
AD-5	-	12	48	-	-	-	-	30	10

a) Mg >50: magnesium was sieved with a mesh size 50 (grain size > 300 µm), b) Epon 813 and Versamid 140 in a weight percent ratio of 80:20

2.3.2 Modified pyrotechnical systems

In preliminary experiments "drop-in" formulations of the investigated lithium salts containing ammonium nitrate oxidizer and the two-component binder system Epon 813/Versamid 140 showed a hygroscopic behavior. Since the latter was attributed to the oxidizing agent and could not be countered by increasing the binder content, these two ingredients were replaced by potassium nitrate and nitrocellulose, respectively. As a consequence, the resulting pyrotechnical formulations are more sensitive towards external stimuli, due to the nitrocellulose as the binder system. All following formulations showed an impact sensitivity of around 10 J, but there was no increase of friction sensitivity.

Lithium dihydrobis(1,2,4-triazol-1-yl)borate • 1.5 H_2O (**59**), lithium 5-aminotetrazolate (**20**), and lithium 4-amino-3,5-dinitropyrazolate • 1.5 H_2O (**14**), which already showed a red flame color, were tested again in the improved pyrotechnic matrix (see **Table 18**). Furthermore, lithium tetrazolate (**18**) with its sensitivity to electrostatic discharge of 1 J as well as insensitive dilithium 5,5'-bistetrazolate • 2 H_2O (**26**) and dilithium 5,5'-bis(tetrazole-1-oxide) • 4 H_2O (**30**) were investigated for their capability to impart red color to the flame.

***Table 18**: "Drop-in" formulations with modified system containing lithium 5-tetrazolate (**18**), lithium 5-aminotetrazolate (**20**), dilithium 5,5'-bistetrazolate dihydrate (**26**), dilithium 5,5'-bis(tetrazole-1-oxide) tetrahydrate (**30**), lithium 4-amino-3,5-dinitropyrazolate sesquihydrate (**14**), lithium dihydrobis(1,2,4-triazol-1-yl)borate sesquihydrate (**59**), lithium dihydrobis(5-aminotetrazol-1-yl)borate (**64**), respectively.*

Formulation	***KNO_3*** **[wt%]**	***Mg 50/100*** **[wt%][a]**	***18*** **[wt%]**	***20*** **[wt%]**	***26*** **[wt%]**	***30*** **[wt%]**	***14*** **[wt%]**	***59*** **[wt%]**	***64*** **[wt%]**	***Nitrocellulose*** **[wt%][b]**
AD-6	48	12	33	-	-	-	-	-	-	7
AD-7	48	12	-	33	-	-	-	-	-	7
AD-8	48	12	-	-	33	-	-	-	-	7
AD-9	48	12	-	-	-	33	-	-	-	7
AD-10	48	12	-	-	-	-	33	-	-	7
AD-11	48	12	-	-	-	-	-	33	-	7
AD-12	48	12	-	-	-	-	-	-	33	7

a) Mg >50: magnesium was sieved with a mesh size 50 (grain size > 300 µm), b) Nitrocellulose is the binder solution in acetone 10 [wt%].

***Table 19**: Measured parameters of "drop-in" formulations with modified system containing lithium 5-tetrazolate (**18**), lithium 5-aminotetrazolate (**20**), dilithium 5,5'-bistetrazolate dihydrate (**26**), dilithium 5,5'-bis(tetrazole-1-oxide) tetrahydrate (**30**), lithium 4-amino-3,5-dinitropyrazolate sesquihydrate (**14**), lithium dihydrobis(1,2,4-triazol-1-yl)borate sesquihydrate (**59**), lithium dihydrobis(5-aminotetrazol-1-yl)borate (**64**), respectively.*

Formulation	Ω_{CO2} **[%][a]**	***BT*** **[s][b]**	λ_d **[nm][c]**	Σ **[%][d]**	***LI*** **[cd][e]**
AD-6	- 8.48	6.7	597	41	3302
AD-7	- 8.52	6.2	600	48	3360
AD-8	- 2.48	3	601	40	3846
AD-9	- 3.73	15	581-596	-	-
AD-10	4.96	4.1	617	28	4114
AD-11	- 37.24	1.8	622	36	8308
AD-12	- 10.8	1.3	614	33	8675

a) Oxygen balance with respect to formation of CO_2, Li_2O, b) *BT* [s]: burn time, c) λ_d [nm]: dominant wavelength, d) Σ [%]: spectral purity, e) *LI* [cd]: luminous intensity.

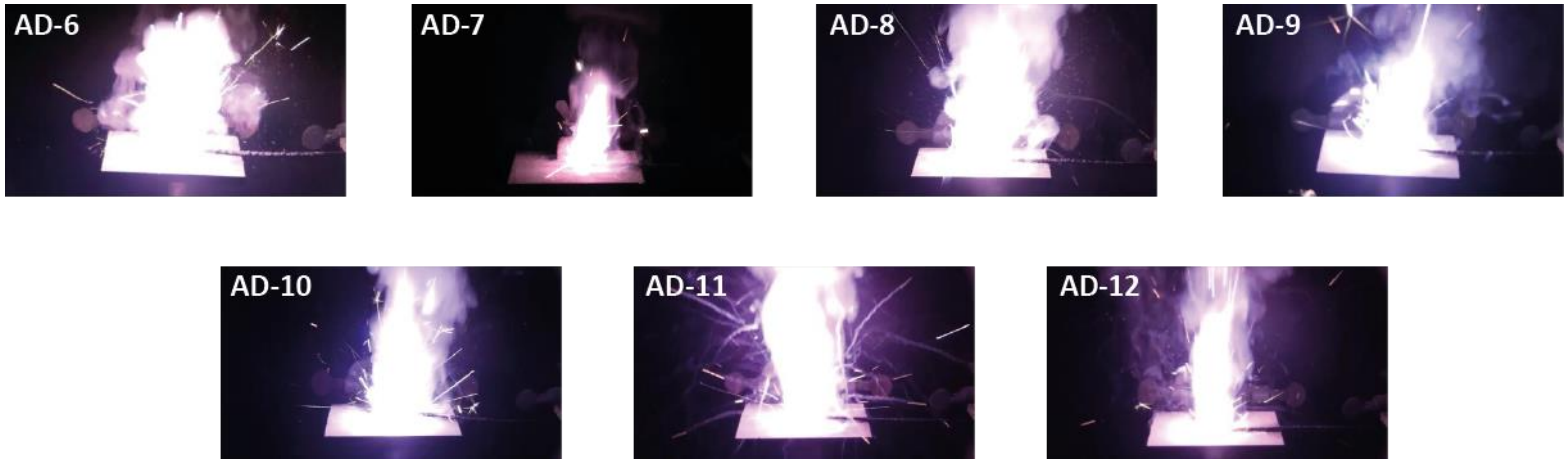

***Figure 32**: Burning images of the "drop-in" formulations with KNO3 as oxidizer and nitrocellulose as binder, with the respective number of the formulation.*

2.3.3 Variation of lithium content

As a subtask of the project, the amount of lithium salt in the mixtures had to be varied. The drop-in formulations of the mixtures containing lithium dihydrobis(1,2,4-triazol-1-yl)borate sesquihydrate (**59**) , lithium dihydrobis(5-aminotetrazol-1-yl)borate (**64**), lithium 4-amino-3,5-dinitropyrazolate sesquihydrate (**14**), and dilithium 5,5'-bistetrazolate dihydrate (**26**) showed a continuous burn and had a dominant wavelength equal or greater than 600 nm. The formulation containing lithium 5-aminotetrazolate (**18**) showed a strobe like behavior. Nevertheless, all formulations had spectral purity below 50%. This could not be improved by the use of multivalent lithium salts. We assume that an oxygen excess in the flame causes the formation of incandescent lithium oxide. In order to proof this assumption we varied the amount of lithium salt at the expense of the oxidizer.

However, this could only be done for the salts **18**, **20**, **26**, **14**, **64**. No further mixtures were carried out for the salt **30** because the performance of the salt in the drop-in formulations was poor (see **Table 20**). In addition, no further studies could be carried out with the lithium salt **59** either, although the previous results were promising. The reason for this is that the performed syntheses could not provide enough pure substance needed for a series of tests. For the same reasons, the magnesium content was not varied in the mixtures containing these salts.

***Table 20**: Variation of the lithium content of pyrotechnical formulations containing the salts lithium 5-tetrazolate (**18**), lithium 5-aminotetrazolate (**20**), dilithium 5,5'-bistetrazolate dihydrate (**26**), lithium 4-amino-3,5-dinitropyrazolate sesquihydrate (**14**), lithium dihydrobis(5-aminotetrazol-1-yl)borate (**64**), respectively.*

Formulation	***KNO_3* [wt%]**	***Mg 50/100* [wt%][a]**	***18* [wt%]**	***20* [wt%]**	***26* [wt%]**	***14* [wt%]**	***64* [wt%]**	***Nitrocellulose* [wt%][b]**
AD-13	30	12	51	-	-	-	-	7
AD-14	20	12	61	-	-	-	-	7
AD-15	10	12	71	-	-	-	-	7
AD-16	30	12	-	51	-	-	-	7
AD-17	20	12	-	61	-	-	-	7
AD-18	10	12	-	71	-	-	-	7
AD-19	30	12	-	-	51	-	-	7
AD-20	20	12	-	-	61	-	-	7
AD-21	10	12	-	-	71	-	-	7
AD-22	30	12	-	-	-	51	-	7
AD-23	20	12	-	-	-	61	-	7

AD-24	10	12	-	-	-	71	-	7
AD-25	30	12	-	-	-	-	51	7
AD-26	20	12	-	-	-	-	61	7
AD-27	10	12	-	-	-	-	71	7

a) Mg >50: magnesium was sieved with a mesh size 50 (grain size > 300 µm), b) Nitrocellulose is the binder solution in acetone 10 [wt%].

As expected, increasing the lithium salt content significantly increased the spectral purity of the mixtures. The dominant wavelength also remained in a range of about 600 nm for all mixtures. Furthermore, an increase in the lithium salt content prolonged the burning time. However, the increase in the colorant also resulted in a significant decrease in the light intensity (see **Table 21**).

***Table 21**: Measured parameters of the pyrotechnical formulations containing an increased amount of the respective lithium salts: 5-tetrazolate (**18**), 5-aminotetrazolate (**20**), 5,5'-bistetrazolate dihydrate (**26**), 4-amino-3,5-dinitropyrazolate sesquihydrate (**14**), dihydrobis(5-aminotetrazol-1-yl)borate (**64**), respectively.*

Formulation	Ω_{CO2} **[%][a]**	***BT* [s][b]**	λ_d **[nm][c]**	***Σ* [%][d]**	***LI* [cd][e]**
AD-13	- 25.08	4.2	597	66	1945
AD-14	- 34.30	6.9	596	87	847
AD-15	- 43.51	9.5	567	40	160
AD-16	- 25.13	4	598	62	1945
AD-17	- 34.36	6.9	597	76	852

AD-18	- 43.58	23.6	590	77	50
AD-19	- 15.80	4	595	67	1515
AD-20	- 23.10	8	592	64	1048
AD-21	- 30.59	9	591	98	900
AD-22	- 4.30	5.1	602	48	1138
AD-23	- 9.44	7.8	601	48	1535
AD-24	- 14.58	10.9	597	85	983
AD-25	- 28.65	2.5	610	41	5100
AD-26	- 38.57	4.1	602	58	1910
AD-27	- 48.48	6.5	599	70	1350

a) Oxygen balance with respect to formation of CO_2, Li_2O, b) *BT* [s]: burn time, c) λ_d [nm]: dominant wavelength, d) Σ [%]: spectral purity, e) *LI* [cd]: luminous intensity.

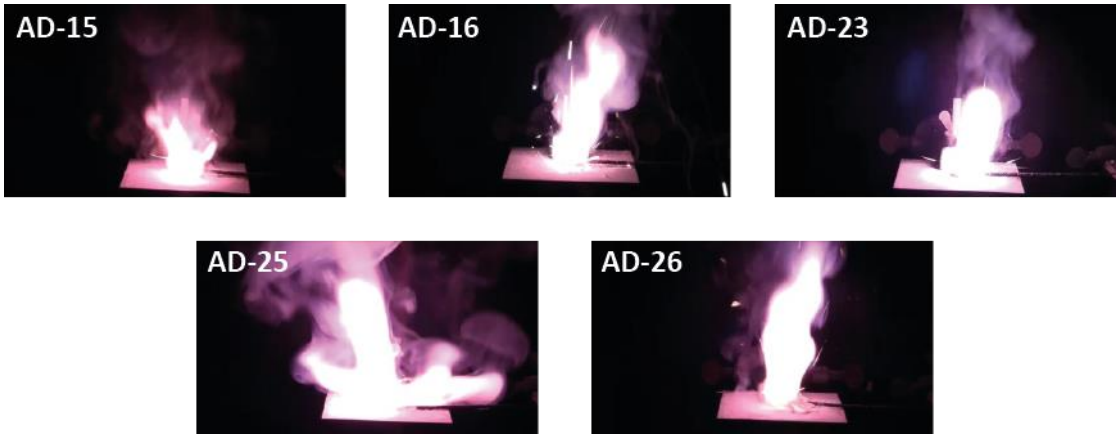

***Figure 33**: Burning images of the best mixtures with the respective number of the formulation, with a variation of the lithium salt content.*

2.3.4 Variation of magnesium content

As already shown in the previous section, a higher spectral purity could be achieved by increasing the colorant. In the drop-in formulations, it was also found that the light intensity deviated far from the desired values. The reduced luminous intensity can be attributed to the fact that we use a lower magnesium content in the prepared drop-in formulations. An increase in the magnesium content is being considered to analyze how strong the influence is on the dominant wavelength, the spectral purity and whether an improvement in the luminous intensity can be observed. For this purpose, salts **14**, **18**, **20**, **26**, and **64** were mixed once at 20 wt% and once at 30 wt% of magnesium, with the amount of oxidizer being reduced at the same time (see **Table 22**). The quantity of the colorant and the nitrocellulose binder was not modified.

***Table 22**: Variation of the magnesium content of pyrotechnical formulations containing the salts lithium 5-tetrazolate (**18**), lithium 5-aminotetrazolate (**20**), dilithium 5,5'-bistetrazolate dihydrate (**26**), lithium 4-amino-3,5-dinitropyrazolate sesquihydrate (**14**), lithium dihydrobis(5-aminotetrazol-1-yl)borate (**64**), respectively.*

Formulation	***KNO_3* [wt%]**	***Mg 50/100* [wt%][b]**	***18* [wt%]**	***20* [wt%]**	***26* [wt%]**	***14* [wt%]**	***64* [wt%]**	***Nitrocellulose* [wt%][e]**
AD-28	40	20	33	-	-	-	-	7
AD-29	30	30	33	-	-	-	-	7
AD-30	40	20	-	33	-	-	-	7
AD-31	30	30	-	33	-	-	-	7
AD-32	40	20	-	-	33	-	-	7
AD-33	30	30	-	-	33	-	-	7
AD-34	40	20	-	-	-	33	-	7
AD-35	30	30	-	-	-	33	-	7
AD-36	40	20	-	-	-	-	33	7
AD-37	30	30	-	-	-	-	33	7

a) Mg >50: magnesium was sieved with a mesh size 50 (grain size > 300 µm), b) Nitrocellulose is the binder solution in acetone 10 [wt%].

Unexpectedly, for formulation **AD-28** and **AD-29** no measurement could be performed, as both mixtures were not stable after the pressing process. For mixture **AD-30** no luminous intensity could be determined, since this mixture showed the behavior of a strobe. The remaining mixtures with an increased magnesium content were able to achieve dominant wavelengths that are above the required value of 600 nm. In addition, the luminous intensity could also be increased to a value of over 14000 cd. Furthermore, the burning rate increased, which reduced the burning time. Thus, burning times of about 2 seconds could be measured for all formulations (see **Table 23**). However, the increasing magnesium content had the consequence that the flame purity dropped to a percentage value of around 30%. These trends are in line with expectations.

***Table 23**: Measured parameters of the pyrotechnical formulations containing an increased amount of magnesium with the respective lithium salts: 5-tetrazolate (**18**), 5-aminotetrazolate (**20**), 5,5'-bistetrazolate dihydrate (**26**), 4-amino-3,5-dinitropyrazolate sesquihydrate (**14**), dihydrobis(5-aminotetrazol-1-yl)borate (**64**), respectively.*

Formulation	Ω_{CO2} **[%][a]**	***BT*** **[s][b]**	λ_d **[nm][c]**	Σ **[%][d]**	***LI*** **[cd][e]**
AD-28	- 16.91	-	-	-	-
AD-29	- 27.45	-	-	-	-
AD-30	- 16.95	3.2	601	37	-
AD-31	- 27.49	1.5	599	44	14400
AD-32	- 10.91	1.7	602	38	14100
AD-33	- 21.45	2.2	603	34	14350
AD-34	- 3.47	2.7	615	27	14100
AD-35	- 14.01	2	606	28	14650

AD-36	-19.23	1.5	610	32	14500
AD-37	- 29.76	1.5	608	23	14600

a) Oxygen balance with respect to formation of CO_2, Li_2O, b) *BT* [s]: burn time, c) λ_d [nm]: dominant wavelength, d) Σ [%]: spectral purity, e) *LI* [cd]: luminous intensity.

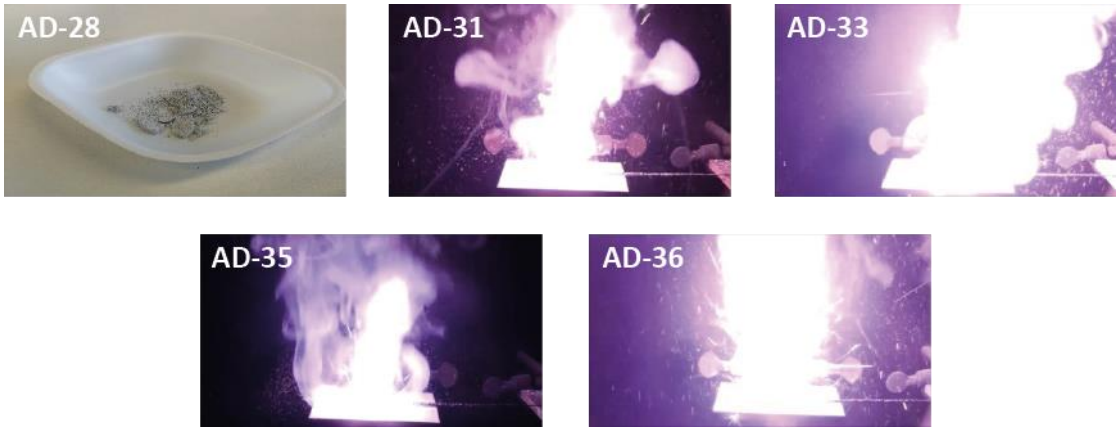

***Figure 34**: Burning images of the mixtures with the respective number of the formulation, with a variation of the magnesium content.*

2.3.5 Variation grain size of magnesium

Although the mixtures containing salt **64** demonstrated good burnup parameters, no further mixtures were prepared with this salt during the course of the project. This was due to the fact that H_2-gas is released during the synthesis of a preliminary stage of the salt, which can lead to complications during the upscaling of the reaction. This topic will also be addressed in chapter 2.2.

For these reasons, only salts **20**, **26** and **14** were used for further formulations. Since the magnesium content was found to have a strong influence on the burning behavior, it was tested whether a change could be made by altering the grain size of the magnesium. For this purpose, the fuel was sieved with different mesh sizes, which are shown in **Table 24**.

***Table 24**: Variation of the magnesium grain size of pyrotechnical formulations containing the salts lithium 5-aminotetrazolate (**20**), dilithium 5,5'-bistetrazolate dihydrate (**26**), lithium 4-amino-3,5-dinitropyrazolate sesquihydrate (**14**), respectively.*

Formulation	***KNO_3* [wt%]**	***Mg > 50* [wt%][a]**	***Mg 100/200* [wt%][b]**	***Mg 200/373* [wt%][c]**	***Mg < 373* [wt%][d]**	***20* [wt%]**	***26* [wt%]**	***14* [wt%]**	***Nitrocellulose* [wt%][e]**
AD-38	48	12	-	-	-	33	-	-	7
AD-39	48	-	12	-	-	33	-	-	7
AD-40	48	-	-	12	-	33	-	-	7
AD-41	48	-	-	-	12	33	-	-	7
AD-42	48	12	-	-	-	-	33	-	7
AD-43	48	-	12	-	-	-	33	-	7
AD-44	48	-	-	12	-	-	33	-	7
AD-45	48	-	-	-	12	-	33	-	7
AD-46	48	12	-	-	-	-	-	33	7

AD-47	48	-	12	-	-	-	-	33	7
AD-48	48	-	-	12	-	-	-	33	7
AD-49	48	-	-	-	12	-	-	33	7

a) Mg >50: magnesium was sieved with a mesh size 50 (grain size > 300 µm) b) Mg 100/200: magnesium was sieved with mesh size 100/200 (150 µm > grain size > 75 µm), c) Mg 200/373: magnesium was sieved with mesh size 200/373 (75 µm > grain size > 40 µm), d) Mg <373: magnesium was sieved with a mesh size 373 (40 µm > grain size), e) Nitrocellulose is the binder solution in acetone 10 [wt%].

For the blends, with the largest grain size of over 300 µm, **AD-38**, **AD-42** and **AD-46** no continuous burnup could be measured. The burnup was associated with a strong smoke development and large bright sparks were visible in the mixture, which are responsible for the relatively high luminous intensity. The burning time was about 6 seconds and a color purity of just about 37% was achieved in the mixtures (see **Table 25**). With a grain size between 150 µm and 75 µm the burning rate increased. For formulation **AD-39**, the behavior of a strobe could be observed. For mixtures **AD-43** and **AD-47**, a continuous burnup was present. Furthermore, a dominant wavelength of more than 600 nm could be achieved, the highest in mixture **AD-47** with even 608 nm. In addition, a color purity of 54% was achieved in blend **AD-43**. The luminous intensity was in the same range as it was in the drop-in formulations, with the respective salt. For even smaller grain sizes, it was found that the measured values for luminous intensity and dominant wavelength deteriorated. Thus, for the mixtures **AD-41**, **AD-45** and **AD-49**, only an intensity of less than 1000 cd could be measured. However, the color purity was again significantly better, as in mixture **AD-41** with 95% spectral purity.

***Table 25**: Measured parameters of the pyrotechnical formulations containing different grain sizes of magnesium and the salts lithium 5-aminotetrazolate (**8**), dilithium 5,5'-bistetrazolate dihydrate (**9**), lithium 4-amino-3,5-dinitropyrazolate sesquihydrate (**11**), respectively.*

Formulation	Ω_{CO2} [%][a]	***BT*** [s][b]	λ_d [nm][c]	***Σ*** [%][d]	***LI*** [cd][e]
AD-38	- 8.52	6	599	37	1493
AD-39	- 8.31	10.9	598	56	1873
AD-40	- 8.31	7.6	596	78	774
AD-41	- 8.52	6.3	596	95	305
AD-42	- 2.47	6.4	605	39	2735
AD-43	- 14.22	4.1	602	54	1675
AD-44	- 2.48	1.7	601	57	2440
AD-45	- 2.48	1.5	598	78	647
AD-46	4.96	5.5	605	38	3280
AD-47	- 2.48	2.5	608	38	3625
AD-48	4.96	1.9	599	64	1510
AD-49	4.96	2.2	589	136	204

a) Oxygen balance with respect to formation of CO_2, Li_2O, b) *BT* [s]: burn time, c) λ_d [nm]: dominant wavelength, d) *Σ* [%]: spectral purity, e) *LI* [cd]: luminous intensity.

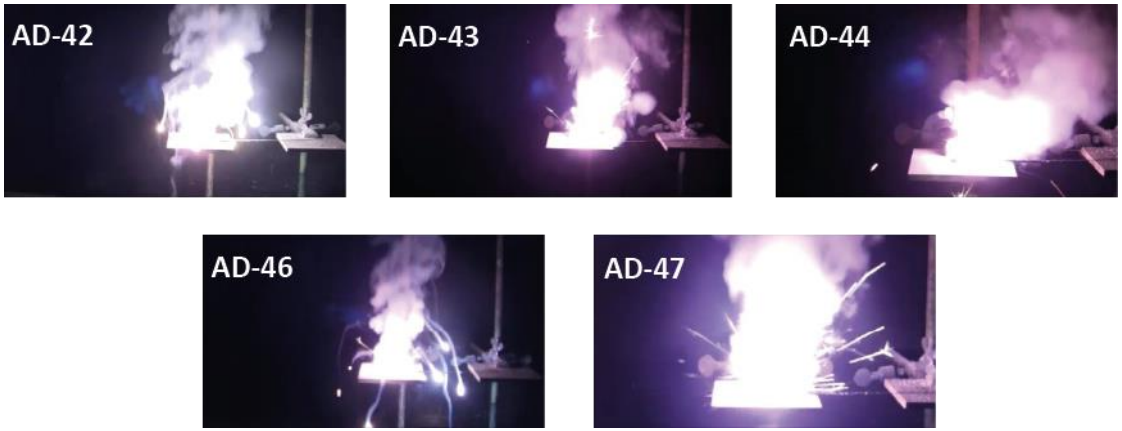

***Figure 35**: Burning images of the mixtures with the respective number of the formulation, with a variation of the magnesium grain size.*

2.3.6 Different fuel and grain size

Furthermore, it was investigated whether it is possible to use a different fuel for the mixture, because magnesium produces high temperatures during the combustion. This is undesirable with lithium, as it leads to a strong activation, which reduces the intensity of the red flame color.[45] One example is aluminum. The latter was also sieved and mixed as shown in **Table 26**. A change in the weight ratio was not considered, since it was tested whether aluminum is generally suitable for use in lithium mixtures.

*Table 26: Pyrotechnical formulations containing different grain sizes of aluminum and the salts lithium 5-aminotetrazolate (**20**), dilithium 5,5'-bistetrazolate dihydrate (**26**), lithium 4-amino-3,5-dinitropyrazolate sesquihydrate (**14**), respectively.*

Formulation	***KNO_3* [wt%]**	***Al 50/100* [wt%][a]**	***Al 100/150* [wt%][b]**	***20* [wt%]**	***26* [wt%]**	***14* [wt%]**	***Nitrocellulose* [wt%][c]**
AD-50	48	12	-	33	-	-	7
AD-51	48	-	12	33	-	-	7
AD-52	48	12	-	-	33	-	7
AD-53	48	-	12	-	33	-	7
AD-54	48	12	-	-	-	33	7
AD-55	48	-	12	-	-	33	7

a) Al 50/100: magnesium was sieved with mesh size 50/100 (300 µm > grain size > 150 µm), b) Al 100/150: magnesium was sieved with mesh size 100/150 (150 µm > grain size > 100 µm), c) Nitrocellulose is the binder solution in acetone 10 [wt%].

As shown in **Table 27**, good results could not be obtained. No constant burnup was observed. In terms of dominant wavelength and luminous intensity, the measured data were far below the desired values. Only in mixtures **AD-51**, **AD-53** and **AD-55** a spectral purity of over 70% was achieved. These were the mixtures that were blended with a smaller grain size of aluminum. All results suggest that this fuel is not suitable for usage in mixtures with a lithium salt.

***Table 27**: Measured parameters of the pyrotechnical formulations containing different grain sizes of aluminum and the salts lithium 5-aminotetrazolate (**20**), dilithium 5,5'-bistetrazolate dihydrate (**26**), lithium 4-amino-3,5-dinitropyrazolate sesquihydrate (**14**), respectively.*

Formulation	Ω_{CO2} [%][a]	***BT*** [s][b]	λ_d [nm][c]	Σ [%][d]	***LI*** [cd][e]
AD-50	- 14.47	8.5	565	38	53
AD-51	- 14.47	9.7	590	94	62
AD-52	- 5.26	10.2	566	38	10
AD-53	- 5.26	6.5	598	76	340
AD-54	2.18	10.9	564	37	4
AD-55	2.18	11.1	587	76	189

a) Oxygen balance with respect to formation of CO_2, Li_2O, b) *BT* [s]: burn time, c) λ_d [nm]: dominant wavelength, d) Σ [%]: spectral purity, e) *LI* [cd]: luminous intensity.

***Figure 36**: Burning images of the mixtures with the respective number of the formulation, with aluminum as the fuel.*

2.3.7 Variation of the mixtures with different additives

Another possibility to influence the burning parameters of pyrotechnic mixtures is the use of additional additives. The compounds 5-aminotetrazole and hexamine were selected and tested for this purpose. The idea behind the use of aminotetrazole came from the high amount of nitrogen in the compound. The high amount of N_2 released during combustion should create a reductive flame atmosphere and the N_2 gas released should cool the flame, which is the basic requirement for producing a good flame color with lithium.[45] The use of hexamine is justified by the fact that the compound has a very high negative oxygen balance, which can influence the oxygen balance. Moreover, this additive was already used by Glück *et al*.[46] and produced good results. To test the effects of the additives, they were mixed individually and in combination. As in the previous test series, the amount of oxidizer was reduced at the expense of the additives (see **Table 28**).

***Table 28**: Pyrotechnical formulations containing pyrotechnical additives and the salts lithium 5-aminotetrazolate (**20**), dilithium 5,5'-bistetrazolate dihydrate (**26**), lithium 4-amino-3,5-dinitropyrazolate sesquihydrate (**14**), respectively.*

Formulation	***KNO_3* [wt%]**	***Mg 50/100* [wt%][a]**	***20* [wt%]**	***26* [wt%]**	***14* [wt%]**	***5-AT* [wt%]**	***Hexamine* [wt%]**	***Nitrocellulose* [wt%][b]**
AD-56	40	12	33	-	-	-	8	7
AD-57	33	12	33	-	-	-	15	7
AD-58	40	12	33	-	-	8	-	7
AD-59	33	12	33	-	-	15	-	7
AD-60	40	12	37	-	-	-	4	7
AD-61	40	12	33	-	-	4	4	7

AD-62	40	12	-	33	-	-	8	7
AD-63	33	12	-	33	-	-	15	7
AD-64	40	12	-	33	-	8	-	7
AD-65	33	12	-	33	-	15	-	7
AD-66	40	12	-	37	-	-	4	7
AD-67	40	12	-	33	-	4	4	7
AD-68	40	12	-	-	33	-	8	7
AD-69	33	12	-	-	33	-	15	7
AD-70	40	12	-	-	33	8	-	7
AD-71	33	12	-	-	33	15	-	7
AD-72	40	12	-	-	37	-	4	7
AD-73	40	12	-	-	33	4	4	7

a) Mg 50/100: magnesium was sieved with mesh size 50/100 (300 µm > grain size > 150 µm), b) Nitrocellulose is the binder solution in acetone 10 [wt%].

In the formulations where hexamine was added, wavelengths above 600 nm could be achieved, but not in the mixtures containing the salt **14**. This may be due to the relatively high negative oxygen balance (Mixture **AD-63**, **AD-69**). With the latter salt, only a very low luminous intensity could be

achieved (Mixture **63**). The maximum luminous intensity was achieved with Mixture **AD-62** with a value of 1780 cd. Likewise, no sufficient spectral purity could be achieved with this additive, which lies in a range of 46-57% (see **Table 29**). In addition, the burnups showed a strobe like behavior and are very smoke-forming. In the mixtures, in which the additive, 5-aminotetrazol is present, the results are the opposite of the previously mentioned mixtures. Only in the case of the salt **14** a dominant wavelength of over 600 nm could be achieved. The best light intensity was also achieved with this salt in mixture **AD-71** with a value of 2370 cd. The worst values in terms of luminous intensity were measured with salt **26**. The burning times were in the same range as with the other additive and were in the range of 4.7-8.8 seconds. However, the burn-offs also resulted in very strong smoke formation. The mixtures containing both additives showed the best burning behavior. Likewise, a dominant wavelength above the required benchmark of 600 nm was achieved for all salts. However, the spectral purity and luminous intensity values are below the required values. The best spectral purity value was achieved with mixture **AD-73** with salt **14** with 58%. The longest burnup was also measured with this mixture with 8.2 seconds. The brightest mixture was measured with mixture **AD-67** with salt **26** with a value of 1675 cd (see **Table 29**).

***Table 29**: Measured parameters of the pyrotechnical formulation containing pyrotechnical additives and the salts lithium 5-aminotetrazolate (**20**), dilithium 5,5'-bistetrazolate dihydrate (**26**), lithium 4-amino-3,5-dinitropyrazolate sesquihydrate (**14**), respectively.*

Formulation	Ω_{CO2} [%][a]	***BT*** [s][b]	λ_d [nm][c]	Σ [%][d]	***LI*** [cd][e]
AD-56	- 28.04	7.0	604	46	1095
AD-57	- 44.91	4.6	604	48	1045
AD-58	- 16.95	5.1	598	37	1102
AD-59	- 21.74	6.7	598	61	1845
AD-60	- 24.12	7.7	603	43	1183

AD-61	- 22.3	7.6	605	47	1070
AD-62	- 22	5.7	604	46	1780
AD-63	- 97.04	6.5	600	55	477
AD-64	- 10.9	4.7	593	73	418
AD-65	- 18.30	8.8	596	33	510
AD-66	- 22	3.9	598	57	2190
AD-67	- 14.22	4.1	602	54	1675
AD-68	- 14.56	8.4	565	39	12
AD-69	- 141.73	7.5	599	57	676
AD-70	- 3.47	7.8	604	48	1045
AD-71	- 10.85	5.4	607	28	2370
AD-72	- 6.85	6.7	603	49	1179
AD-73	- 9.01	8.2	603	58	1215

a) Oxygen balance with respect to formation of CO_2, Li_2O. b) *BT* [s]: burn time, c) λ_d [nm]: dominant wavelength, d) Σ [%]: spectral purity, e) *LI* [cd]: luminous intensity.

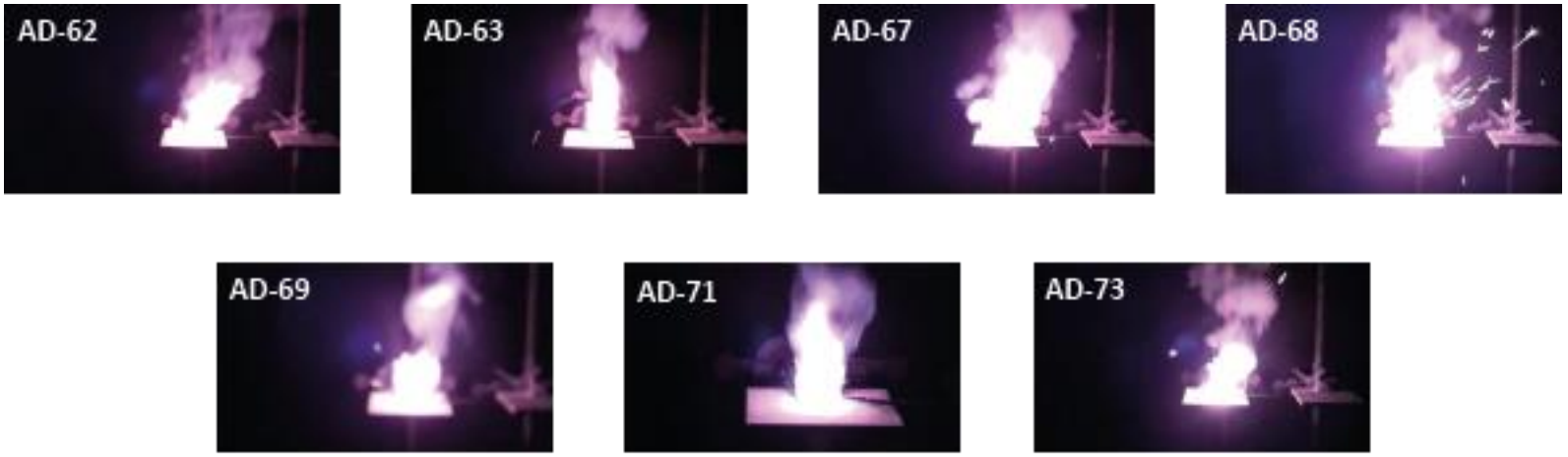

***Figure 37**: Burning images of the mixtures with the respective number of the formulation, with pyrotechnical additives.*

2.3.8 Thermal measurement

Another issue that has been worked on in course of this project is the determination of the burnup temperatures of the pyro mixtures. For this reason, the most promising mixtures were reproduced and the burnup was recorded with a thermal camera from FLIR.

Table 30: *Compositions of the pyrotechnical formulation containing lithium 5-aminotetrazolate (**20**), dilithium 5,5`-bistetrazole dihydrate (**26**), lithium 4-amino-3,5-dinitropyrazolate sesquihydrate (**14**), lithium dihydrobis(1,2,4-triazol-1-yl)borate (**59**) and lithium dihydrobis(5-aminotetrazol-1-yl)borate monohydrate (**64**), respectively.*

Formulation	***KNO_3* [wt%]**	***Mg 50/100* [wt%][a]**	***Nitrocellulose* [wt%][b]**	***20***	***26***	***14***	***59***	***64***
AD-7	48	12	7	33	-	-	-	-
AD-32	40	20	7	-	33	-	-	-
AD-34	40	20	7	-	-	33	-	-
AD-11	40	20	7	-	-	-	33	-
AD-36	48	12	7	-	-	-	-	33

a) Mg 50/100: magnesium was sieved with mesh size 50/100 (300 µm > grain size > 150 µm), b) Nitrocellulose is the binder solution in acetone 10 [wt%].

***Table 31**: Measured values of the pyrotechnical formulation containing lithium 5-aminotetrazolate (**20**), dilithium 5,5`-bistetrazole dihydrate (**26**), lithium 4-amino-3,5-dinitropyrazolate sesquihydrate (**14**), lithium dihydrobis(1,2,4-triazol-1-yl)borate (**59**) and lithium dihydrobis(5-aminotetrazol-1-yl)borate (**64**).*

Formulation	λ_d **[nm]**	***Σ* [%]**	***LI* [cd]**	***BT* [s]**	***T* [°C]**
AD-7	600	48	3360	6	-
AD-32	602	38	14100	1.7	1016
AD-34	615	27	14100	2.7	1449
AD-11	622	36	8308	1.8	1100
AD-36	610	32	14500	1.5	1285

As shown in **Table 31**, all burnup temperatures are in a range of above 1000°C. This result was expected, since the burnup temperature of the mixtures is determined by the fuel (in this case magnesium). However, it could be seen that the difference of 8 wt% of magnesium makes a temperature difference of about 200°C. For a more precise result concerning the burning temperatures, the mixtures have to be prepared in larger scale and a longer measuring time.

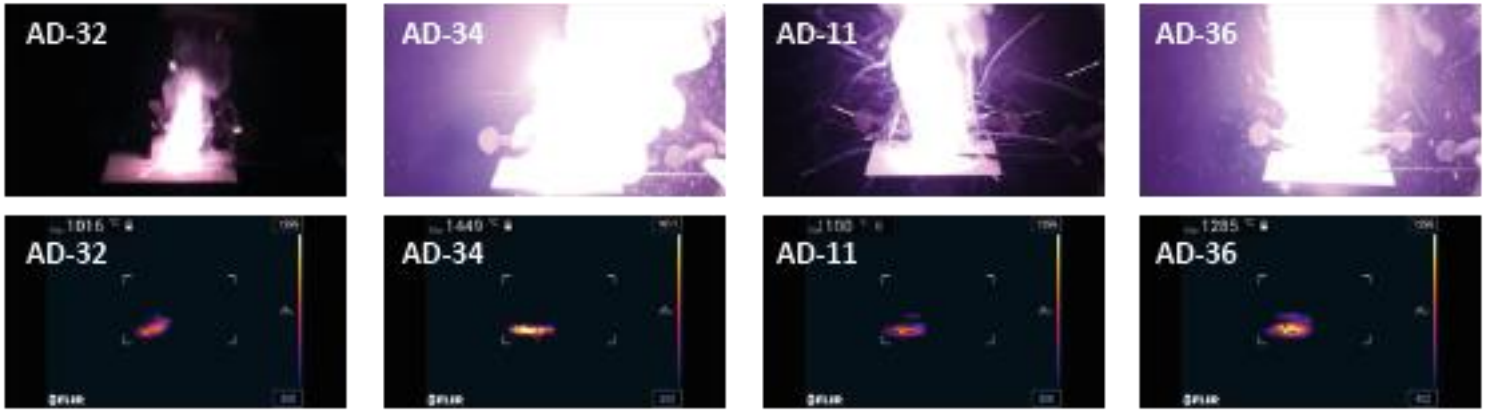

***Figure 38**: Thermal measurements of the most promising formulations.*

2.3.9 Overview of the selected salts after measuring pyrotechnical formulations

Based on the preceding criteria (stability, hygroscopicity, toxicity and sensitivity) only four lithium salts remained, namely lithium tetrazolate (**18**), lithium 5-aminotetrazolate (**20**), dilithium 5,5`-bistetrazolate dihydrate (**26**) and dilithium 5,5`-bis(tetrazole-1-oxide) tetrahydrate (**30**).Although, several salts were considered for use, salts **20** and **26** prevailed due to their performance in the pyrotechnic mixtures. In the **AD-7** and **AD-32** mixtures, several required parameters could be achieved. On the other hand, most mixtures containing salt **18** did not show a continuous burning. This result was unexpected, since there is no crystal water reported for this compound. Also, mixtures **AD-28** and **AD-29**, which contained salt **18**, were not stable after processing and these are the only mixtures were this was observed.

Same goes for salt **30** in context of the burning behavior. The explanation for the latter salt is the high chance the amount of crystal water, which could not be removed via drying. Therefor a poor performance was expected. For these aforementioned reasons, salts **18** and **30** were not considered in the toxicity measurements, as the poor performance in the mixtures was known prior to the test.

Table 32: *Overview of the selected lithium salts after the pyrotechnical measurements.*

Compound number	Ageing/hygroscopicity behavior	Sensitivity	Toxicity	Pyrotechnical performance
18	No ageing / hygroscopicity visible	Not sensitive	Not determined	Poor performance
20	No ageing / hygroscopicity visible	Not sensitive	Not toxic	✓
26	No ageing / hygroscopicity visible	Not sensitive	Not toxic	✓
30	No ageing / hygroscopicity visible	Not sensitive	Not determined	Poor performance

2.4 Preparation of prototypes

2.4.1 Objective

To assemble pyrotechnic flare prototypes based on two lithium salt colorants, lithium 5-aminotetrazolate (**20**) and dilithium 5,5'-bistetrazolate dihydrate (**26**), and compare their optical emissive properties to those of a control formulation based on strontium nitrate.

2.4.2 Approach

After the selection process at the Ludwig-Maximilians-Universität (LMU) in Munich, the chosen lithium salts, named in the section above, were transferred to the *U.S. Army Combat Capabilities Development Command* (DEVCOM). The chemicals provided by LMU were postally shipped via *FedEx* as dangerous goods. Initial tests were performed by DEVCOM to ensure the quality and stability of the delivered chemicals. The performed testing comprised differential scanning calorimetry (DSC), thermogravimetric analysis (TGA) and an isothermal analysis at 60 °C. The measured values were in accordance with the provided data of the LMU, from which it could be concluded, that the delivered compounds are pure, unaltered and thermal stable.

For the following tests, three baseline formulations, labeled "control," **I**, and **II**, were blended alongside experimental formulations **III** – **VI** containing lithium salts **20** and **26** (**Table 33**). The "control" formulation is a conventional red-burning illuminant composition based on strontium nitrate ($Sr(NO_3)_2$) that provides a red display via excitation/relaxation of the gas-phase, molecular strontium monochloride (SrCl) photochemical species. Formulation **I**, on the other hand, emits by gas-phase atomic lithium excitation/relaxation, but the lithium source is (Li_2CO_3) instead of either salt **20** or **26**. Formulation **II** also uses lithium emission but combines the ingredients to synthesize salt **20**, in an effort to obtain similar formulation performance as **20** with only commercial off the shelf (COTS) ingredients. The goal was to compare the prototype scale performance of these three baseline formulations to those of formulations **III** – **VI** containing **20** and **26**, which had only been studied to date in smaller, bench-scale sized pellets.

***Table 33**: Chemical makeup of the red illuminant compositions.*

	Illuminant Composition Percentages by Weight						
Ingredient	**Control**	**I**	**II**	**III**	**IV**	**V**	**VI**
$Sr(NO_3)_2$	48.4						
KNO_3		39	39	30	48	30	48
Li_2CO_3		33	13.4				
5-AT			19.6				

20				33	33		
26						33	33
Mg 50/100		21	21	30	12	30	12
Mg 30/50	30.5						
PVC	14.1						
4:1 Epoxy	7						
NC		7	7	7	7	7	7

2.4.3 Blending of illuminant compositions

Lithium salts **20** and **26** were received from LMU and ground with a mortar and pestle; only the material passing through a 30-mesh US Standard sieve was collected and oven-dried for at least 18 hours prior to mixing. Likewise, strontium nitrate (50 microns max for the control formulation) and potassium nitrate (30 microns max for formulations I – VI) were passed through a 30-mesh US Standard sieve and dried in an oven for at least 18 h at 60 ^{o}C, after which time all ingredients were weighed according to their corresponding formulation weight percentages in **Table 33**. For the control formulation, a binder system (80:20 Epon 813/Versamid 140) was weighed in a steel Hobart mixing bowl and vigorously mixed by hand with a wooden tongue depressor for 1 min; for formulations **I** – **VI**, the binder was an 8.1% w/w solution of NC in acetone and required no manual mixing. For each formulation, magnesium powder was next added to the bowl and the mixture was blended with the aid of a B-blade at 40 rpm for 10 min. Then, for each formulation, the remaining ingredients were added to the bowl and each mixture was blended at 40 rpm for 20 min. After blending, each pyrotechnic mixture was poured from the mixer bowl to a large ceramic evaporating dish and dried overnight at 60 °C, except for the control which was dried overnight at ambient temperature. The next day, granulation of all compositions except the control was highly cumbersome and required extensive processing. This consisted of manually breaking the dried agglomerate, temporarily re-wetting with ~40 mL of acetone, manually kneading the dough to near-dryness, passing through a US standard 6-mesh sieve, and oven drying at 60 °C overnight once more. A photograph of every granulated formulation can be seen in **Figure 39**. All eight formulations were then ready for pressing. The above procedures were followed to prepare 500 grams of the control formulation and 400 grams each of formulations **I** – **VI**.

***Figure 39**: Photographs of the granulated pyrotechnic mixes.*

2.4.4 Assembly of cluster flares

Each cluster flare with perforated core (ID = 0.44”) was assembled by adding the following energetic materials sequentially to a kraft paper tube (ID= 1.13”, wall thickness = 0.11”) inside a stainless steel tooling: 1.0 g black powder (MIL-P-223B, Class 7), 2.5 g igniter, and 16.0 g illuminant composition. Here the igniter was a thermite composition consisting of the following ingredients as a percent by weight: 33.0% KNO_3, 24.5% silicon powder, 20.8% black iron oxide, 12.3% aluminum powder, 3.8% charcoal, and 5.6% NC. The three powder layers were pressed in one increment at 10,000 lb. dead load with a 10-second dwell (**Figure 40**). An overview of all prepared cluster flares can be seen in **Figure 41**.

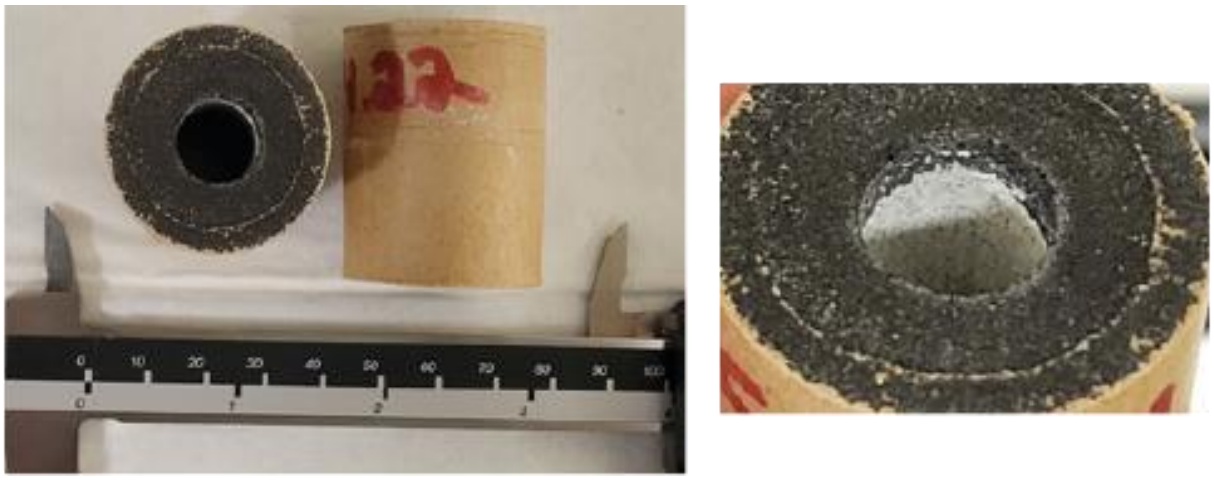

***Figure 40**: Images of a finished cluster flare; (left) top and side view, (right) inner diameter view showing igniter (black) and illuminant (gray) layers.*

***Figure 41**: Images of all finished cluster flares; (left) top view, (right) angled view.*

2.4.5 Assembly of parachute flares

Each parachute flare with solid core was assembled by adding the following energetic materials sequentially to a kraft paper tube (ID= 1.23”, wall thickness = 0.05”) inside a stainless steel tooling: 1.0 g black powder (MIL-P-223B, Class 7), 2.5 g igniter from above cluster section, and 50.0 g illuminant composition. The three powder layers were also pressed in one increment at 10,000 lb. dead load with a 10-second dwell (**Figure 42**). An overview of all prepared parachute flares can be seen in **Figure 43**.

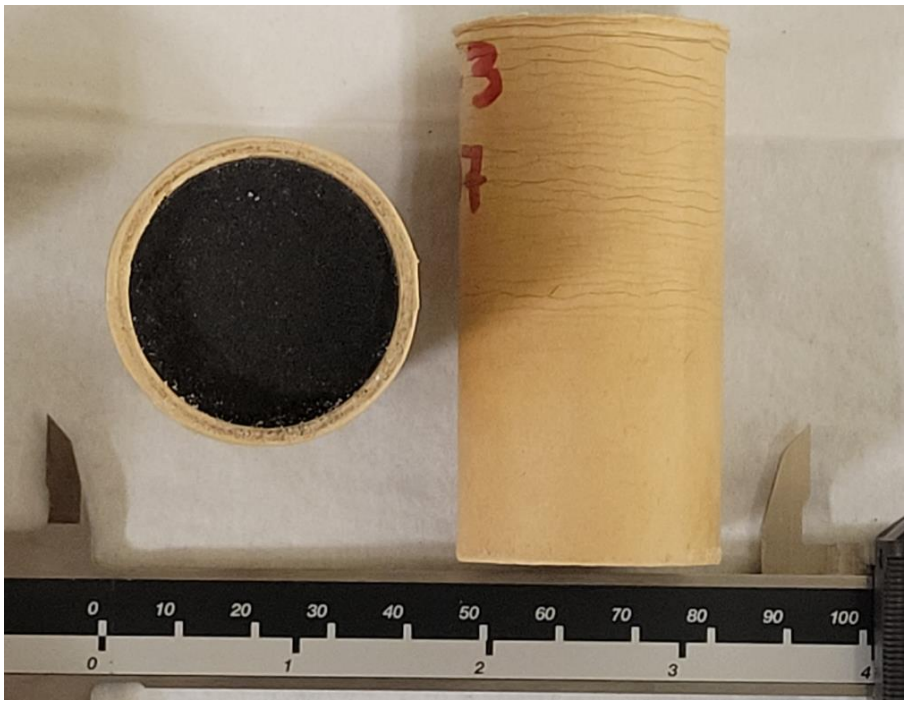

***Figure 42**: Top and side view of a finished parachute flare.*

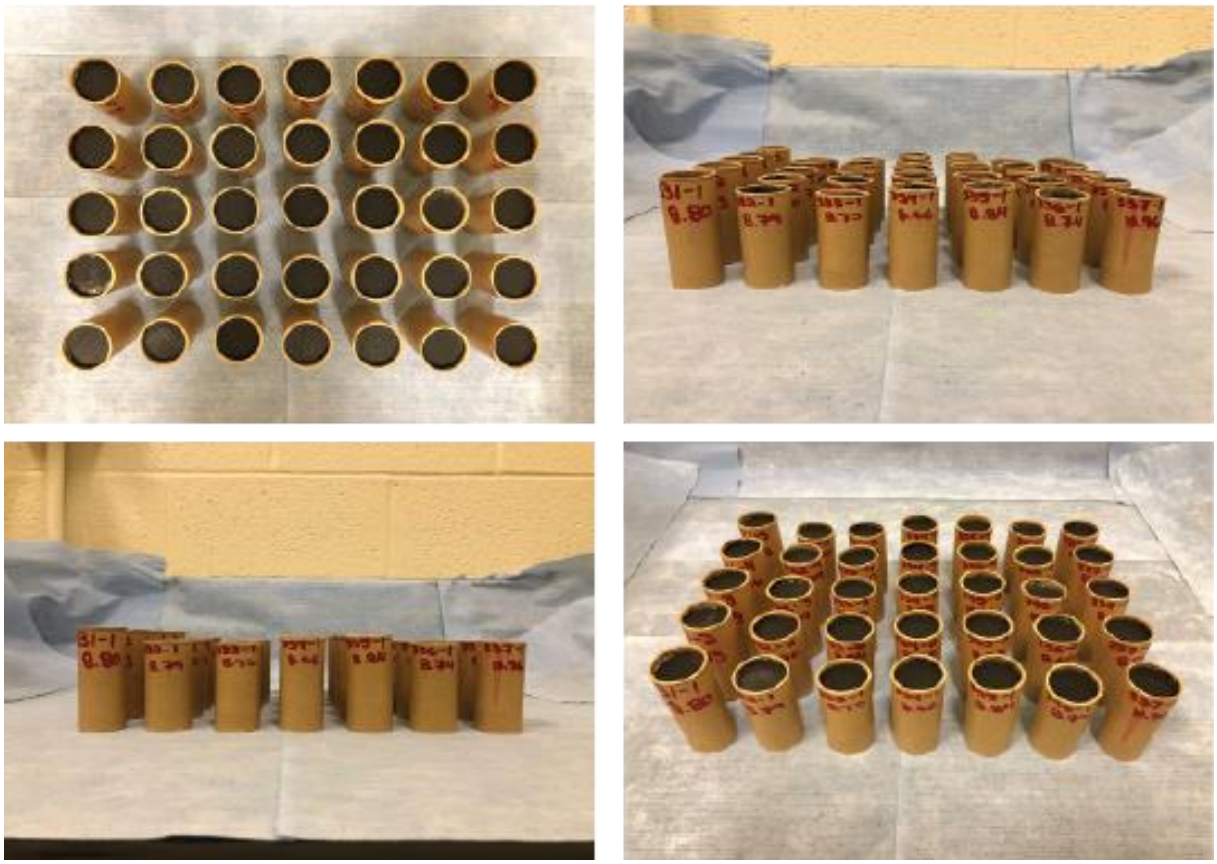

***Figure 43**: Images of all finished flares; (top left) top view, (top right/bottom left) side view, (bottom right) angled view of the flares.*

2.5 Prototype testing and results

In **Figure 44** and **Figure 45** the setup of the measurements of the cluster and parachute flares is shown.

***Figure 44**:Set up for the measurement of the cluster flares; (left/middle) angled view, (right) frontal view.*

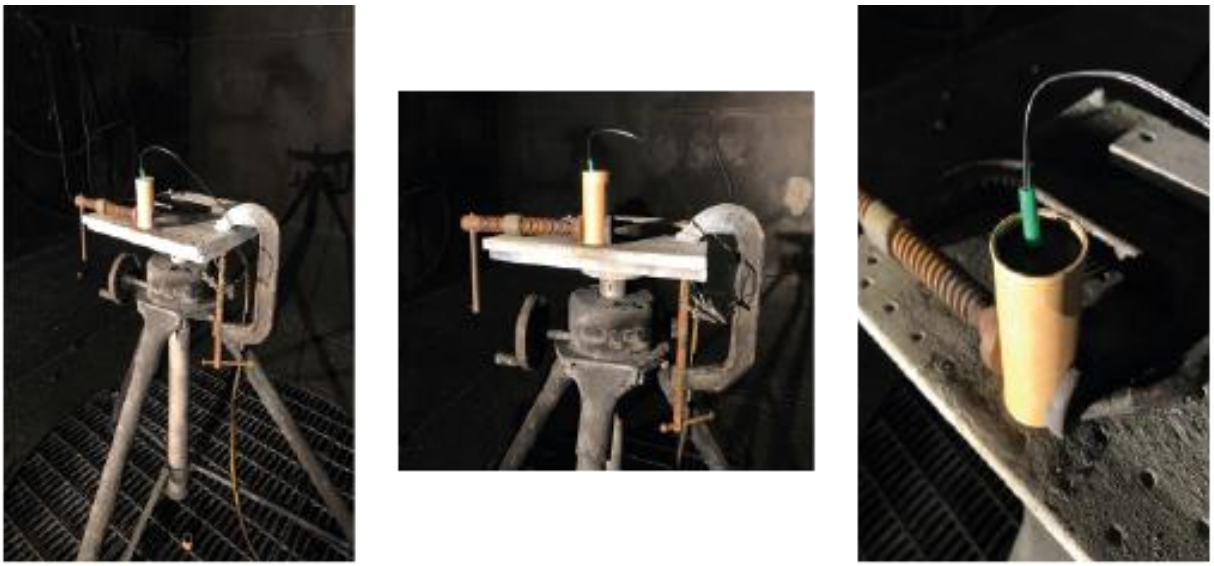

***Figure 45**: Set up for the measurement of the parachute flares from different angles.*

Spectral data was acquired with an Ocean Insight Flame spectrometer with a 230 micron core diameter multimode fiber as the input optic. The spectrometer was calibrated using the light output from a calibrated Labsphere integrating sphere (7.62 cm diameter aperture). The irradiance was calculated at the fiber probe (positioned 1.52 m from the aperture) and was input into the Oceanview software to build the absolute irradiance calibration file. This calibration file was input into the software when collecting data to produce absolute irradiance spectra (used in dominant wavelength and spectral purity calculations) that are free from instrument artifacts. The spectrometer's integration time was adjusted to keep all the spectral lines within the linear range of the spectrometer. Dominant wavelength and spectral purity were calculated based on illuminant C as the white point. Individual datapoints were averaged from the middle of the burn to get an average dominant wavelength and average spectral purity for each sample.

Photometric data was measured using an international light SED033 silicon detector with a Y3 filter and field of view limiting hood (H). The output from the photometer was connected to a DL instruments 1211 transimpedance amplifier. The voltage from the amplifier was digitized using a 16-bit National Instruments datacard and the data was collected with in-house developed Labview software. The calibration of the entire system was validated using the integrating sphere previously described as the calibrated light source. The photometer was placed 1.52 m from the integrating sphere's aperture and the luminous intensity was compared for both the integrating sphere and the photometer (using the manufacturer's provided calibration constant for the calculation). The luminous intensity of the integrating sphere and the calculated photometer's luminous intensity were nearly identical, thus validating the calibration of the system.

Data for each candle and parachute was collected at a rate of 500 samples/second or 1000 samples/sec (parachute and cluster, respectively). A threshold of 250 Cd was used to determine the start and end times of the burn. All data points between the threshold points were averaged to produce the average luminous intensity. The burn time was calculated from the difference between end and start times as determined by the threshold value.

***Table 34**: Geometry and optical emissive output of all cluster flares.*

Cluster Identification	Pellet Density	Burn Time	Luminous Intensity	Dominant Wavelength	Spectral Purity
	(g/cc)	(s)	(cd)	(nm)	(%)
Control – 1	1.87	10.27	19,196	611.3	86.8
Control – 2	1.96	10.31	16,934	612.0	88.0
Control – 3	1.83	9.95	18,534	611.8	87.9
Control – 4	1.85	9.80	19,723	611.9	88.0
Control – 5	1.82	9.82	16,413	611.7	87.5
I – 1	1.37	6.40	4,134	597.7	31.2
I – 2	1.55	6.70	3,862	597.7	34.5
I – 3	1.46	6.04	4,602	598.7	34.1
I – 4	1.49	6.40	3,941	598.6	31.7
I – 5	1.45	6.63	3,851	599.3	31.0
II – 1	1.41	8.75	1,672	601.9	45.8
II – 2	1.38	8.46	1,752	600.8	46.3
II – 3	1.40	8.39	1,742	601.4	46.0
II – 4	1.46	8.49	1,699	601.3	46.9
II – 5	1.44	8.57	1,602	601.4	45.8
III – 1	1.40	4.87	3,761	595.3	61.5
III – 2	1.46	5.02	4,311	595.7	61.3
III – 3	1.54	5.25	4,027	595.7	60.4
III – 4	1.55	4.96	4,684	595.6	60.9
III – 5	1.42	4.78	3,916	596.1	60.5
IV – 1	1.39	5.08	608	596.5	58.7
IV – 2	1.54	5.55	620	596.0	59.4
IV – 3	1.50	5.14	613	596.7	59.2
IV – 4	1.55	5.51	578	596.7	59.8
IV – 5	1.52	5.65	592	596.8	58.2

V – 1	1.36	5.40	2,985	596.1	54.2
V – 2	1.34	5.69	2,758	596.8	54.9
V – 3	1.35	5.41	3,098	596.1	53.8
V – 4	1.36	5.28	3,021	596.4	53.6
V – 5	1.37	5.30	3,027	596.3	54.9
VI – 1	1.45	4.24	1,282	601.3	52.3
VI – 2	1.41	4.05	1,201	598.2	51.3
VI – 3	1.44	4.18	1,196	597.3	51.2
VI – 4	1.40	4.12	1,201	597.8	50.8
VI – 5	1.48	4.06	1,194	597.9	50.4

***Table 35**: Geometry and optical emissive output of all parachute flares.*

Parachute Identification	**Pellet Density**	**Burn Time**	**Luminous Intensity**	**Dominant Wavelength**	**Spectral Purity**
	(g/cc)	(s)	(cd)	(nm)	(%)
Control – 1	1.94	33.06	16,994	611.4	79.5
Control – 2	1.92	32.91	21,001	611.6	78.6
Control – 3	1.88	33.15	18,961	612.5	80.2
Control – 4	1.90	33.44	15,544	612.8	81.6
I – 1	1.43	28.23	1,180	604.1	29.1
I – 2	1.41	28.63	938	604.2	28.3
I – 3	1.43	27.83	1,031	600.1	27.2
I – 4	1.47	28.95	982	604.7	30.9
I – 5	1.45	29.45	1,138	600.6	26.3
II – 1	1.47	37.35	944	612.3	36.4
II – 2	1.52	38.74	659	614.0	38.6
II – 3	1.48	37.33	840	611.1	38.8
II – 4	1.46	38.64	760	611.5	37.2
II – 5	1.45	36.92	996	608.8	38.0

III – 1	1.49	21.39	3,684	598.5	48.0
III – 2	1.49	21.65	3,212	597.8	52.0
III – 3	1.46	21.44	3,639	598.0	49.3
III – 4	1.47	21.52	3,543	597.7	51.1
III – 5	1.47	21.60	3,708	597.7	51.0
IV – 1	1.52	24.64	482	No data*	
IV – 2	1.51	25.19	451	No data*	
IV – 3	1.51	24.90	488	605.1	58.8
IV – 4	1.51	24.82	509	600.0	54.2
IV – 5	1.50	25.10	513	599.9	53.2
V – 1	1.43	25.42	2,513	597.1	50.3
V – 2	1.44	25.59	2,372	599.0	47.7
V – 3	1.40	24.77	2,561	599.2	48.2
V – 4	1.43	26.15	2,470	598.6	50.4
V – 5	1.42	25.82	2,530	599.0	49.2
VI – 1	1.40	22.03	811	602.0	45.4
VI – 2	1.43	21.40	814	603.9	42.0
VI – 3	1.41	22.64	736	602.4	46.3
VI – 4	1.47	21.62	799	602.9	43.9
VI – 5	1.49	21.10	655	605.0	41.5

* Color data for parachute flares **IV** – 1 and **IV** – 2 removed due to low signal levels.

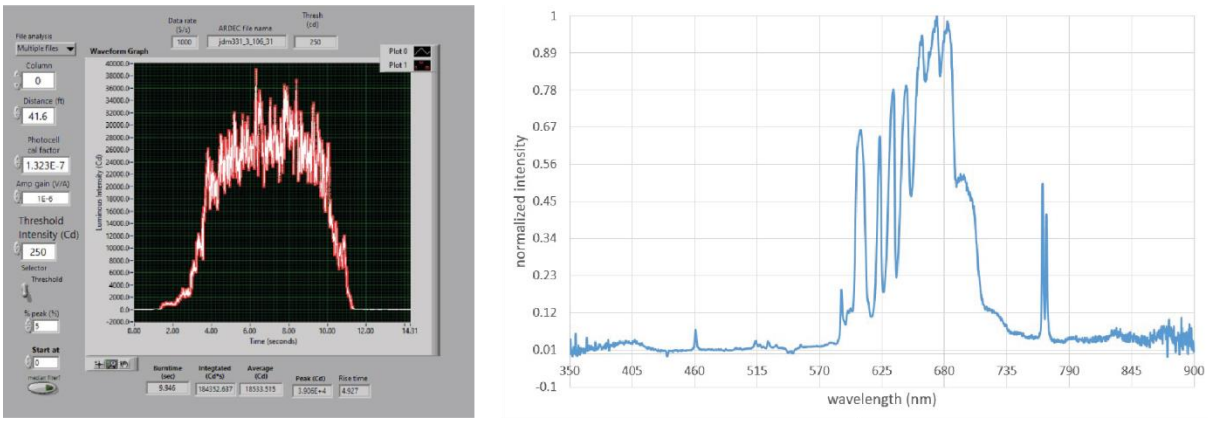

***Figure 46**: Photometric and spectrometric waveform for **Control - 3** cluster flare.*

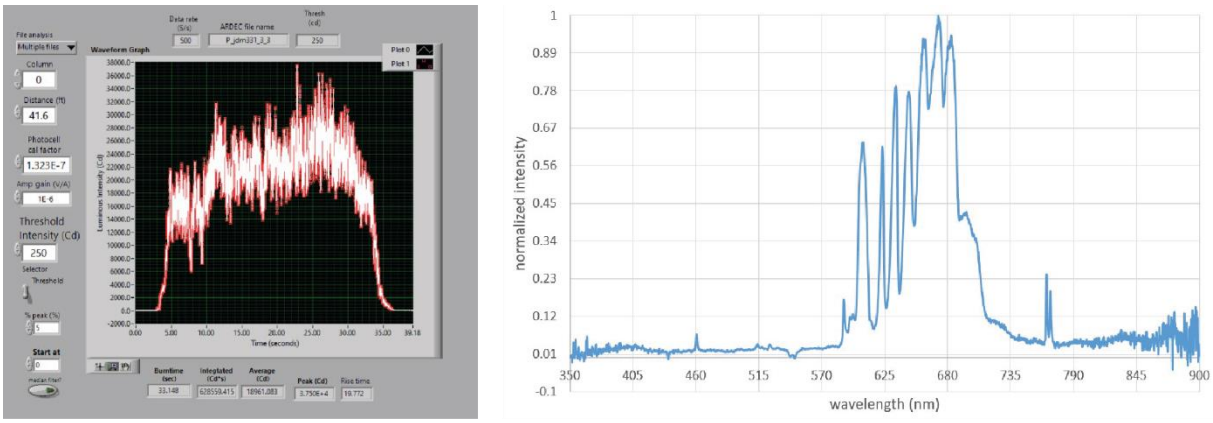

***Figure 47**: Photometric and spectrometric waveform for **Control - 3** parachute flare.*

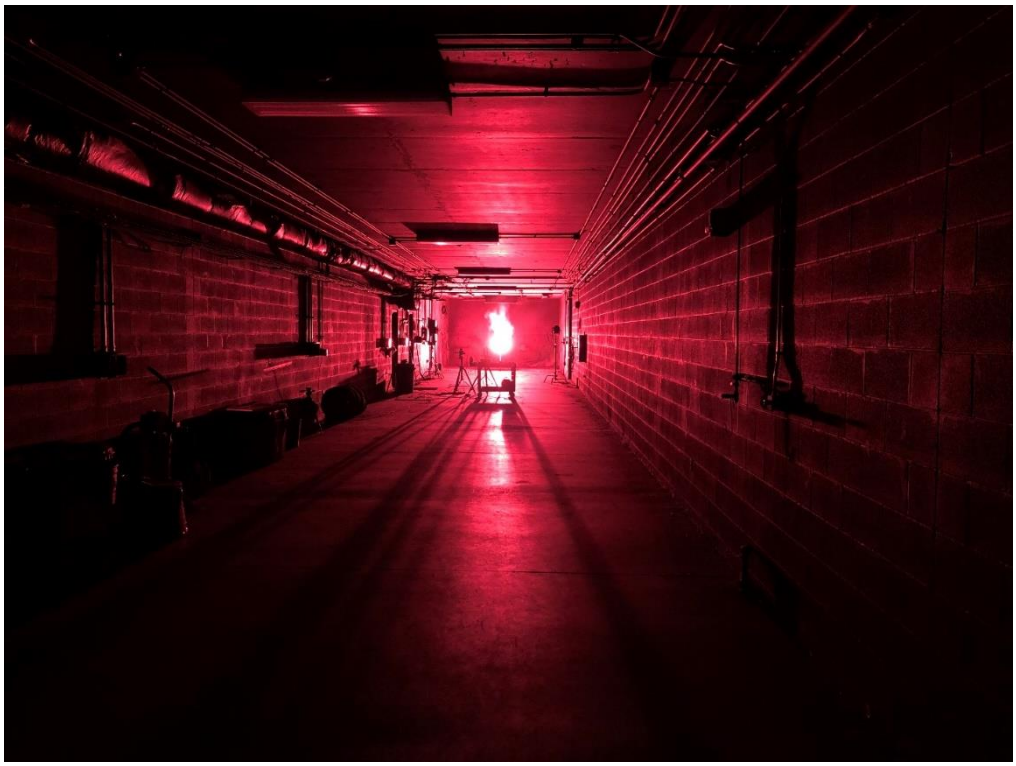

***Figure 48**: The **Control** composition, containing strontium nitrate, burns in the hand-held signal parachute flare configuration on a test stand (picture 1).*

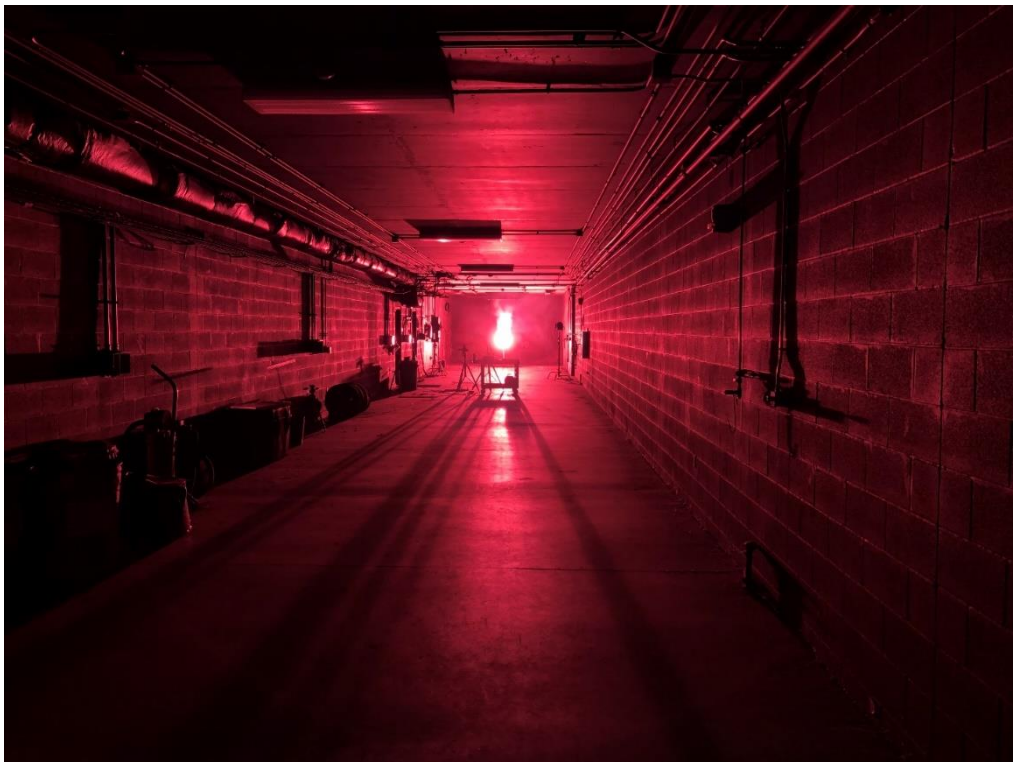

***Figure 49**: The **Control** composition, containing strontium nitrate, burns in the hand-held signal parachute flare configuration on a test stand (picture 2).*

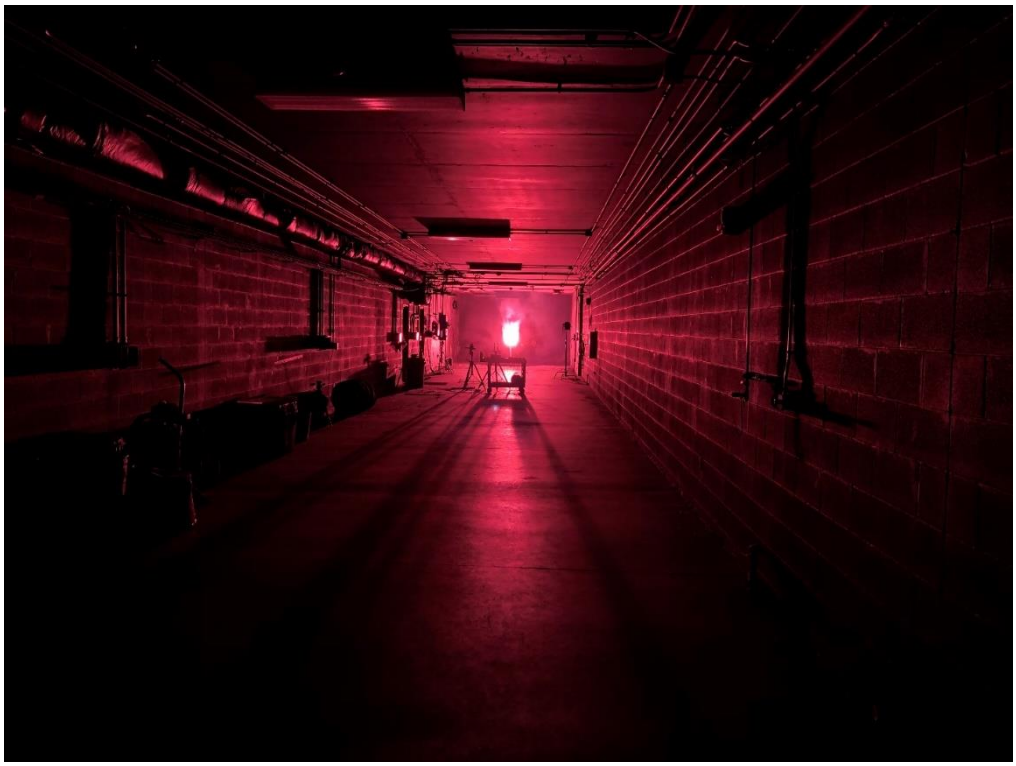

***Figure 50**: The **Control** composition, containing strontium nitrate, burns in the hand-held signal parachute flare configuration on a test stand (picture 3).*

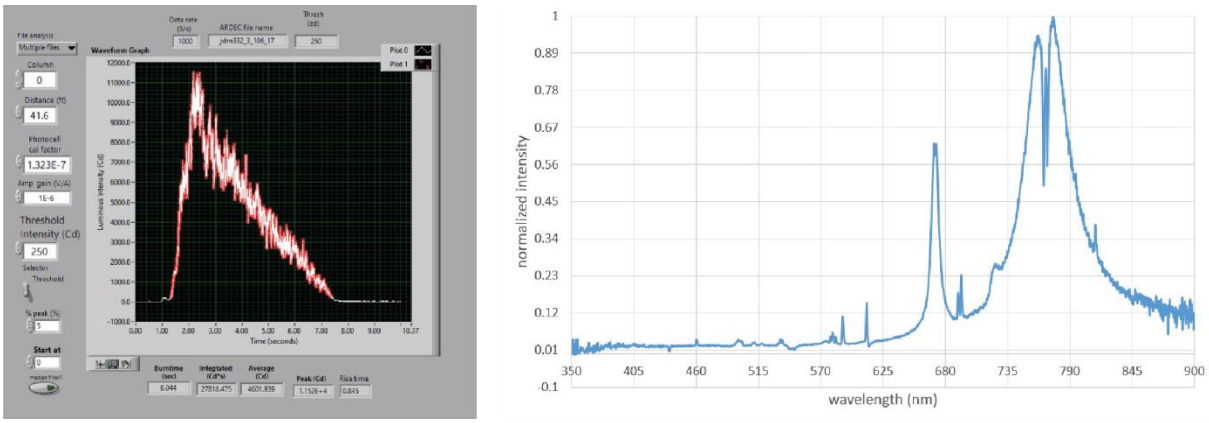

***Figure 51**: Photometric and spectrometric waveform for cluster flare **I - 3**.*

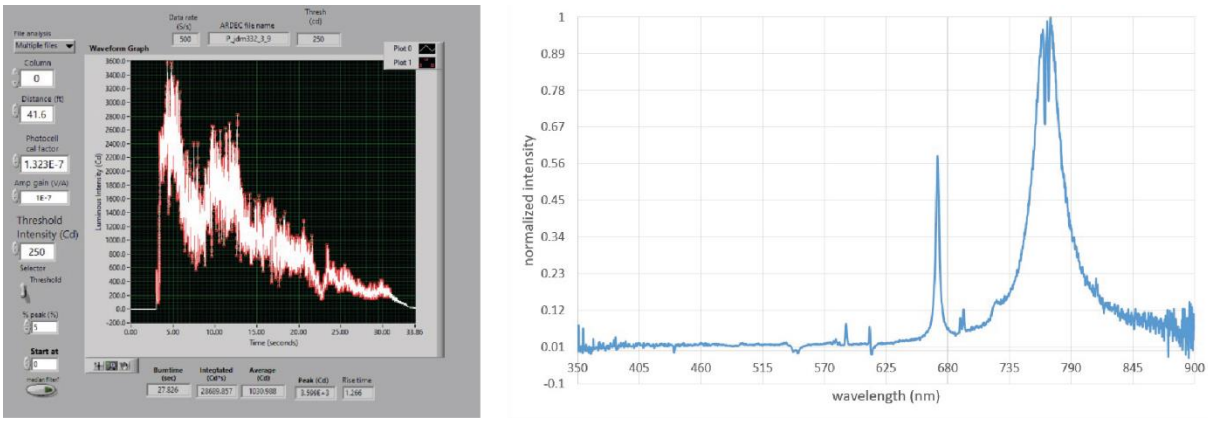

***Figure 52**: Photometric and spectrometric waveform for parachute flare **I – 3**.*

***Figure 53**: Composition **I**, which contained 33 wt-% Li2CO3, produced large amounts of slag upon combustion, as shown by this photograph taken after a test of a parachute flare.*

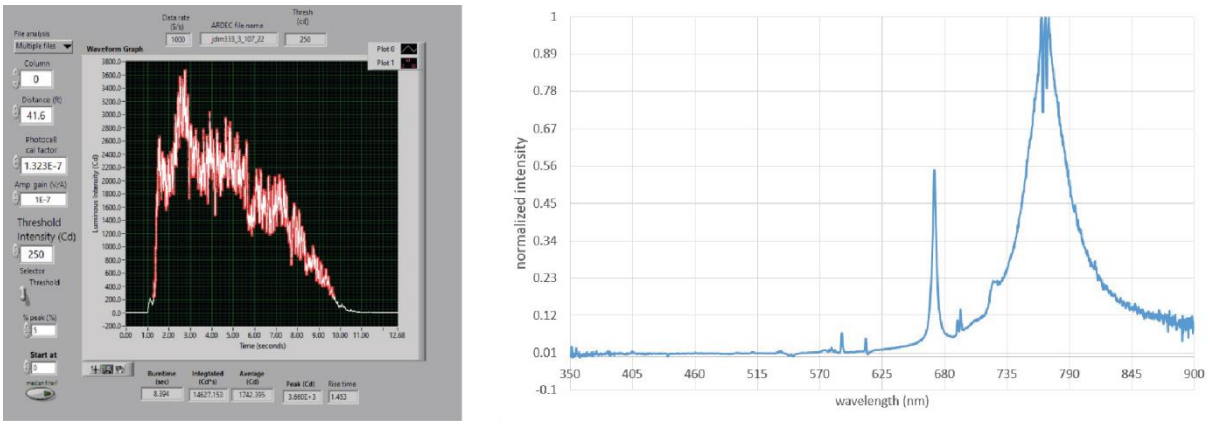

***Figure 54**: Photometric and spectrometric waveform for cluster flare **II - 3**.*

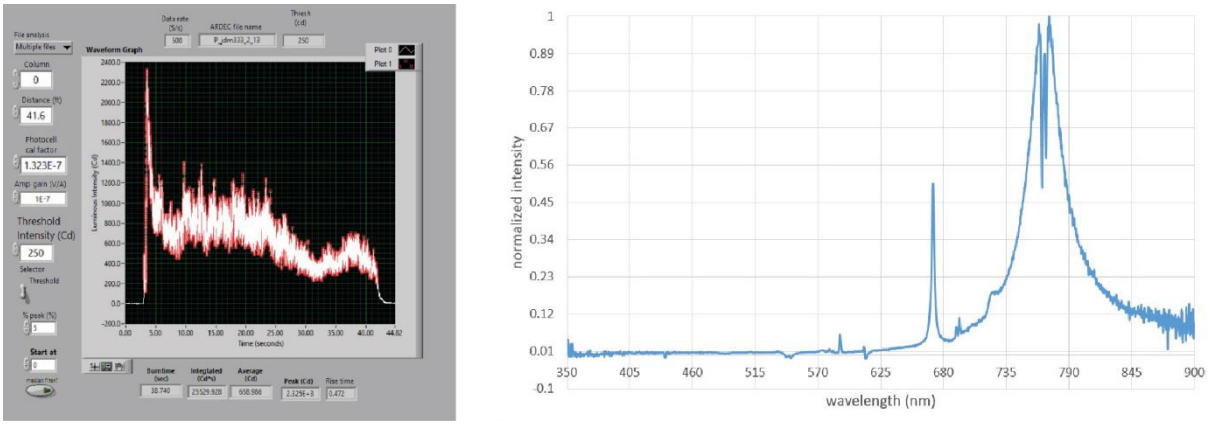

***Figure 55**: Photometric and spectrometric waveform for parachute flare **II – 3**.*

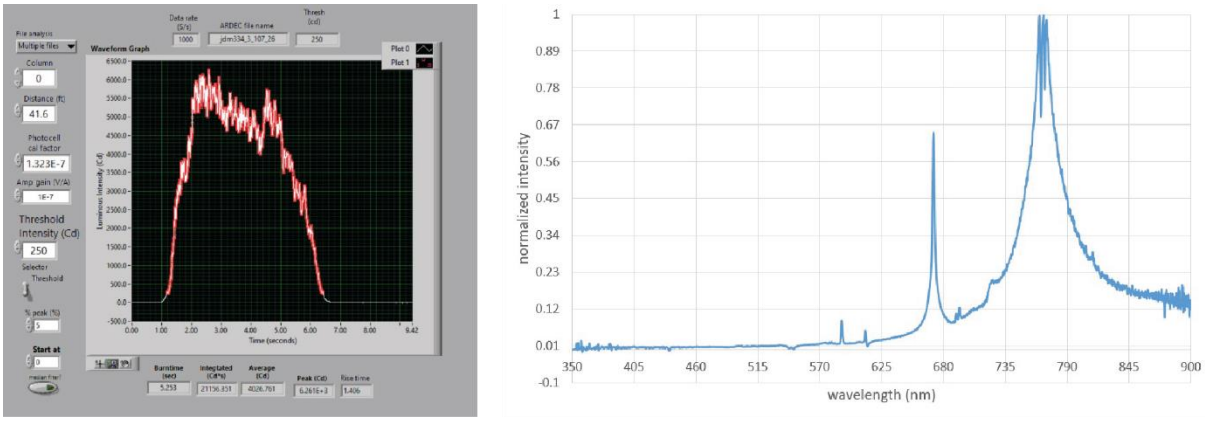

***Figure 56**: Photometric and spectrometric waveform for cluster flare **III – 3**.*

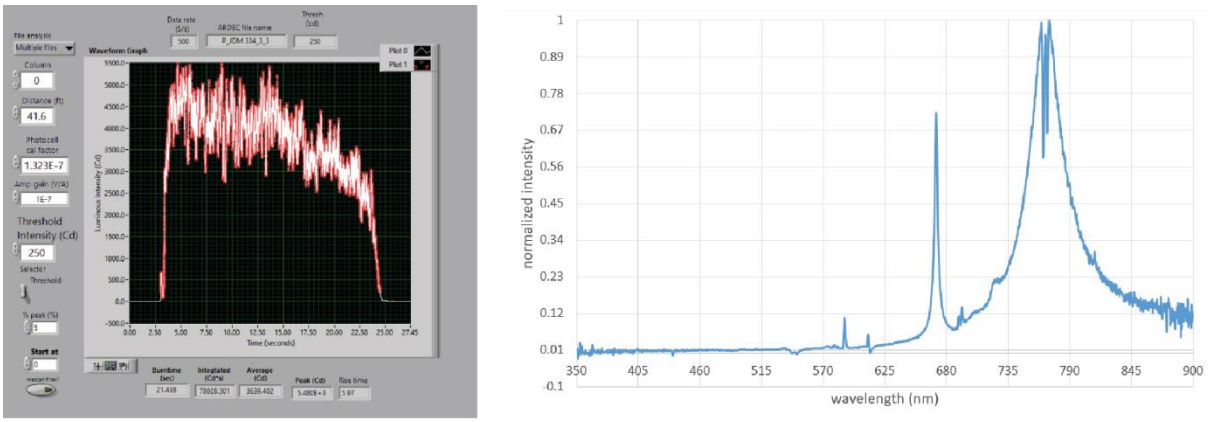

***Figure 57**: Photometric and spectrometric waveform for parachute flare **III – 3**.*

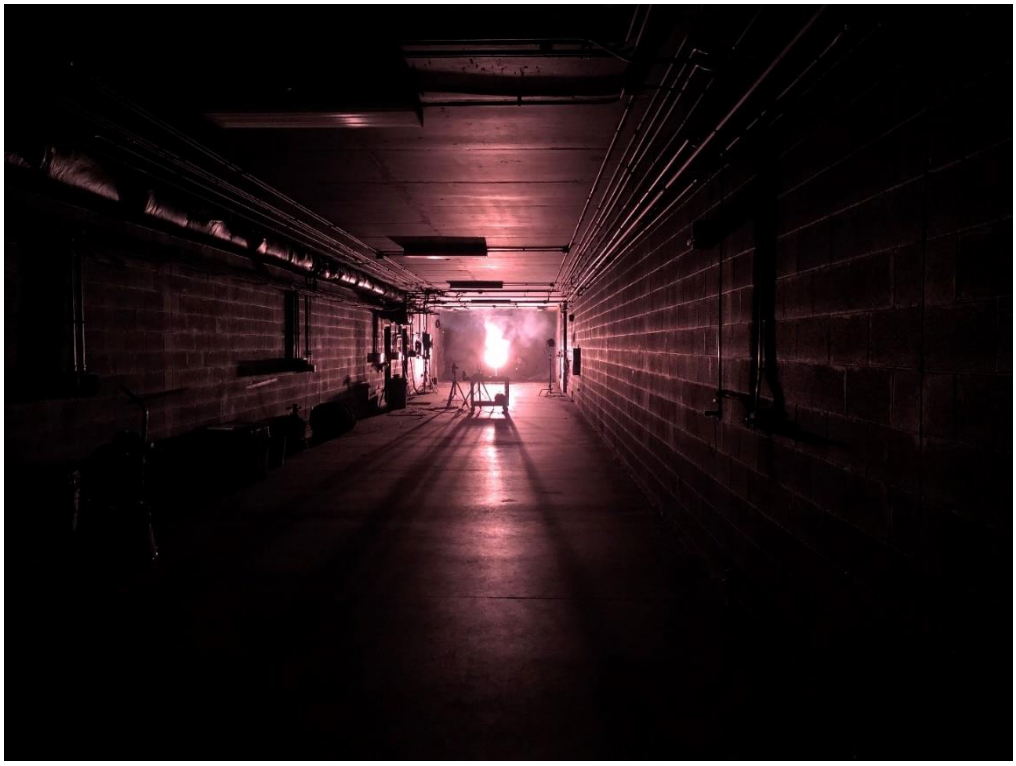

***Figure 58**: Composition **III**, containing 33 wt-% Li 5-aminotetrazole and 30 wt-% Mg, burns in the hand-held signal parachute flare configuration on a test stand (picture 1).*

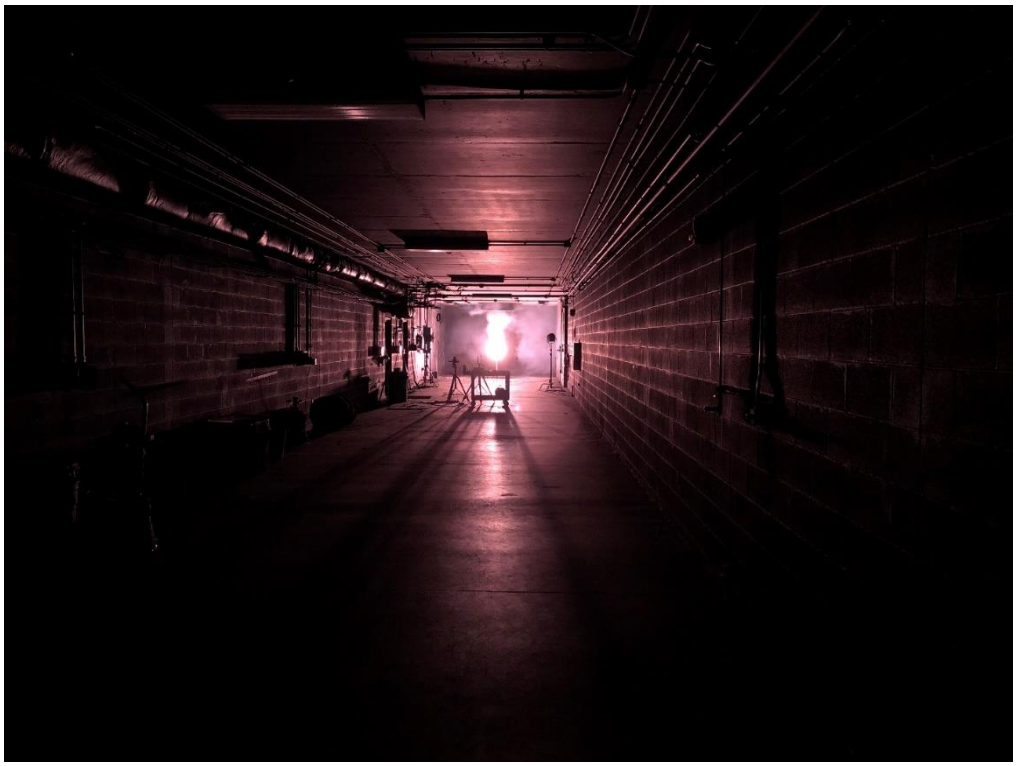

Figure 59: *Composition **III**, containing 33 wt-% Li 5-aminotetrazole and 30 wt-% Mg, burns in the hand-held signal parachute flare configuration on a test stand (picture 2).*

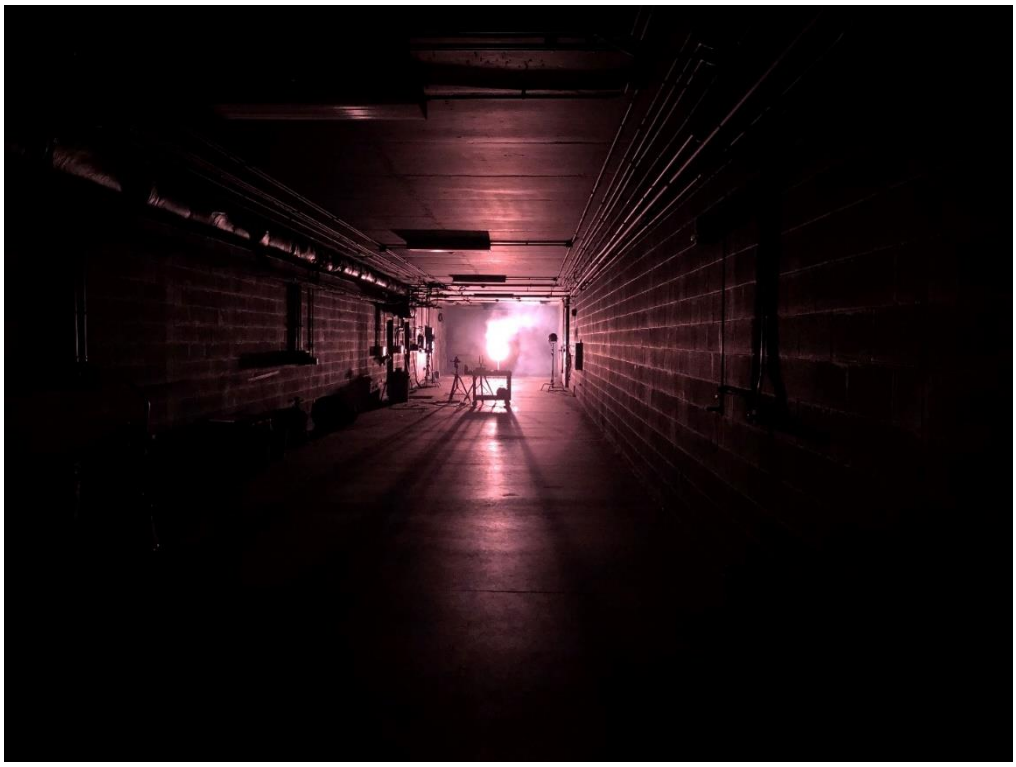

Figure 60*: Composition **III**, containing 33 wt-% Li 5-aminotetrazole and 30 wt-% Mg, burns in the hand-held signal parachute flare configuration on a test stand (picture 3).*

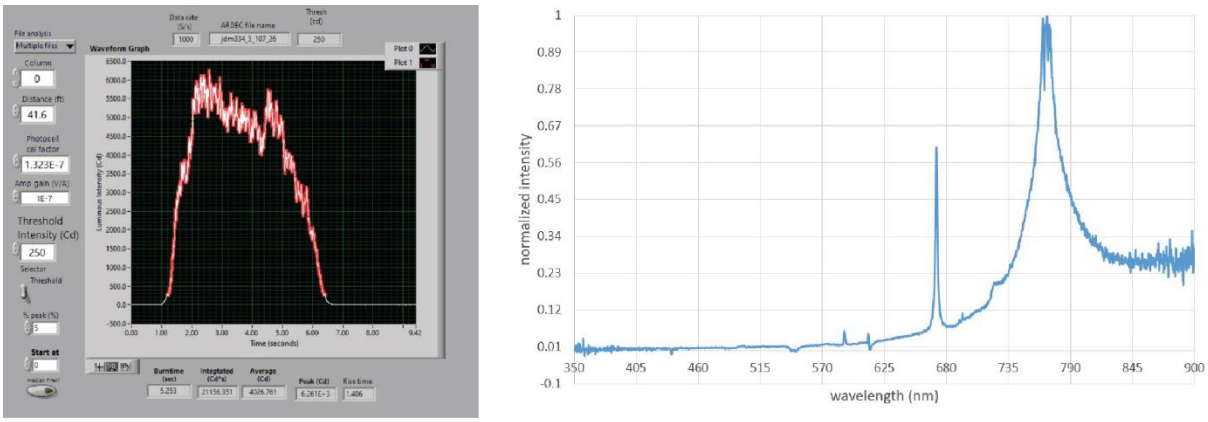

***Figure 61**: Photometric and spectrometric waveform for cluster flare **IV – 3**.*

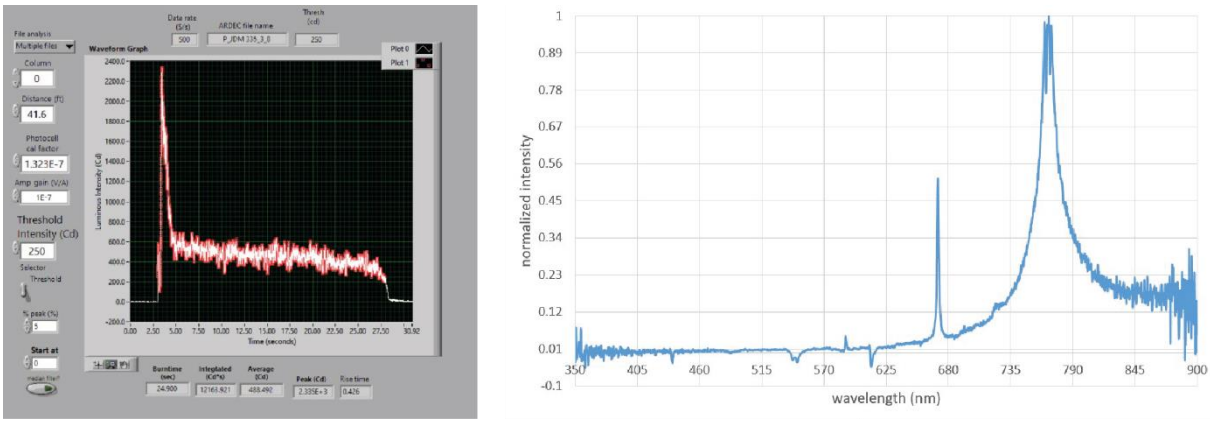

***Figure 62**: Photometric and spectrometric waveform for parachute flare **IV – 3**.*

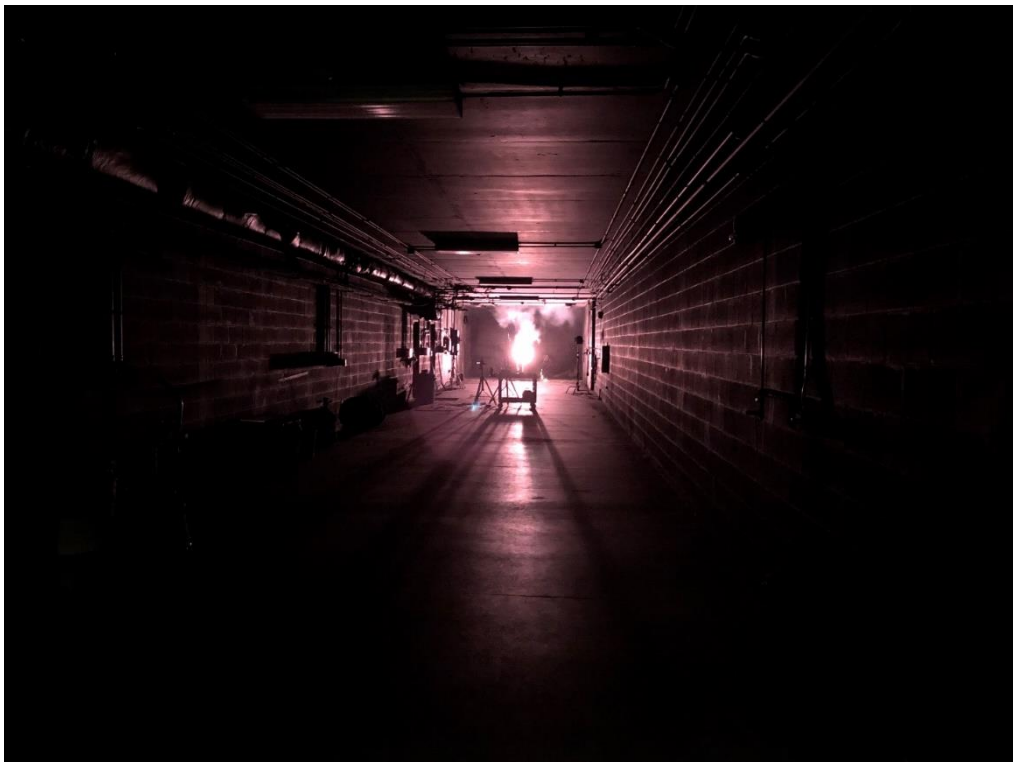

***Figure 63**: Composition **IV**, containing 33 wt-% Li 5-aminotetrazole and 12 wt-% Mg, burns in the hand-held signal parachute flare configuration on a test stand (picture 1).*

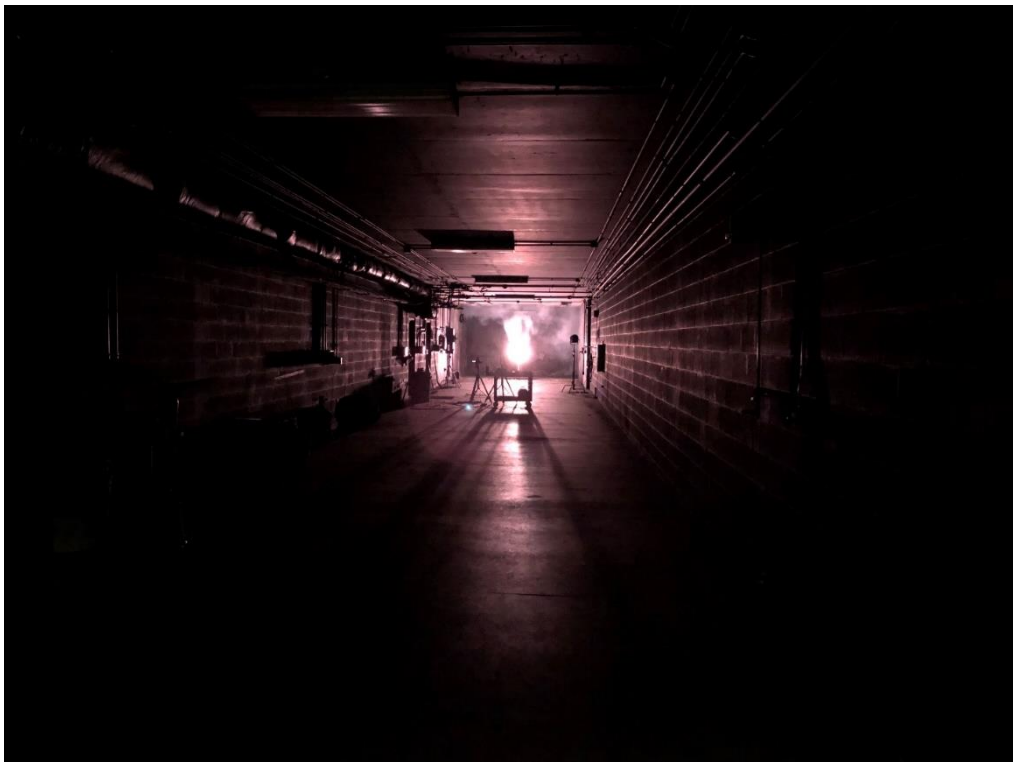

***Figure 64**: Composition **IV**, containing 33 wt-% Li 5-aminotetrazole and 12 wt-% Mg, burns in the hand-held signal parachute flare configuration on a test stand (picture 2).*

***Figure 65**: Composition **IV**, containing 33 wt-% Li 5-aminotetrazole and 12 wt-% Mg, burns in the hand-held signal parachute flare configuration on a test stand (picture 3).*

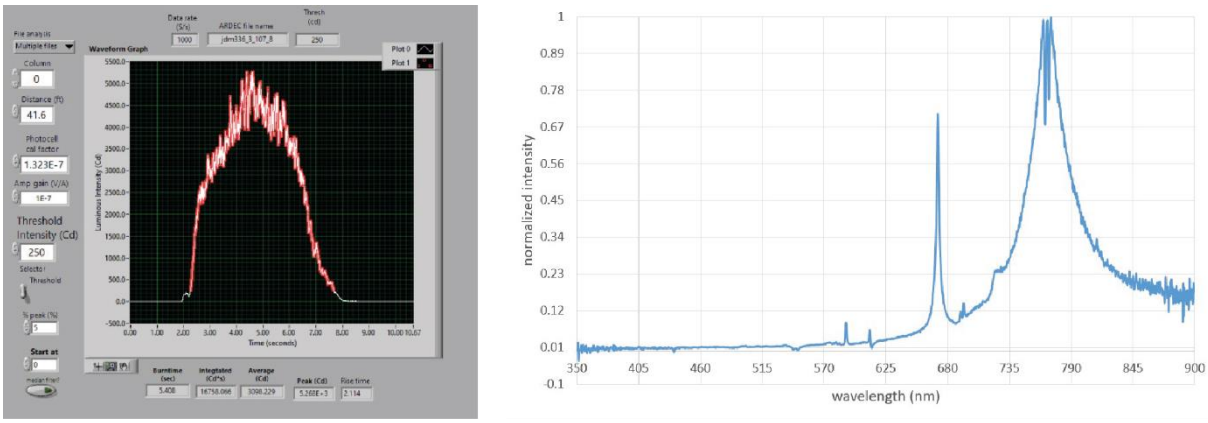

***Figure 66**: Photometric and spectrometric waveform for cluster flare **V – 3**.*

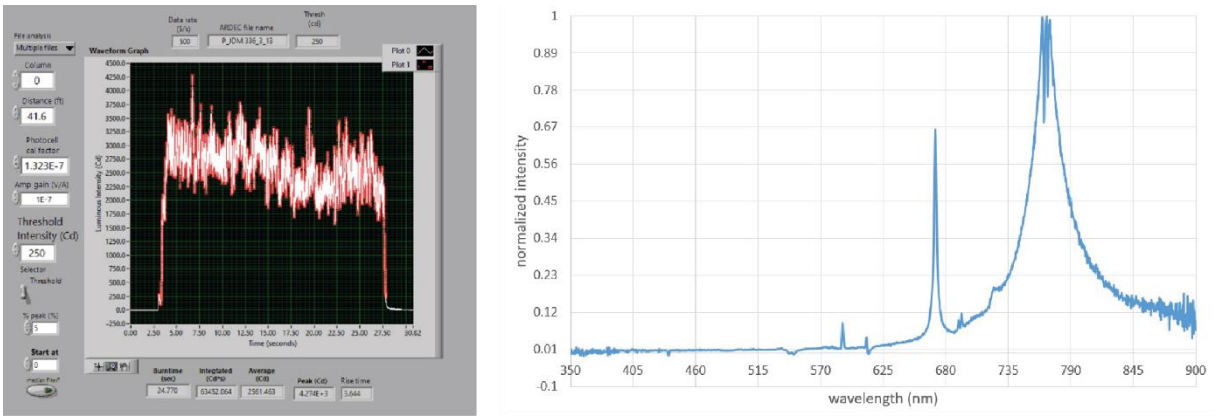

***Figure 67**: Photometric and spectrometric waveform for parachute flare **V – 3**.*

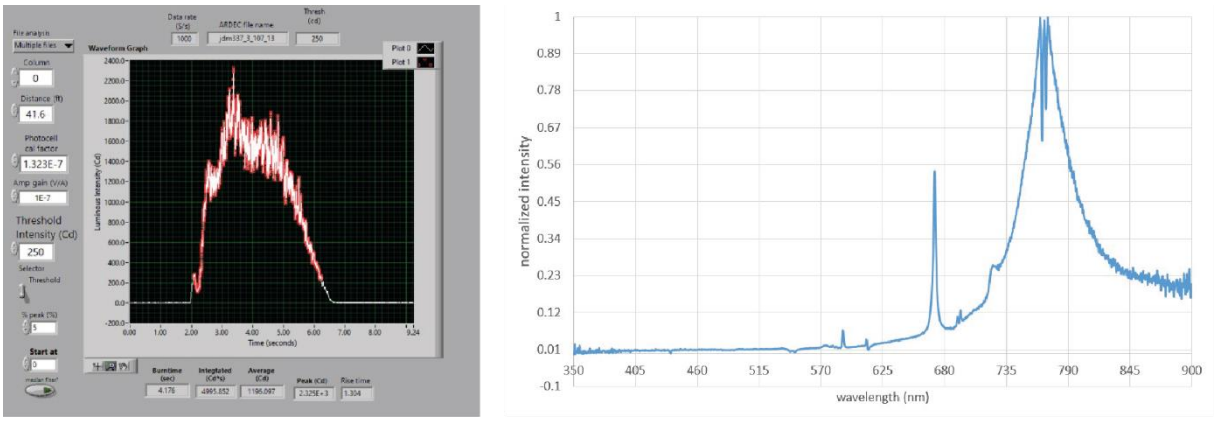

***Figure 68**: Photometric and spectrometric waveform for cluster flare **VI – 3**.*

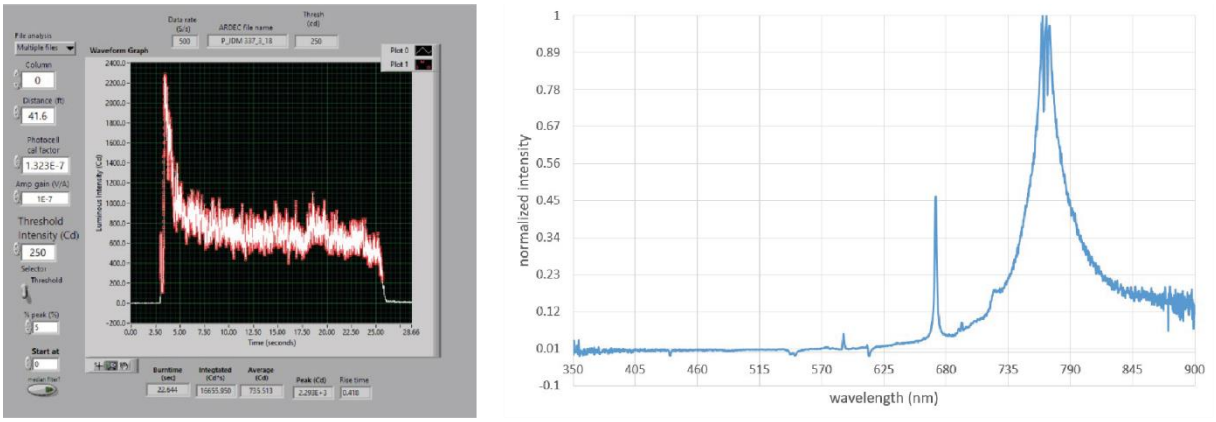

***Figure 69**: Photometric and spectrometric waveform for parachute flare **VI – 3**.*

3 Executive Summery

3.1 Introduction

Traditional red-light-emitting pyrotechnic formulations are based on strontium and chlorinated organic materials. These mixtures mostly contain strontium nitrate in combination with a chlorine donor, such as polyvinyl chloride (PVC), to form metastable strontium (I) chloride as the red-light-emitting species.[1] During the combustion of these formulations, highly carcinogenic polychlorinated biphenyl, dibenzofuran and dibenzo-*p*-dioxin derivates are formed.[2] According to a recent report from the United States Environmental Protection Agency (U.S. EPA), strontium is potentially harmful to human health.[3] It is also reported that strontium replaces calcium in the bone, interferes with bone strength, and thus affects the skeletal development of children and adolescents. In 2014, the U.S. EPA made a preliminary decision to start regulating the amount of strontium in drinking water.[47]Strontium has been detected in 99 % of all public water systems and at levels of concern in 7 % of the public water systems in the USA.[48] While U.S. military training grounds were not included in the study, these facilities may show evaluated concentrations of strontium as well, given the presence of strontium in former and currently used red-light-illuminating signaling pyrotechnic compositions. This includes the red star cluster as well as the red star parachute illuminant.[4,49] In addition, the emergency highway signals (civilian sector) are also based on strontium nitrate.

Table 36: *Sr-based red-light illuminant formulations of a cluster and a parachute flare.*

Formulation	***$Sr(NO_3)_2$*** **[wt%]**	**Mg 30/50 [wt%]**	***PVC*** **[wt%]**	***Mg 50/100*** **[wt%]**	***Laminac 4116/Lupersol*** **[wt%]**	***$KClO_4$*** **[wt%]**
In-service M158 red star cluster	48	33	15	-	4	-
M126A1 red star parachute illuminant	39.3	14.7	14.7	14.7	6.8	6.8

The only element that is capable of producing a similar color impression to strontium is lithium. Until this point, lithium is not considered toxic for humans, and it is applied in medicine to treat various mental disorders.[50] The intended main emitter for lithium-containing flames is atomic $Li^0_{(g)}$.[51]

3.2 Objectives

In general, the goal of the project WP19-1287 is to find a novel pyrotechnic system that will significantly reduce the environmental impact of pyrotechnics. The requirements of these pyrotechnic system can be divided into several points such as

- Enhancing the color while reducing the size and weight of the project
- High color purity and luminous intensity
- Low smoke generation
- Free of chlorine (perchlorate), heavy metals and strontium
- No toxic solvents involved in synthesis and purification

In accordance with these points, we propose to:

- Develop new lithium based pyrotechnical compositions as red illuminates
- Synthesize high-nitrogen Li-salts which are new or as described in literature
- Focus on simple reactions with a low number of reaction steps for potential scale-up and industrial adaption
- Develop completely Sr/chlorine and perchlorate-free formulations which are nonpolluting
- Increase the intensity of lithium containing formulations

The presented approach here describes several strategies for a lithium-based red pyrotechnical illuminant signal meeting the military requirement for the dominant wavelength (620±20 nm) and spectral purity (≥ 76 %). The developed new formulations will be completely chlorine-/heavy metal/strontium-free meeting potential U.S. EPA future regulations regarding strontium. This could avoid future health problems for all people related to pyrotechnical applications worldwide.

3.3 Technology Description

After the synthesis the lithium salts were completely characterized. NMR (were measured on a JEOL Bruker 400, Eclipse 270, JEOL EX 400, or a JEOL Eclipse 400 instrument.), IR (Perkin-Elmar BXII FT-IR system provided with a Smith DuraSampler IR II diamond ATR), elemental analysis and DTA measurements were performed to achieve a complete characterization. In some cases, a crystal structure could also be measured to provide information about the structure of the compounds. An important information is the sensitivity of the new or literature-known compounds produced. For this purpose, impact, friction and electrostatic discharge measurements were performed in order to provide information on the following. Impact and friction sensitivity were tested using BAM standardized (Bundesanstalt für Materialforschung und -prüfung) devices. In addition, all substances were tested for hazard to electrostatic discharge using an OZM Electric Spark Tester XSpark10[52]. In all three

procedures, sensitivities were determined using the 1 out of 6 method to evaluate the no-fire level.

***Figure 70**: Analytical devices: Xcalibur Sapphire 3 for X-ray measurements, OZM DTA 552-Ex for differential thermal analysis, BAM standardized friction and impact device and an OZM Electric Spark Tester XSpark10, respectively.*

When a lithium salt met the requirements, pyro mixtures were prepared containing the salts. Afterwards, all constituents of the compositions had been weighed out according to their weight percentages with a deviation of 2 mg and had been hand-blended to homogeneous mixtures. Then a 10 wt% solution of nitrocellulose in acetone was added. The resulting gum-like mass was kneaded, until the solvent had completely evaporated. For the mixtures containing the epoxy binder, solutions of Epon 813 and Versamid 140 in ethyl acetate with concentrations in the range of 20 or 10 g L^{-1}, respectively, were added resulting in a weight percent ratio of 80:20. The slurries thus obtained were blended approximately every ten minutes, until the solvent had completely evaporated. Subsequently, the mixtures were cured at 60 °C over night and blended to fine powders. Portions of 500 mg with a deviation of 2 mg had been weighed out, before they were pressed to pellets in one increment at a consolidation dead load of 3 t with a dwell time of roughly 10 s. The latter were ignited by the tip of a sparkler and their combustions recorded with a digital DCR-HC37E video camera from Sony. The dominant wavelengths, spectral purities, and luminous intensities were measured over the full burn of the pellets with the aid of a HR2000+ES spectrometer with an ILX 511B linear silicon CCD-array detector (range 190 to 1100 nm) provided with software from OCEAN OPTICS. The distance between the detector of the spectrometer and the sample was calibrated to 1.000 m and the acquisition time was set to 20 ms. The dominant wavelengths as well as the color purities were evaluated based on the 1931 CIE method using illuminant C as the white reference point. Average values of all emissive parameters and burn time were gained by taking two samples into account, respectively.

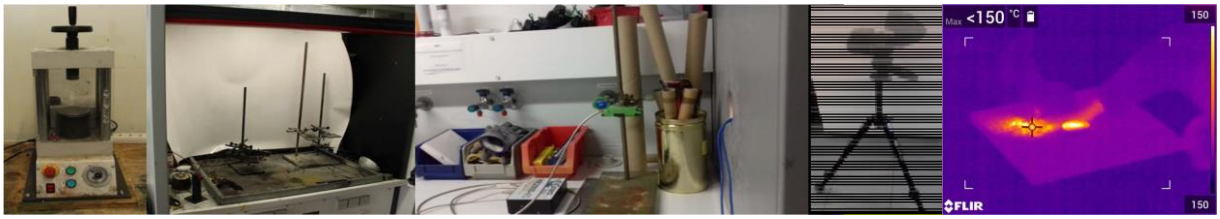

***Figure 71**: Representation of the pyrometric setup: Press, fume hood for the burn-off, spectrometer (Ocean Optics), FLIR thermal camera and display of the thermal measurement.*

After the transfer of the lithium salts to DEVCOM, cluster flares and parachute flares were produced and their pyrotechnical parameters were measured.

Figure 72: *Display of a parachute flare manufactured by DEVCOM.*

Each cluster flare with perforated core (ID = 0.44”) was assembled by adding the following energetic materials sequentially to a kraft paper tube (ID= 1.13”, wall thickness = 0.11”) inside a stainless steel tooling: 1.0 g black powder (MIL-P-223B, Class 7), 2.5 g igniter, and 16.0 g illuminant composition

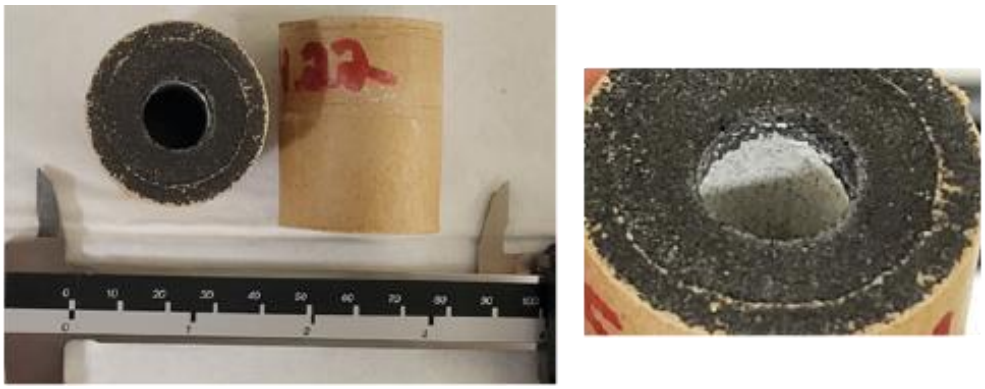

Figure 73: *Images of a finished cluster flare; (left) top and side view, (right) inner diameter view showing igniter (black) and illuminant (gray) layers.*

Each parachute flare with solid core was assembled by adding the following energetic materials sequentially to a kraft paper tube (ID= 1.23”, wall thickness = 0.05”) inside a stainless steel tooling: 1.0 g black powder (MIL-P-223B, Class 7), 2.5 g igniter from above cluster section, and 50.0 g illuminant composition.

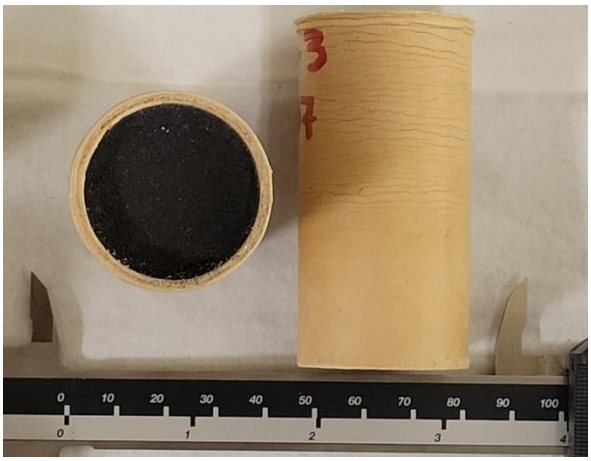

Figure 74: *Top and side view of a finished parachute flare.*

3.4 Performance Assessment

In the context of this project, several topics were worked on. First, several new lithium pyrazolate and borate salts have been synthesized and completely characterized by standard techniques such as infrared spectroscopy (IR), nuclear magnetic resonance spectroscopy (NMR), elemental analysis (EA) and low-temperature single-crystal X-ray diffraction. Additionally, decomposition temperatures were measured by means of an OZM Research differential thermal analysis (DTA) 552-Ex instrument in the range of 25-400 °C at a heating rate of 5 °C min^{-1} and the sensitivities toward friction, impact and electrostatic discharge were determined using a Bundesanstalt für Materialforschung (BAM) friction tester, a BAM drop hammer and an OZM Electric Spark XSpark10 instrument[33] according to NATO standardization agreement (STANAG) 4487[35] and STANAG 4489[36] with modified instructions[53,54], respectively.

All new or already literature-known lithium salts were evaluated in multiple aspects for example, external stimuli (friction, impact and electrostatic discharge), decomposition temperatures, simplicity of the reactions and toxicological aspects. Based on the results thus obtained from these various methods, a selection of salts was made to be used for further pyro mixtures. The most promising salts were lithium 4-amino-3,5-dinitropyrazolate sesquihydrate (**14**), lithium tetrazolate (**18**), lithium 5-aminotetrazolate (**20**), dilithium 5,5`-bistetrazolate dihydrate (**26**), dilithium 5,5`-bis(tetrazole-1-oxide) tetrahydrate (**30**), lithium picramate sesquihydrate (**36**), lithium dihydrobis(1,2,4-triazol-1-yl)borate sesquihydrate (**59**) and lithium dihydrobis(5-aminotetrazol-1-yl)borate (**64**). The salts **18** and **30** were not further investigated due to poor performance in the drop-in formulations. The lithium compounds **14** and **36** are unusable for the project, because these salts are toxic. The borate salts **59** and **64** were not considered for further testing because upscaling was not possible and the burnup products are on the watch list to be cancerogenic.[39]

Table 37: *Most promising formulations.*

Formulation	***KNO_3*** **[wt%]**	***Mg 50/100*** **[wt%][a]**	***20*** **[wt%]**	***26*** **[wt%]**	***Nitrocellulose*** **[wt%][b]**
AD-7	48	12	33	-	7
AD-30	40	20	33	-	7
AD-8	48	12	-	33	7
AD-32	40	20	-	33	7

Table 38: Measured pyrotechnic values of the most promising mixtures.

Formulation	Ω_{CO2} [%][a]	*BT* [s][b]	λ_d [nm][c]	Σ [%][d]	*LI* [cd][e]
AD-7	- 8.52	6.2	600	48	3360
AD-30	- 16.95	3.2	601	37	-
AD-8	- 2.48	3	601	40	3846
AD-32	- 10.91	1.7	602	38	14100

a) Oxygen balance with respect to formation of CO_2, Li_2O. b) *BT* [s]: burn time, c) λ_d [nm]: dominant wavelength, d) Σ [%]: spectral purity, e) *LI* [cd]: luminous intensity.

The blends that performed the best were reported to the US Army's cooperating partner, *DEVCOM Armaments Center* (*DEVCOM AC*). And the associated lithium salts, lithium 5-aminotetrazolate (**20**) and dilithium 5,5`-bistetrazolate dihydrate (**26**) were produced on a larger scale at the *Ludwig-Maximilians-Universität* in Munich and dispatched to the cooperation partner. At *DEVCOM AC*, the mixtures were reproduced and tested for their applicability. To verify the applicability, the mixtures were pressed into cluster and parachute flares and the resulting key parameters were determined. The only additional parameter measured with the flares is the pellet density. The photometric and spectrometric waveforms were also measured and displayed graphically. Additional mixtures with Li_2CO_3 were prepared to obtain a comparison with an inorganic salt.

Table 39: Prepared formulations at DEVCOM.

	Illuminant Composition Percentages by Weight						
Ingredient	**Control**	**I**	**II**	**III**	**IV**	**V**	**VI**
$Sr(NO_3)_2$	48.4						
KNO_3		39	39	30	48	30	48
Li_2CO_3		33	13.4				
5-AT			19.6				
20				33	33		
26						33	33
Mg 50/100		21	21	30	12	30	12
Mg 30/50	30.5						
PVC	14.1						
4:1 Epoxy	7						
NC		7	7	7	7	7	7

For each formulation in the cluster flares that have lithium salts as color donors, worse parameters have been measured. The luminous intensity was a factor of 10 worse than in the control mixture. Likewise, the values for the dominant wavelength dropped below the required 600 nm. Likewise, none of the lithium-based mixtures achieved the desired spectral purity of over 76% (see **Table 40**).

***Table 40**: Geometry and optical emissive output of all cluster flares.*

Cluster Identification	**Pellet Density**	**Burn Time**	**Luminous Intensity**	**Dominant Wavelength**	**Spectral Purity**
	(g/cc)	(s)	(cd)	(nm)	(%)
Control – 1	1.87	10.27	19,196	611.3	86.8
Control – 2	1.96	10.31	16,934	612.0	88.0
Control – 3	1.83	9.95	18,534	611.8	87.9
Control – 4	1.85	9.80	19,723	611.9	88.0
Control – 5	1.82	9.82	16,413	611.7	87.5
I – 1	1.37	6.40	4,134	597.7	31.2
I – 2	1.55	6.70	3,862	597.7	34.5
I – 3	1.46	6.04	4,602	598.7	34.1
I – 4	1.49	6.40	3,941	598.6	31.7
I – 5	1.45	6.63	3,851	599.3	31.0
II – 1	1.41	8.75	1,672	601.9	45.8
II – 2	1.38	8.46	1,752	600.8	46.3
II – 3	1.40	8.39	1,742	601.4	46.0
II – 4	1.46	8.49	1,699	601.3	46.9
II – 5	1.44	8.57	1,602	601.4	45.8
III – 1	1.40	4.87	3,761	595.3	61.5
III – 2	1.46	5.02	4,311	595.7	61.3
III – 3	1.54	5.25	4,027	595.7	60.4
III – 4	1.55	4.96	4,684	595.6	60.9
III – 5	1.42	4.78	3,916	596.1	60.5
IV – 1	1.39	5.08	608	596.5	58.7

IV – 2	1.54	5.55	620	596.0	59.4
IV – 3	1.50	5.14	613	596.7	59.2
IV – 4	1.55	5.51	578	596.7	59.8
IV – 5	1.52	5.65	592	596.8	58.2
V – 1	1.36	5.40	2,985	596.1	54.2
V – 2	1.34	5.69	2,758	596.8	54.9
V – 3	1.35	5.41	3,098	596.1	53.8
V – 4	1.36	5.28	3,021	596.4	53.6
V – 5	1.37	5.30	3,027	596.3	54.9
VI – 1	1.45	4.24	1,282	601.3	52.3
VI – 2	1.41	4.05	1,201	598.2	51.3
VI – 3	1.44	4.18	1,196	597.3	51.2
VI – 4	1.40	4.12	1,201	597.8	50.8
VI – 5	1.48	4.06	1,194	597.9	50.4

The same result was observed for all parachute flares (see **Table 41**)

***Table 41**: Geometry and optical emissive output of all parachute flares.*

Parachute Identification	**Pellet Density**	**Burn Time**	**Luminous Intensity**	**Dominant Wavelength**	**Spectral Purity**
	(g/cc)	(s)	(cd)	(nm)	(%)
Control – 1	1.94	33.06	16,994	611.4	79.5
Control – 2	1.92	32.91	21,001	611.6	78.6
Control – 3	1.88	33.15	18,961	612.5	80.2
Control – 4	1.90	33.44	15,544	612.8	81.6
I – 1	1.43	28.23	1,180	604.1	29.1
I – 2	1.41	28.63	938	604.2	28.3
I – 3	1.43	27.83	1,031	600.1	27.2
I – 4	1.47	28.95	982	604.7	30.9
I – 5	1.45	29.45	1,138	600.6	26.3

II – 1	1.47	37.35	944	612.3	36.4
II – 2	1.52	38.74	659	614.0	38.6
II – 3	1.48	37.33	840	611.1	38.8
II – 4	1.46	38.64	760	611.5	37.2
II – 5	1.45	36.92	996	608.8	38.0
III – 1	1.49	21.39	3,684	598.5	48.0
III – 2	1.49	21.65	3,212	597.8	52.0
III – 3	1.46	21.44	3,639	598.0	49.3
III – 4	1.47	21.52	3,543	597.7	51.1
III – 5	1.47	21.60	3,708	597.7	51.0
IV – 1	1.52	24.64	482	No data*	
IV – 2	1.51	25.19	451	No data*	
IV – 3	1.51	24.90	488	605.1	58.8
IV – 4	1.51	24.82	509	600.0	54.2
IV – 5	1.50	25.10	513	599.9	53.2
V – 1	1.43	25.42	2,513	597.1	50.3
V – 2	1.44	25.59	2,372	599.0	47.7
V – 3	1.40	24.77	2,561	599.2	48.2
V – 4	1.43	26.15	2,470	598.6	50.4
V – 5	1.42	25.82	2,530	599.0	49.2
VI – 1	1.40	22.03	811	602.0	45.4
VI – 2	1.43	21.40	814	603.9	42.0
VI – 3	1.41	22.64	736	602.4	46.3
VI – 4	1.47	21.62	799	602.9	43.9
VI – 5	1.49	21.10	655	605.0	41.5

* Color data for parachute flares **IV** – 1 and **IV** – 2 removed due to low signal levels.

3.5 Cost Assessment

The costs were within the expected range. However, there was a redistribution of funds with regard to travel expenses. Most of the travel money was spent on the purchase of a thermal camera. This was justified by the fact that a study of burnup temperatures was considered necessary for this project. Also, the travel funds could not be used for the original purpose, as from 2020 on meetings have either taken place online or have been cancelled due to the corona pandemic. Additionally, many trips were cancelled or significantly restricted due to local permissible ordinances.

Cost Category	***Details***	***Subcategory***	***Costs***
Salaries & Wages	In this section the total labor costs are included Hourly or salary (40h/week)	1 PhD student loan (for three years)	$145,500
		Overhead expenses (20%)	$29,100
		TOTAL SALARIES	**$174,600**
Expendable Supplies	Including costs of chemicals, lab space, infrastructure, power, water and disposal	Consumables incl. chemicals, solvents, analytical costs	$43,250
		Overhead expenses (20%)	$8,650
		TOTAL EXPENDABLES SUPPLIES	**$51,900**
Non-expendable Equipment	Including costs of new equipment, which was required for complete analysis	Bench Top Mixing System	$18,000
		Equipment (safety equipment, pump, magnetic stirrer, etc.)	$10,000
		Thermal camera (FLIR)	$55,000
		Overhead expenses (20%)	$16,600
		TOTAL NON-EXPENDABLES EXPENSES	**$99,600**
Work Cost Partner *DEVCOM*	Prototyping and testing of 2 colorants	US Army *DEVCOM* (involved personal: 2 pilot plant technicians, 1 lead test engineer, 2 pyro engineers)	$40,000
		Overhead expenses (20%)	$8,000
		TOTAL WORK COST *DEVCOM*	**$48,000**
Travel	Travel cost	Due to Covid-19 no travels possible	$0
TOTAL COSTS OF THE PROJECT (36 MONTHS)			**$371,400**

3.6 Implementation Issues

In this work it was shown, that multiple lithium salts are able to produce red light in pyrotechnics. Multiple mixtures reached the required benchmarks of 620±20 nm for the dominant wavelength and showed spectral purity of ≥70 %. It was also possible to push the boundaries for the luminous intensity into a magnitude of the strontium standard formulations. Unfortunately, these parameters were not fulfilled simultaneously. As an example, in formulation **AD-33**, containing the lithium salt dilithium 5,5`-bistetrazolate dihydrate (**26**), a dominant wavelength of 603 nm with a luminous intensity of over 14000 cd could be obtained, but the spectral purity was around 30%. This mixture gave a more pinkish flame impression. As another example in formulation **AD-24** a spectral purity of 85% was achieved. But on the other hand the dominant wavelength only reached 597 nm and the luminous intensity was 100 times weaker as in the other example mixture. The trend that the dominant wavelength and spectral purity are antagonist to the luminous intensity and the other way around, was observed in all pyrotechnical tests we executed over the last three years. The same trend was also observed by the cooperation partner *DEVCOM AC*. In the application tests, in which the most promising mixtures determined by the *LMU* were pressed and placed into cluster and parachute flares the results remained below the expectations. Instead of producing a bright red color, the mixtures with the lithium salts remained in a pink color range.

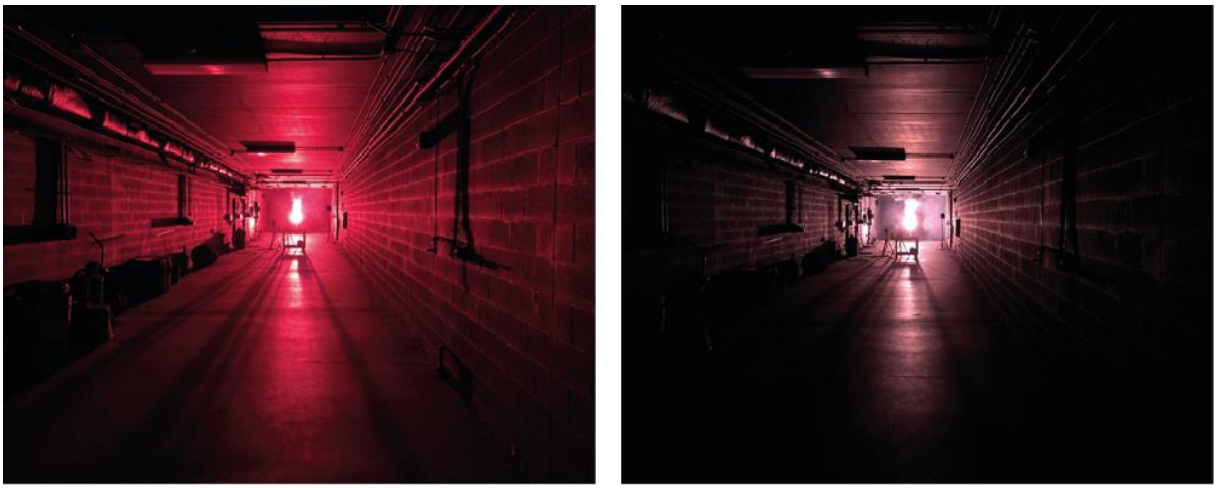

***Figure 75**: Comparison of a strontium-based control formulation and the tested formulation containing lithium-5-aminotetrazol (**20**).*

It turned out that the measured values in the application testing were worse than the results obtained on a small laboratory scale. This can be explained by the fact that the mixtures were measured at the LMU without any “impurities”. This is not the case with DEVCOM's tests, as they include additional material that burns during the test, like the paper tubes in which the mixtures are pressed.

The reason for the poor performance of the formulations is lithium itself. This can be explained by the oxophilicity of the element. Lithium forms lithium hydroxide (LiOH) and lithium oxide

(Li_2O) during the burnup. The latter compounds are masking the red color impression of the Li^0 species.[55]

To summarize the project **WP19-1287 "Lithium Based Red Colorants in Environmentally Friendly Pyrotechnical Illuminants"**, the replacement of strontium to this point is not possible. Further ideas for following projects are the investigation of other lithium salts for example the dilithium 3,3`-diamino-4,4`-dinitramino-5,5`-bi-1,2,4-triazolate trihydrate synthesized by *Glück* et al.[46], which was not included in the investigation in this work due to the complex synthesis scheme. The investigation of lithium nitrate ($LiNO_3$) as an oxidizer and the colorant of pyrotechnical mixtures would be interesting, although this topic was already dealt with in the past. However, the idea of coating the material and the pyrotechnical mixtures would open new opportunities. These ideas would be the fundamentals for a subsequent project.

4 Publications

4.1 In peer reviewed journals

1) The Lithium Salts of Bis(azoyl)borates as Strontium- and Chlorine-free Red Pyrotechnic Colorants
   Alicia M. W. Dufter, Thomas M. Klapötke, Magdalena Rusan, and Jörg Stierstorfer
   Z. Anorg. Allg. Chem. **2020**, *646*, 580–585.
2) Comparison of Functionalized Lithium Dihydrobis(azolyl)borates with Their Corresponding Azolates as Environmentally Friendly Red Pyrotechnic Coloring Agents.
   Alicia M. W. Dufter, Thomas M. Klapötke, Magdalena Rusan, Alexander Schweiger and Jörg Stierstorfer
   ChemPlusChem. **2020**, *85*, 2044–2050.
3) Lithium Nitropyrazolates as Potential Red Pyrotechnic Colorants.
   A. M. W. Dufter-Münster, Alexander G. Harter, Thomas M. Klapötke, Elena Reinhardt, Julia Römer and Jörg Stierstorfer
   Eur. J. Inorg. Chem. ***2022****, in press.*

4.2 Poster

1) Lithium-Based Red Colorants In Environmetnally Friendly Pyrotechnical Illuminats
   Alicia M. W. Dufter, Thomas M. Klapötke, Jared D. Moretti, Anthony P. Shaw, Jörg Stierstorfer
   SERDP ESTCP SYMPOSSIUM, Washington, D. C., December 3 – December 5, 2019.

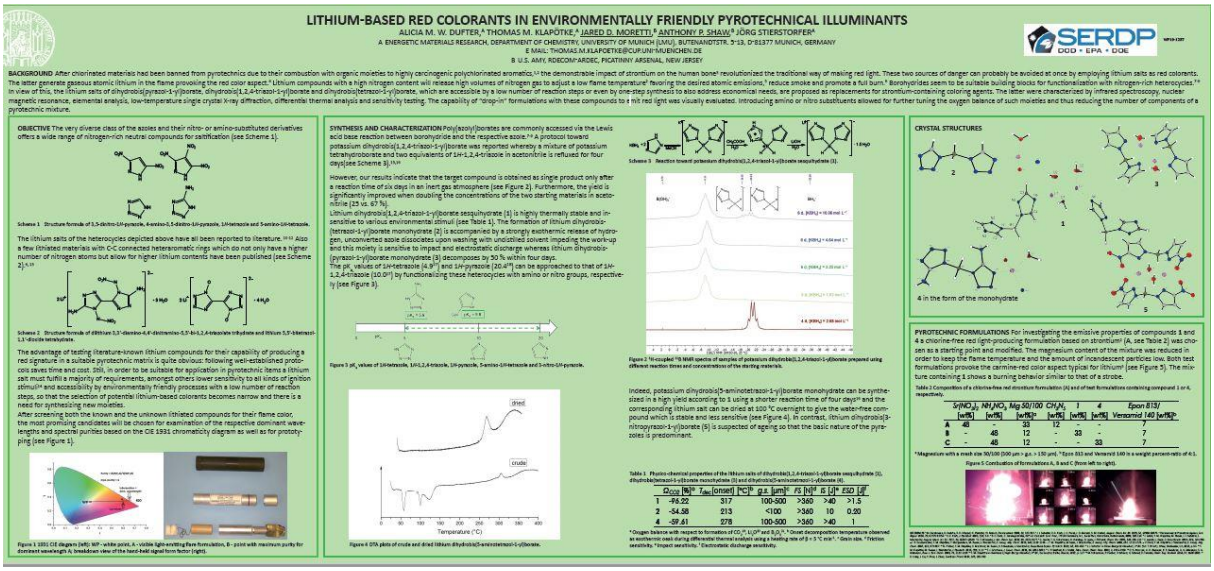

Figure 76: *Poster presented at SERDP ESTCP SYMPOSSIUM in 2019.*

2) Lithium 2,2,2-trinitroethyl nitrocarbamate monohydrate as colorant in red-burning pyrotechnics
Thomas M. Klapötke, Alexander Schweiger, Jörg Stierstorfer
NTREM 2022, Pardubice, Czech Republic, April 6 – April 8, 2022.

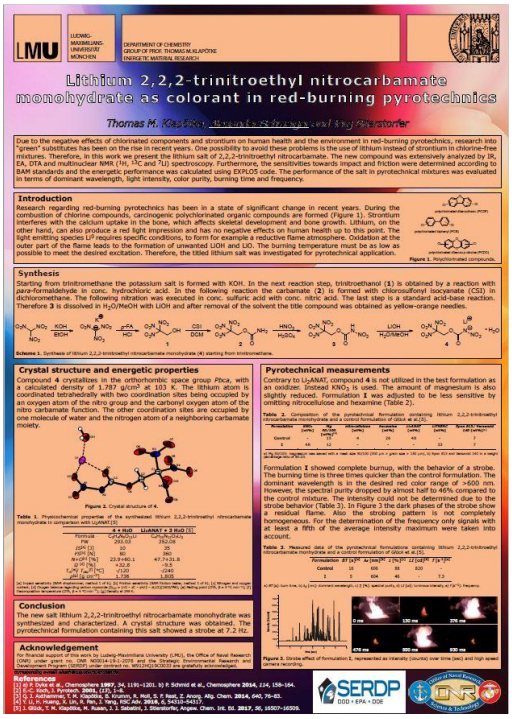

***Figure 77**: Poster presented at NTREM 2022.*

5 Literature Cited

[1] J. A. Conkling and C. Mocella, Chemistry of Pyrotechnics: Basic Principles and Theory, Taylor & Francis, 2010.

[2] W. Christmann, D. Kasiske, K. D. Klöppel, H. Partscht and W. Rotard, Chemosphere, 1989, 19, 387–392.

[3] a) U.S. Environmental Protection Agency (EPA) Makes Preliminary Determination to Regulate Strontium in Drinking Water, b) https://yosemite.epa.gov/opa/admpress.nsf/6427a6b7538955c585257359003f0230/327f339e63facb5a85257d77005f4bf9!OpenDocume nt, Accessed Oct 2017.

[4] J. J. Sabatini, E.-C. Koch, J. C. Poret, J. D. Moretti, S. M. Harbol, *Angew. Chem.* **2015**, *127*, 11118–11120; *Angew. Chem. Int. Ed.* **2015**, *54*, 10968–10970.

[5] a) S. Trofimenko, *J. Am. Chem. Soc.* **1967**, *89*, 3170–3177. b) C. Janiak, T. G. Scharmann, H. Hemling, D. Lentz, J. Pickardt, *Chem. Ber.* **1995**, *128*, 235–244. c) C. Janiak, L. Esser, *Z. Naturforsch.* **1992**, *48 b*, 394–396. d) T. J. Groshens, *J. Coord. Chem.* **2010**, *63*, 1882–1892. e) T. M. Klapötke, M. Rusan, J. Stierstorfer, *J. Pyrotech.* **2014**, (33), 1–14.

[6] M. F. Bölter, A. Harter, T. M. Klapötke, J. Stierstorfer, *ChemPlusChem* **2018**, *83*, 804–811.

[7] J. W. A. M. Janssen, H. J. Koeners, C. G. Kruse, C. L. Habraken, *J. Org. Chem.* **1973**, *38*, 1777–1782.

[8] I. E. Drukenmüller, T. M. Klapötke, Y. Morgenstern, M. Rusan, J. Stierstorfer, *Z. Anorg. Allg. Chem.* **2014**, *640*, 2139–2148.

[9] D. Fischer, J. L. Gottfried, T. M. Klapötke, K. Karaghiosoff, J. Stierstorfer, T. G. Witkowski, *Angew. Chem. Int. Ed.* **2016**, *55*, 16132-16135.

[10] Y. Zhang, Y. Guo, Y.-H. Joo, D. A. Parrish, J. M. Shreeve, *Chem. Eur. J.* **2010**, *16*, 10778–10784.

[11] T. M. Klapötke, M. Stein, J. Stierstorfer, *Z. Anorg. Allg. Chem.* **2008**, *634*, 1711–1723.

[12] V. Ernst, T. M. Klapötke, J. Stierstorfer, *Z. Anorg. Allg. Chem.* **2007**, *633*, 879–887.

[13] T. M. Klapötke, J. Stierstorfer, *Helv. Chim. Acta* **2007**, *90*, 2132–2150.

[14] N. Fischer, T. M. Klapötke, J. Stierstorfer, *J. Energ. Mater.* **2011**, *29*, 61–74.

[15] E. Lieber, E. Sherman, R. A. Henry, J. Cohen, *J. Am. Chem. Soc.* **1951**, *73*, 2327–2379.

[16] A. D. Vasiliev, A. M. Astakhov, M. S. Molokeev, L. A. Kruglyakova, A. M. Sirotinin, R. S. Stepanov, *J. Struct. Chem.* **2004**, *45*, 360–364.

[17] D. E. Chavez, M. A. Hiskey, D. L. Naud, *J. Pyrotech.* **1999**, (10), 17–36.

[18] J. H. Nelson, N. E. Takach, R. A. Henry, D. W. Moore, W. M. Tolles, G. A. Gray, *Magn. Reson. Chem.* **1986**, *24*, 984–994.

[19] L. H. Finger, F. G. Schröder, J. Sundermeyer, *Z. Anorg. Allg. Chem.* **2013**, *639*, 1140–1152.

[20] N. Fischer, T. M. Klapötke, S. Marchner, M. Rusan, S. Scheutzow, J. Stierstorfer, *Propellants Explos. Pyrotech.* **2013**, *38*, 448–459.

[21] J. Hoare, R. Duddu, R. Damavarapu, *Org. Process Res. Dev.* **2016**, *20*, 683–686.

[22] L. Molard, J. Vaganay, *Meml. Poudres* **1957**, *39*, 123–136.

[23] M. H. H. Wurzenberger, J. T. Lechner, M. Lommel, T. M. Klapötke, J. Stierstorfer, *Propellants Explos. Pyrotech.* **2020**, *45*, 898–907.

[24] A. Langlet, N. V. Latypov, U. Wellmar, U. Bemm, P. Goede, *J. Org. Chem*. **2002**, 67, 7833–7838.

[25] N. Latypov, U. Wellmar, A. Langlet, Method of Preparing Salts of Dinitromethane, **2002**, US6340780B1.

[26] Q. J. Axthammer, B. Krumm, T. M. Klapötke, *J. Org. Chem.* **2015**, *80*, 6329–6335.

[27] Q. J. Axthammer, T. M. Klapötke, B. Krumm, R. Moll, Sebastian F. Rest, *Z. Anorg. Allg. Chem.* **2014**, *640*, 76−83.
[28] Q. J. Axthammer, B. Krumm, T. M. Klapötke, *Eur. J. Org. Chem.* **2015**, 723–729.
[29] T. M. Klapötke, B. Krumm, C. C. Unger, *Inorg. Chem.* **2019**, *58*, 2881–2887.
[30] A. M. W. Dufter, T. M. Klapötke, M. Rusan, J. Stierstorfer, *Z. anorg. allg. Chem.*, in press.
[31] J. F. Satchell, B. J. Smith, Phys. *Chem. Chem. Phys.* **2002**, *4*, 4314–4318.
[32] G. Herve, C. Roussel, H. Graindorge, *Angew. Chem. Int. Ed.* **2010**, *49*, 3177–3181.
[33] http://www.ozm.cz, Accessed February 17, 2020.
[34] UN Recommendations on the Transport of Dangerous Goods –Manual of Tests and Criteria, 5th Ed, ST/SG/AC. 10/11/Rev.5, **2009**.
[35] NATO standardization agreement (STANAG) on explosives, impact sensitivity tests, no. 4489, 1st ed., Sept. 17, **1999**.
[36] NATO standardization agreement (STANAG) on explosive, friction sensitivity tests, no. 4487, 1st ed., Aug. 22, **2002**.
[37] UN Recommendations on the Transport of Dangerous Goods –Manual of Tests and Criteria, 5th Ed, **2009**, S 76.
[38] UN Recommendations on the Transport of Dangerous Goods –Manual of Tests and Criteria, 5th Ed, **2009**, S 104–105.
[39] https://echa.europa.eu/de/substance-information/-/substanceinfo/100.013.751, Accessed June 1, 2021.
[40] Z. Jalový, J. Ottis, A. Růžička, A. Lyčka, N. V. Latypov, *Tetrahedron*, **2009**, *65*, 7163–7170.
[41] G. I. Sunahara, S. Dodard, M. Sarrazin, L. Paquet, G. Ampleman, S. Thiboutot, J. Hawari, A. Y. Renoux, *Ecotoxicology and Environmental Safety* **1998**, *39*, 185-194.
[42] T. M. Klapötke in *Chemistry of High-Energy Materials, 4th Ed.*, De Gruyter, Berlin, Boston, **2017**, p. 127.
[43] M. Schiemann, P. Fischer, V. Scherer, G. Schmid, D. Taroata, *Chem. Eng. Technol.* **2014**, *37*, 1600–1605.
[44] D. Liang, J. Liu, Y. Zhou, J. Zhou, *Combust. Flame* **2017**, *185*, 292–300.
[45] a) E.-C. Koch, *J. Pyrotech.* **2001**, (13), 1-8. b) E.-C. Koch, C. Jennings-White, *Int. Pyrotech. Sem.*, *Proc. Semin.*, *36th*, Rotterdam, Netherlands, **2009**, 105-110
[46] J. Glück, T. M. Klapötke, M. Rusan, J. J. Sabatini, J. Stierstorfer, *Angew. Chem*. **2017**, *129*, 16733–16736; *Angew. Chem. Int. Ed*. **2017**, *56*, 16507–16509.
[47] J. Roberts, Wisconsin strontium levels among highest in U.S. drinking water supplies, http://wisconsinwatch.org/2016/03/wisconsin-strontium-levels-among-highest-in-u-sdrinking-water-supplies/, Accessed Oct 2017.
[48] A. J. O'Donnell, D. A. Lytle, S. Harmon, K. Vu, H. Chait and D. D. Dionysiou, Water Res., 2016, 103, 319–333.
[49] J. J. Sabatini and J. D. Moretti, Chem. - Eur. J., 2013, 19, 12839–12845.
[50] S. H. Zyoud, W. S: Waring, W. M. Sweileh, S. W. Al-Jabi, *Basic Clin. Pharmacol. Toxical.* **2017**, *121*, 67–73.
[51] a) E.-C. Koch, *J. Pyrotech*. **2002**, *15*, 9. b) B. E. Douda, Theory of Colored Flame Production, Report, RDTN No. 71, **1964**, U.S. Naval Ammunition Depot, Crane, IN, USA.
[52] http://www.ozm.cz, Accessed February 17, 2020.
[53] Wehrwissenschaftliches Institut für Werk- und Betriebsstoffe (WIWEB)-Standardarbeitsanweisung 4-5.1.03, Ermittlung der Explosionsgefährlichkeit oder der Reibeempfindlichkeit mit dem Reibeapparat, Nov. 8, **2002**.
[54] WIWEB-Standardarbeitsanweisung 4-5.1.02, Ermittlung der Explosionsgefährlichkeit, hier der Schlagempfindlichkeit mit dem Fallhammer, Nov. 8, **2002**.

[55] E.-C. Koch, *Propellents, Explosives, Pyrotechnics* **2004**, *29*, 67–80.